UNIVERSIDAD AUTÓNOMA DE MADRID

Departamento de Bioquímica

ATHEROSCLEROSIS IN PROGERIA: INSIGHT FROM NEW MOUSE MODELS WITH SYSTEMIC AND TISSUE-SPECIFIC PROGERIN EXPRESSION

MAGDA RITA HAMCZYK

Madrid, 2017

Departamento de Bioquímica
Facultad de Medicina
Universidad Autónoma de Madrid

Atherosclerosis in progeria: insight from new mouse models with systemic and tissue-specific progerin expression

PhD student: Magda Rita Hamczyk, M.Sc. in Biotechnology

Thesis directors: Vicente Andrés, PhD and Ricardo Villa-Bellosta, PhD

Centro Nacional de Investigaciones Cardiovasculares Carlos III (CNIC)

D. Vicente Andrés García, Doctor en Biología, y **D. Ricardo Villa Bellosta**, Doctor por la Universidad de Zaragoza,

CERTIFICAN:

Que Dña. **Magda Rita Hamczyk**, licenciada en Biotecnología por la Universidad **Jaguelónica** (Polonia) ha realizado bajo su dirección el trabajo de Tesis Doctoral que lleva por título ***"Atherosclerosis in progeria: insight from new mouse models with systemic and tissue-specific progerin expression"***.

Revisado el presente trabajo, expresan su conformidad para la presentación del mismo por considerar que reúne los requisitos necesarios para ser sometido a discusión ante el Tribunal correspondiente, para optar al grado de Doctora.

En Madrid, a 26 de Junio de 2017

Dr. Vicente Andrés García Dr. Ricardo Villa Bellosta

ACKNOWLEDGEMENTS

This thesis would not have been possible without the help of many people. Thus, I would like to express my sincere gratitude to:

- **Dr. Vicente Andrés**, my thesis director, for giving me the opportunity to perform my PhD at the CNIC and for all the support during more than 5 years of hard work and sacrifice (it would be impossible to list all the tasks that were accomplished and all the obstacles that were overcome during this period).
- **Dr. Ricardo Villa-Bellosta**, my thesis co-director, labmate and friend, for believing in me and being there for me 24/7. I am grateful to have been a part of this unstoppable arteriosclerosis duo; thank you for the motivation, immense knowledge and for teaching me the essential lab (survival) skills.
- **Dr. Carlos López-Otín** for giving me the opportunity to develop a part of my project during a (too) short stay at the University of Oviedo. Thank you for all the precious support in this ER stress story. Without your help, it would not have been possible to conduct this research; and thank you for giving me hope that a scientist does not have to sacrifice their personal life to be successful.
- **Dr. Antonio Maraver** and **Dr. Andrés Hidalgo**, my thesis committee members, for their insightful comments and encouragement, and also for the hard questions which stimulated me to improve my research. And thank you **Andrés** for cheering me up during my PhD blues and always finding the time to talk to me even when you were up to your neck in work.
- **Dr. Krzysztof Guzik**, my former research supervisor, for encouraging me to pursue a career in research and providing advice during my postgraduate work.
- **María Jesús Andrés** for the priceless technical support in many tedious laboratory techniques (genotyping, lesion quantification, etc.) and for being like a mother to me.
- **Dr. Pilar Gonzalo** for the optimism and invaluable help during the last year of my PhD which allowed me to focus on writing my thesis and research articles; without you, it would not have been possible to complete the project on time.
- **Antonio de Molina** and **Roisin Doohan** for the support with histology. Thank you for sharing your enthusiasm for exciting aortic and cardiac pathologies; I wish everybody had the same commitment and love for their work as you have.
- **Rubén Mota** for being the best vet for my mice and for teaching me many amazing things about mouse pathology.

- The animal facility technicians, especially **Virginia Zorita** and **Eva Santos**, for the laborious, day-to-day animal care.
- **Marta García Camacho** and **Ana Belén Ricote** for the support with hematology, serum biochemistry, ECG and blood pressure techniques.
- **Dr. Beatriz Dorado** for keeping the lab in check and for the hard labor of managing the group.
- **Eduardo Bieger** and **Eeva Soininen** for the invaluable help with the Spanish bureaucracy.
- **Javier Mateos** for the technical support.
- My students, **Lucia**, **Carmen**, **Miriam** and **Rosa**, for teaching me how to be a leader rather than a boss, for asking adequate questions, and for making me think out of the box.
- Former (**Carlos**, **Pedro**, **Laia**, **Raphael**, **Alba**, **Óscar**, **José**) and current lab members (**José María**, **Raquel**, **Amanda**, **Víctor**, **Alberto**, **Lara**, **Álvaro**, **Elba**, **Cristina**) for the stimulating discussions and all the time spent together at the CNIC.
- CNIC´s Polish team (**Magda**, **Ola**, **Dori**, and **Ania**) for sharing those good and bad moments on this PhD emotional rollercoaster, for all the scientific and non-scientific support, pierogi cooking, pączki eating and much more.
- **Carlos López-Otín´s group members** for the warm reception at the University of Oviedo during my internship.
- **Riju** for entertaining me during our 12:45 lunch sessions. Thank you for making me believe that there are still good people out there.
- **Víctor**, my soul-mate, for being a true and great emotional-scientific supporter at all times, and for telling awful jokes that made me forget how bad the situation was. Thank you for being non-judgmental of me and instrumental in instilling confidence, and for inspiring me to strive towards my goal.
- **Maria**, my flatmate and friend, for all the time spent together talking, laughing, dancing, cooking; thank you for becoming a part of my life.
- **Ania**, **Roman**, **Sofia** and **Maxim** for being my eastern family here in Madrid; thank you for sharing many precious moments with me.
- My **parents** for their love and encouragement, for providing me with the best education they could, and most importantly for teaching me how to think rather than what to think.
- My siblings (**Sylwia** and **Rafał**) and friends back in Poland (**Łukasz**, **Justyna**, **Gosia, Monika, Madzia** and **many others**) for putting up with me and my endless excuses related

to continuous lack of time. Special thanks to **Łukasz** for encouraging me to relax and enjoy life during the most difficult moments of my PhD and for being the best friend I could dream of.

RESUMEN

Las enfermedades cardiovasculares (ECV) son la causa principal de morbimortalidad en el mundo debido en gran parte al envejecimiento progresivo de nuestras sociedades. El deterioro cardiovascular está acelerado en un trastorno genético muy raro llamado síndrome de progeria Hutchinson-Gilford (HGPS). Esta enfermedad está causada por una mutación puntual *de novo* en el gen *LMNA*, que conduce a la expresión de "progerina", una forma mutante de la lamina A que provoca numerosas anomalías estructurales y funcionales en el núcleo. Los niños con HGPS presentan síntomas de envejecimiento prematuro, incluyendo alopecia, osteoporosis, lipodistrofia, rigidez de las articulaciones, arrugas de la piel y moteado, siendo la característica más importante de la enfermedad la aterosclerosis acelerada, proceso que conduce a muerte prematura a una edad media de 14,6 años, predominantemente por infarto de miocardio o accidente cerebrovascular. Existe un gran desconocimiento sobre los mecanismos por los que la progerina acelera la aterosclerosis, en gran parte debido a la falta de modelos animales adecuados. En esta tesis hemos generado nuevos modelos de ratón que permiten estudiar la aterosclerosis asociada a HGPS. Comparado con controles con el gen *Lmna* intacto, los ratones mutantes que expresan progerina de forma ubicua presentan envejecimiento prematuro asociado con pérdida de peso corporal y menor longevidad. Además, mostraron patología vascular similar a la observada en pacientes HGPS, incluyendo aterosclerosis acelerada, pérdida de células de músculo liso vascular (CMLVs), aumento del contenido de colágeno, retención de lípidos en la capa media y fibrosis de la capa adventicia. También hemos demostrado que los ratones que expresan progerina específicamente en CMLVs, pero no en macrófagos, recapitulan la patología vascular del modelo ubicuo. Además, tanto en el modelo ubicuo como en el específico de CMLVs, los ateromas mostraron evidencia de ruptura de la placa que podría provocar infarto de miocardio. Por otra parte, mediante transcriptómica de alto rendimiento identificamos en ambos modelos de ratón el estrés de retículo endoplásmico (RE) y la respuesta a proteínas desplegadas como posibles mecanismos inductores de muerte de CMLVs y aterosclerosis acelerada. De acuerdo con esta hipótesis, el tratamiento con ácido tauroursodeoxicólico (TUDCA), una chaperona química que aumenta la capacidad celular para soportar el estrés de RE, disminuyó en ambos modelos la aterosclerosis, la pérdida de CMLVs y el grosor de la adventicia. TUDCA también prolongó en un 35% la supervivencia de los ratones con expresión de progerina específica en CMLVs. En resumen, nuestros resultados sugieren el uso de TUDCA para prevenir la aterosclerosis y eventos cardiovasculares asociados a HGPS. Dado que la progerina se acumula con la edad en individuos sin HGPS, nuestros resultados también podrían arrojar luz sobre el envejecimiento fisiológico.

SUMMARY

Cardiovascular disease (CVD) is a major cause of morbidity and mortality worldwide due to the progressive aging of our societies. Age-related decline in cardiovascular health is accelerated in a rare genetic disorder called Hutchinson-Gilford progeria syndrome (HGPS). The disease is caused by a *de novo* point mutation in the *LMNA* gene, which leads to the expression of "progerin", a mutant form of the nuclear protein lamin A. Since lamin A possesses important structural and functional properties, progerin expression triggers numerous nuclear abnormalities. Children with HGPS exhibit premature aging symptoms, including alopecia, osteoporosis, lipodystrophy, joint stiffness, and skin wrinkling and mottling. However, the most clinically relevant feature of the disease is accelerated atherosclerosis, which leads to premature death at an average age of 14.6 years, predominantly from myocardial infarction or stroke. The mechanisms through which progerin provokes enhanced atherosclerosis remain poorly understood, in part due to the paucity of suitable models. To address this, we sought to generate new mouse models that allow the study of atherosclerosis in the context of HGPS. When compared with control mice expressing wild-type lamin A/C, mice with ubiquitous progerin expression exhibited a premature aging phenotype, including reduced body weight and shortened survival. In addition, progerin-expressing mice showed increased atherosclerosis burden together with a severe vascular pathology, including the depletion of vascular smooth muscle cells (VSMCs), increased collagen content, medial lipid retention and adventitial fibrosis, resembling most aspects of CVD observed in HGPS. We also found that mice expressing progerin specifically in VSMCs, but not in macrophages, fully recapitulated the vascular pathology observed in the ubiquitous progeria model. Atheromas of both ubiquitous and VSMC-specific models showed evidence of plaque disruption, which might lead to myocardial infarction. Using a transcriptomic approach, we identified endoplasmic reticulum (ER) stress and the unfolded protein response as possible driver mechanisms of progerin-induced VSMC death and accelerated atherosclerosis. Accordingly, treatment with tauroursodeoxycholic acid (TUDCA), a chemical chaperone that increases the capacity of a cell to sustain ER stress, was effective at ameliorating vascular disease (atherosclerosis, VSMC loss and adventitial thickening) in both ubiquitous and VSMC-specific mouse models. TUDCA also prolonged the survival of mice with VSMC-specific progerin expression by 35%. Taken together, these findings indicate that TUDCA may be effective in the treatment of atherosclerosis and associated cardiovascular events in HGPS. Moreover, since progerin accumulates with age in non-HPGS individuals, our data may also shed some light on the mechanisms of normal aging.

INDEX

ABBREVIATIONS 1

I. INTRODUCTION 7

I.1. Physiological aging and cardiovascular disease (CVD) 9

I.1.1. Aging as a risk factor for CVD 9

I.1.2. Atherosclerosis 9

I.2. Premature aging and CVD 10

I.2.1. Hutchinson-Gilford progeria syndrome (HGPS) 10

I.2.2. CVD in HGPS 11

I.2.3. Mechanism leading to progerin production 13

I.3. Progerin and prelamin A in physiological aging 15

I.4. Mouse models of progeria 15

I.5. General mechanisms of HGPS 17

I.6. Mechanisms underlying CVD in progeria 19

I.6.1. VSMC loss 19

I.6.2. Vascular calcification 21

I.6.3. Endothelial dysfunction 22

I.6.4. Cardiac electrical alterations 22

I.7. Endoplasmic reticulum (ER) stress and the unfolded protein response (UPR) 23

II. OBJECTIVES 27

III. MATERIALS AND METHODS 31

III.1. Mice 33

III.2. Longevity study 33

III.3. High-fat diet (HFD) experiments 33

III.4. Hematology and serum biochemical analysis 34

III.5. Blood pressure measurement 34

III.6. ECG 34

III.7. Treatment 35

III.8. Quantification of atherosclerosis burden 35

III.9. Histology and immunofluorescence 35

III.10. Sample collection and preparation for RNAseq 36

III.11. RNAseq library preparation, sequencing, and generation of FastQ files 37

III.12. Differential expression analysis 37

III.13. Pathway analysis 38

III.14. RNA extraction and cDNA preparation 38

III.15. PCR detection of lamin A and progerin 38

III.16. Quantitative real-time PCR 39

III.17. Statistical analysis 39

IV. RESULTS AND DISCUSSION 41

IV.1. Ubiquitous progerin expression aggravates atherosclerosis in HFD-fed *Apoe*$^{-/-}$ mice 43

IV.2. VSMC-specific progerin expression in HFD-fed *Apoe*$^{-/-}$ mice aggravates atherosclerosis and shortens lifespan 48

IV.3. Progerin triggers plaque vulnerability 57

IV.4. Progerin expression accelerates atherosclerosis in *Apoe*$^{-/-}$ mice fed normal chow 59

IV.5. Progerin expression in VSMCs leads to progressive hypotension 62

IV.6. *Apoe*$^{-/-}$*Lmna*$^{G609G/G609G}$ mice develop arrhythmias 64

IV.7. *Apoe*$^{-/-}$*Lmna*$^{LCS/LCS}$*SM22αCre* die from atherosclerosis-related causes 66

IV.8. Progerin expression in VSMCs activates endoplasmic ER stress and the UPR 72

IV.9. Therapeutic effects of ER stress response targeting in progeroid mice 78

V. CONCLUSIONS 87

V. CONCLUSIONES 93

VI. REFERENCES 99

VII. ANNEX 121

ABBREVIATIONS

53BP1 - 53 binding protein-1

APOE - apolipoprotein E

ATF4 - activating transcription factor 4

ATF6 - activating transcription factor 6

ATF6f - ATF6 fragment

BAC - bacterial artificial chromosome

BMP2 - bone morphogenetic protein 2

BSA - bovine serum albumin

CVD - cardiovascular disease

DDIT3 - DNA damage-inducible transcript 3

DNA-PK - DNA-dependent protein kinase

DNA-PKcs - DNA-dependent protein kinase catalytic subunit

EC(s) - endothelial cell(s)

ECG - electrocardiogram

eIF2α - eukaryotic translation initiator factor 2α

ePPi - extracellular inorganic pyrophosphate

ER - endoplasmic reticulum

ERAD - ER-associated protein degradation

FTI(s) - farnesyl transferase inhibitor(s)

GRP78 - 78 kDa glucose-regulated protein

H&E - hematoxylin-eosin

HDL - high-density lipoproteins

HFD - high-fat diet

HGPS - Hutchinson-Gilford progeria syndrome

ICMT - isoprenylcysteine carboxyl methyltransferase

IPA - Ingenuity Pathway Analysis

iPSC(s) - induced pluripotent stem cell(s)

IRE1 - inositol-requiring enzyme 1

LDL - low-density lipoproteins

mTOR - mammalian target of rapamycin

NHEJ - non-homologous end joining

ORO - Oil Red O

PBA - 4-phenyl butyric acid

PBS - phosphate-buffered saline

PERK - protein kinase RNA-like ER kinase

RT - room temperature

RUNX2 - Run-related transcription factor-2

SEM - standard error of the mean

SMC(s) - smooth muscle cell(s)

TUDCA - tauroursodeoxycholic acid

UPR - unfolded protein response

VSMC(s) - vascular smooth muscle cell(s)

XBP1 - X box-binding protein 1

XBP1s - spliced X box-binding protein 1

I. INTRODUCTION

I.1. Physiological aging and cardiovascular disease (CVD)

I.1.1. Aging as a risk factor for CVD

Aging is the main risk factor for the development of CVD (*1*). Although much progress has been made in the prevention, diagnosis, and treatment of CVD, it remains the leading cause of death worldwide (*2*). According to the World Health Organization, approximately 17.5 million people die annually from CVD, representing 31% of all deaths (www.who.int/cardiovascular_diseases). CVD is the outcome of complex interactions between modifiable and non-modifiable risk factors (*3*). Many modifiable risk factors for CVD have been identified, and the causal relevance of several of these factors is now well proven, including tobacco exposure, physical inactivity, obesity, hypertension, hypercholesterolemia and diabetes. Non-modifiable risk factors include age, gender, ethnicity and genetic susceptibility to the disease (family history).

Age-related changes in the vasculature include luminal dilatation and arterial wall thickening, especially of the intima (e.g. atherosclerosis), leading to increased vascular stiffness (*1, 4*). Various changes in the vessel wall that show causal relationships with arterial stiffening have been described, including calcification, augmented content and crosslinking of collagen fibers, increased elastin breakage, and diminished elastin content (*5-8*). Moreover, endothelial function is impaired with age, further contributing to the reduced vascular compliance (*1*), defined as the capacity of a blood vessel to enlarge and contract in response to changes in the pressure.

I.1.2. Atherosclerosis

Atherosclerosis underlies most manifestations of CVD, including coronary heart disease and cerebrovascular disease, and can lead to myocardial infarction or stroke. Atherosclerosis is characterized by thickening of the arterial wall and luminal narrowing due to atherosclerotic plaque buildup. The disease is initiated by endothelial dysfunction triggering low-density lipoprotein (LDL) infiltration and accumulation in the intima, principally at sites with disturbed blood flow (*9*). The presence of proteoglycans in the subendothelial space can further increase the retention of LDL particles (*10*), which are subsequently oxidized by reactive oxygen species. Oxidized LDL induces endothelial activation, which is characterized by the expression of adhesion molecules and the secretion of chemokines that trigger the recruitment of monocytes to the intima and their differentiation into macrophages. Neointimal macrophages begin to ingest modified LDL via the scavenger receptor

pathway (*11*), leading to their transformation into foam cells that secrete pro-inflammatory molecules, recruiting more immune cells to the lesion site. Impairment in the processing of oxidized lipoproteins leads to foam cell death (*12*). Progressive accumulation of cell debris and cholesterol crystals results in the formation of a necrotic core. Growth factors and cytokines present within the lesion induce the phenotypic transition of vascular smooth muscle cells (VSMCs) from a "contractile" to a "synthetic" state, and their migration from the media to the growing neointimal lesion. Neointimal synthetic VSMCs proliferate and abundantly synthesize extracellular matrix, normally stabilizing plaques. Mature fibroatheromatous plaques have a collagen- and VSMC-rich fibrous cap covering the necrotic core, which prevents its rupture and the subsequent life-threatening thrombus formation.

Plaque destabilization, including plaque rupture, plaque erosion and the formation of calcified nodules, is a complex process that depends on both structural features and biomechanical forces. Plaque rupture, which is the best characterized and the most common manifestation of plaque destabilization, is characterized by fibrous cap disruption and the ensuing exposure of the necrotic core to blood constituents, resulting in thrombus formation. Plaque destabilization may also occur due to plaque erosion and the accumulation of calcified nodules. Atherosclerotic lesions that are prone to rupture are termed "vulnerable" plaques, and are usually characterized by large necrotic cores, thin fibrous caps (related to decreased collagen and VSMC content), intraplaque hemorrhage, neoangiogenesis and large inflammatory infiltrates (*13*). Since plaque disruption can lead to myocardial infarction or stroke, it is of considerable importance to characterize and detect vulnerable plaques in order to prevent cardiovascular events in patients.

I.2. Premature aging and CVD

I.2.1. Hutchinson-Gilford progeria syndrome (HGPS)

HGPS is an extremely rare disorder characterized by signs of premature aging. This devastating disease was first described by Jonathan Hutchinson in 1886 and Hastings Gilford in 1897 (*14, 15*). The prevalence of HGPS is 1 in 20 million and it has no ethnic or gender bias (*16*). Affected children are normal at birth but within the first two years of life they begin to present the first symptoms of the disease, such as failure to thrive and skin abnormalities. Patients progressively develop other signs of premature aging, including alopecia, mottled and wrinkled skin, loss of body fat, joint stiffness and osteoporosis (*16, 17*). Importantly, they show generalized atherosclerosis, which leads to death from

myocardial infarction or stroke at an average age of 14.6 years (*18*). While HGPS resembles most aspects of normal aging, patients do not show signs of neurodegenerative disease or cancer.

I.2.2. CVD in HGPS

The most clinically relevant feature of HGPS is atherosclerosis, which is responsible for more than 90% of deaths (*16*). Atherosclerosis in HGPS is particularly intriguing because patients lack the classical risk factors for CVD development, such as hypercholesterolemia and increased serum C-reactive protein (*19*). Although levels of athero-protective high-density lipoproteins (HDL) are similar between prematurely-aged and healthy children, there is an age-dependent decline in HDL levels in HGPS (*19*). Autopsy findings have revealed that patients with HGPS present a wide spectrum of plaque phenotypes, ranging from early to late stage (*20*). These atherosclerotic lesions usually exhibit calcification, inflammation, and evidence of plaque erosion or rupture, similar to what is observed in physiological aging (*20*). The overall absence of pronounced dyslipidemia in progeria could partially explain why HGPS lesions tend to have smaller atheromatous cores than those of typical age-associated atheromas (*20*).

The severity of atherosclerosis in progeria usually correlates with VSMC depletion in the media (*21, 22*). This severe loss of VSMCs is accompanied by extracellular matrix deposition and altered elastin structure (*20-22*). In contrast to what is seen in normal aging, HGPS arteries and veins present prominent thickening of the adventitia (*20*), which together with VSMC loss may result in vessel stiffening and reduced vascular compliance, triggering plaque development. Accordingly, patients with HGPS exhibit an increase in both carotid-femoral pulse wave velocity and arterial wall echodensity, confirming that vascular stiffening is an essential contributor to cardiovascular decline in progeria (*23*). Aortic stiffness can then lead to augmented afterload and the subsequent left ventricular hypertrophy observed in some HGPS patients (*16, 17, 20, 22*).

The ability of blood vessels to stretch in response to changes in the pressure plays an important role in the regulation of blood pressure. Although some authors reported development of hypertension in HGPS subjects, it does not seem to be a generalized symptom of the disease. Merideth *et al.* described elevated systolic or diastolic blood pressures in 7/15 patients as compared with both age- and height-matched healthy controls (*17*). However, they reported only the highest reading even though blood pressure was measured an average of six times during the course of the study, which questions the validity of their results and conclusions. Further work by Gerhard-Herman *et al.* reported increased

systolic pressure in 7/26 patients and increased diastolic pressure in 9/26 patients as compared with age-matched controls (*23*). When they applied height-age standards to account for the growth impairment, systolic and diastolic blood pressures were higher in approximately half of the patients. Nonetheless, pulse pressure, which is defined as the difference between systolic and diastolic blood pressure and positively correlates with CVD risk during physiological aging (*24, 25*), was within the normal range for both chronologic age and height age (*23*). Of note, none of the studies analyzed hypotension incidence in HGPS, albeit raw data from some reports clearly show that some blood pressure measurements are below the normal range for the age-matched controls (*20*).

These somewhat contradictory observations on blood pressure may in fact indicate that progeria patients have blood pressure instability and variability, which has been recently shown to be a strong predictor of stroke (*26, 27*). This could be of special relevance for HGPS because arterial ischemic strokes are common during the disease progression and may lead to death in about 10% of patients (*18*). A retrospective study by Silvera *et al.* found evidence of stroke in 60% of patients, of which half was clinically silent (*28*). Likewise, vascular alterations in the brain, including intracranial and distal vertebral artery steno-occlusive disease with collateral vessel formation, are frequently found in HGPS (*28*). Remarkably, this arteriopathy is different from other vasculopathies of childhood and cerebrovascular disease during physiological aging (*28*). In spite of evident vascular alterations in the brain, progeric patients have normal cognitive function with the exception of stroke-related defects (*16, 29*).

While stroke accounts for some mortality in HGPS, the most common cause of death is myocardial infarction. As in the case of stroke, patients may have clinically silent myocardial infarcts during their lifetime (*16*). Indeed, autopsy findings provided evidence of remote (months), subacute (2-3 weeks), and acute (2-3-day-old) myocardial infarctions in the same patient (*20*). These acute and chronic infarcts may lead to arrhythmia and death. In a recent study, Rivera-Torres *et al.* showed age-related repolarization abnormalities in HGPS patients, manifested as ST segment depression/elevation and negative or biphasic T waves on the electrocardiogram (ECG), which can lead to an increased risk of arrhythmias (*30*). Another study also reported age-related ECG abnormalities in some patients, such as prolonged QT interval (*17*). Cardiac electrical defects in HGPS may be a consequence of heart fibrosis caused by non-fatal infarcts as well as valvular dysfunction. Likewise, various studies described severe degenerative aortic and mitral valvular disease in HGPS, characterized by thickening, fibrosis and calcification of the valve leaflets (*16, 17, 20, 31, 32*).

In summary, HGPS patients present severe cardiovascular defects in the vessels, heart, brain and valves, which resemble many aspects of physiological aging. Thus, progeria is a model of cardiovascular aging isolated from classical cardiovascular risk factors and may enhance our knowledge about the initiation and progression of vascular stiffening, atherosclerosis and the incidence of cardiovascular events.

I.2.3. Mechanism leading to progerin production

HGPS is caused by a heterozygous *de novo* point mutation within the *LMNA* gene (*33, 34*). In normal cells, alternative splicing of the *LMNA* gene gives rise to two major isoforms, lamin A and lamin C (*35*). Some minor forms are also produced, such as lamin AΔ10 and the germline-specific lamin C2 variant (*36, 37*). Lamin A and lamin C are expressed in the majority of differentiated somatic cells, and play important roles in maintaining nuclear structure and function (*38*).

Various posttranslational modifications of prelamin A (664 amino acid residue) give rise to mature lamin A (646 amino acid residue) (**Fig. 1**). First, the CaaX motif located at the C-terminus of prelamin A is farnesylated by farnesyl protein transferase (*39, 40*). Next, the last three residues (-aaX) are removed usually by the zinc metallopeptidase STE24 (ZMPSTE24), also known as farnesylated proteins-converting enzyme 1 (*40*). The newly exposed C-terminal cysteine is then carboxymethylated by isoprenylcysteine carboxylmethyltransferase (ICMT) (*40*). These modifications are believed to enhance hydrophobic interactions with the inner nuclear membrane and to facilitate assembly into the nuclear lamina (*41*). Finally, ZMPSTE24 cleaves the last 15 amino acids together with the farnesyl and carboxymethyl groups (after tyrosine in position 646), resulting in mature lamin A (*42-44*).

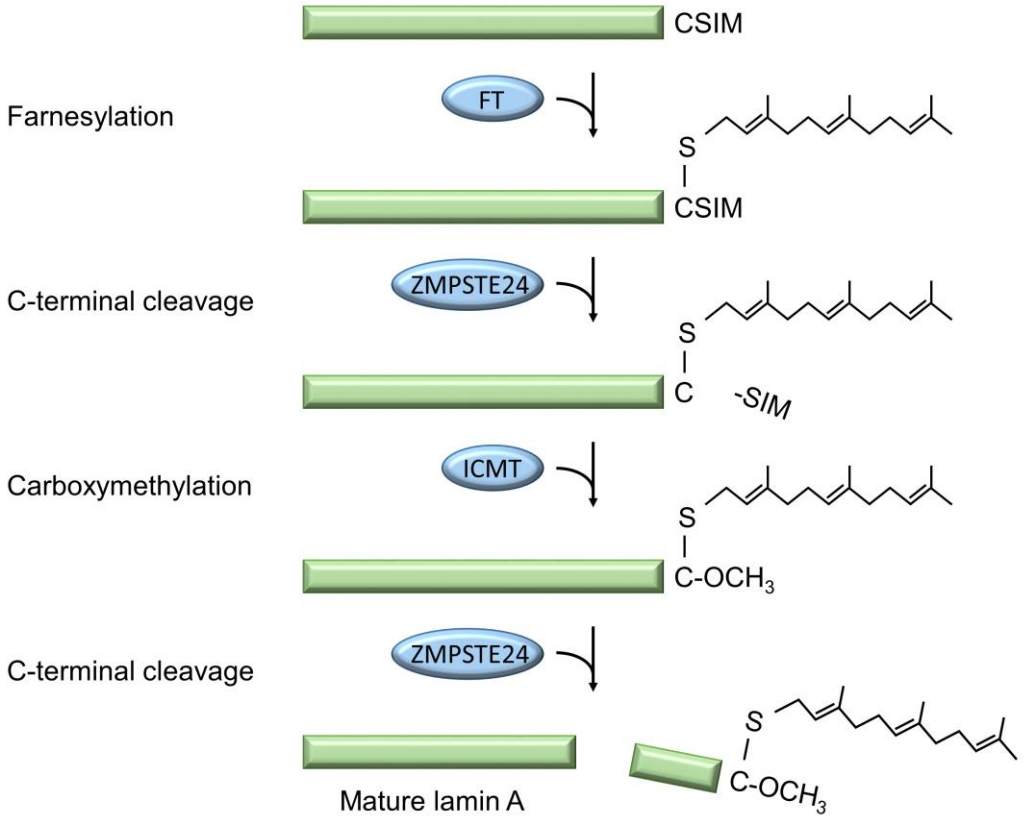

Figure 1. Lamin A maturation. Lamin A is formed from a precursor termed prelamin A. Prelamin A is first farnesylated by a farnesyltransferase (FT) on the cysteine residue within the CaaX motif (where "C" is cysteine, "a" is an aliphatic amino acid, and "X" is variable, in case of prelamin A: CSIM). Next, the C-terminal tripeptide (–SIM) is removed, usually by ZMPSTE24, a zinc metalloendoprotease. This is followed by carboxymethylation of the newly-exposed cysteine by isoprenylcysteine carboxylmethyltransferase (ICMT). Finally, the last 15 amino acids containing the farnesyl and carboxymethyl modifications are cleaved by ZMPSTE24, resulting in mature lamin A.

"Classical" HGPS is caused by a single nucleotide substitution in exon 11 (c.1824C>T; p.G608G) (*33, 34*). This cytosine-to-thymine substitution does not change the amino acid encoded (both GGC and GGT codons encode glycine), but activates a cryptic splice site leading to a deletion of 150 nucleotides in the mRNA. This aberrant splicing results in the production of a truncated form of lamin A, referred to as progerin, missing 50 amino acids close to the C-terminus. Progerin lacks the cleavage site for ZMPSTE24 and therefore retains the last 15 residues together with farnesyl and carboxymethyl groups. Permanently farnesylated and carboxymethylated progerin stays anchored in the inner nuclear membrane, leading to abnormalities in the nuclear shape and function (*45, 46*).

I.3. Progerin and prelamin A in physiological aging

Under normal conditions, prelamin A is almost undetectable in cells because it is rapidly processed into mature lamin A after translation. Farnesylated prelamin A accumulation due to inactivating mutations in the *ZMPSTE24* gene also leads to progeria-like syndromes, such as restrictive dermopathy (*47-49*) and mandibuloacral dysplasia (*50*). Remarkably, increased amounts of prelamin A have been also observed during physiological aging, presumably due to an age-dependent downregulation of ZMPSTE24 (*51*). Interestingly, inhibitors of proteases used for human immunodeficiency virus treatment result in increased levels of prelamin A and accelerated vascular aging (*52, 53*).

Many studies revealed that non-HGPS individuals accumulate small amounts of progerin with age (*20, 54, 55*). One possible explanation for this is because in healthy subjects the cryptic donor splice site shares 5 of 7 bases with the consensus splice sequence, leading to sporadic usage of the splice site. In HGPS, the cryptic donor splice site shares 6 of 7 nucleotides with the consensus splice sequence due to the C-to-T substitution, resulting in the frequent occurrence of aberrant splicing.

Thus, the accumulation of permanently farnesylated prelamin A and progerin in both normal and premature aging strongly suggests that some mechanisms are shared between these physiological and pathological processes. Accordingly, conclusions derived from the study of progeria may also shed some light on normal aging.

I.4. Mouse models of progeria

As of 1st April 2017, there were 148 identified children living with progeria worldwide (www.progeriaresearch.org). Of these, 115 carry the HGPS classical mutation, and the remaining 33 children have a mutation within the lamin A pathway but do not express progerin. This extremely low number of HGPS patients leads to challenges in conducting both clinical trials and research on the mechanisms driving the disease. Because of this, various mouse models of progeria have been created over the past 15 years that resemble many, but not all, premature aging features. This may be in part attributed to interspecies differences (e.g., in lipid metabolism) and distinct toxicity of progerin in mice and humans. Furthermore, the differences in the phenotype between different mouse models may be a consequence of diverse strategies used during their generation, which lead to variable progerin levels, as well as the absence or presence of other *Lmna* gene products, such as lamin A and lamin C.

The first progerin-expressing mouse model was developed by Yang *et al.* in 2005. The authors created a mutant allele called *Lmna*^{HG} ("Hutchinson-Gilford") that, unlike in the human disease, gives rise exclusively to progerin (*56, 57*). Heterozygous *Lmna*$^{HG/+}$ mice, which express progerin from the mutant allele and lamin A/C from the wild-type allele, showed reduced weight gain around 6-8 weeks of age and died by 4-6 months of age (compared with a lifespan of more than 2 years for wild-type mice). Homozygous *Lmna*$^{HG/HG}$ mice expressing solely progerin presented a more severe aging phenotype and died by 3-4 weeks of age. Both, *Lmna*$^{HG/+}$ and *Lmna*$^{HG/HG}$ mice displayed some of the symptoms common to HGPS, such as hair loss, osteoporosis, loss of subcutaneous fat, but no cardiovascular alterations were observed (*57*).

Varga *et al.* generated a transgenic mouse model by introducing a bacterial artificial chromosome (BAC) containing the human *LMNA* gene carrying an HGPS-causing mutation (c.1824C>T; p.G608G) (*58*). In addition to the mutated *LMNA* gene, the BAC also contained *RAB25* (coding for another isoprenylated protein), *UBQLN4* and *MAPBPIP* genes. In consequence, G608G BAC mice expressed mouse endogenous lamin A/C together with human progerin and 3 other human proteins. While these mice did not present any evident signs of premature aging, progressive VSMC depletion was observed in the media, beginning at 5 months of age. Reduced VSMC number was accompanied by an increased deposition of collagen and proteoglycan in the media, altered elastic fiber structure, and thickened adventitial and medial layers. Remarkably, the vascular pathology was similar to that observed in HGPS (*20-22*). In line with the aortic phenotype, vascular responsiveness to sodium nitroprusside administration was decreased in G608G BAC mice. Nevertheless, no evidence of atherosclerotic plaque formation was found (*58*).

Lmna^{HG} and G608G BAC mice fail to fully recapitulate the human disease, showing only premature aging or vascular alterations. Thus, Osorio *et al.* created a knock-in mouse model harboring a c.1827C>T (p.G609G) mutation within the mouse *Lmna* gene, which is equivalent to the human c.1824C>T (p.G608G) HGPS-causing single nucleotide substitution (*59*). Similar to what is observed in HGPS, the presence of the *Lmna*^{G609G} allele leads to the synthesis of progerin via aberrant splicing, together with lamin C and some residual lamin A. Homozygous *Lmna*$^{G609G/G609G}$ mice showed growth retardation after 3 weeks of age and died at an average age of 15 weeks. They also presented a loss of subcutaneous fat, attrition of hair follicles, and bone alterations. Notably, *Lmna*$^{G609G/G609G}$ mice presented VSMC depletion in the medial layer of the aortic arch, but not of the thoracic aorta. Despite the loss of VSMCs, no changes in the blood pressure were detected; however, animals developed age-dependent bradycardia. Moreover, prolonged QRS duration was observed on the ECG, indicating

alterations in cardiac conduction. Heterozygous *Lmna*$^{G609G/+}$ mice appeared normal until 8 months of age, when they started presenting an aging-phenotype similar to that of homozygotes, and died at an average age of 35 weeks. Remarkably, *Lmna*$^{G609G/+}$ mice developed severe calcification of the aortic media (*60*), a relevant symptom observed in HGPS. In summary, whereas *Lmna*$^{G609G/G609G}$ mice recapitulate most of the clinical features of progeria, atherosclerosis has not been reported.

Lee *et al.* have recently created a new *Lmna*$^{G609G/G609G}$ mouse model that, similar to the model developed by Osorio *et al.,* harbors an HGPS-causing mutation in the *Lmna* gene that yields progerin via abnormal splicing (*61*). Homozygous *Lmna*$^{G609G/G609G}$ mice display a phenotype similar to that of other formerly described progeria models (*43, 57, 59, 62*), including VSMC depletion in the media of the ascending aorta and adventitial fibrosis by 4 month of age. No detailed examination of the other phenotypical characteristics was provided by the authors (*61*).

Other important models of premature aging are *Zmpste24*-deficient mice, which were generated in parallel by two different groups (*43, 62*). These mice accumulate permanently-farnesylated prelamin A due to a loss of function of the metalloproteinase involved in lamin A maturation. The *Zmpste24*$^{-/-}$ mouse model created by Bergo *et al.* showed growth impairment, decreased subcutaneous fat content, alopecia, muscle weakness and bone abnormalities, and died at 6-7 months of age (*62*). *Zmpste24* null mice generated by Pendas *et al.* presented a slightly more severe phenotype, characterized by growth delay, lipodystrophy, alopecia, skeletal and muscular atrophy, cardiac abnormalities (heart interstitial fibrosis, thinning of the ventricular wall and dilatation of both ventricles), and death at an average age of 5 months (*43*). Consistent with the cardiac phenotype described by Pendas *et al*. (*43*), recent studies revealed electrical cardiac alterations in *Zmpste24*-deficient mice (*30*).

I.5. General mechanisms of HGPS

Lamin A plays important roles in a wide variety of cellular functions, ranging from maintaining the mechanical stability of the nucleus to regulating gene transcription and signal transduction (*38*). Accordingly, accumulation of progerin and prelamin A may trigger the disease through various non-mutually exclusive mechanisms. These mechanisms might differ across tissues due to the variable amount of lamin A (and progerin) produced, depending on tissue stiffness (*63, 64*).

Progerin elicits its detrimental effects in a dose-dependent manner. Different progerin-causing *LMNA* point mutations lead to a wide spectrum of disease severity, ranging from neonatal to late-onset

premature aging, which correlates with the expression level of progerin (*65, 66*). Thus, antisense oligonucleotide treatment, which reduced the amount of progerin, ameliorated the vascular or aging phenotype in two different *Lmna*$^{G609G/G609G}$ mouse models (*59, 61*).

The farnesyl group, which anchors progerin in the inner nuclear membrane, is believed to account for at least part of its toxic effect. This hypothesis was initially supported by findings on ZMPSTE24 deficiency in humans and mice, which results in the accumulation of farnesylated prelamin A and causes various HGPS-like phenotypes (*43, 47, 48, 62*). The progeroid phenotype is milder in patients that carry both a heterozygous *LMNA* mutation and a homozygous loss-of-function *ZMPSTE24* mutation, possibly due to a reduced amount of farnesylated prelamin A (*67*). Likewise, *Zmpste24*$^{-/-}$ mice with *Lmna* haplodeficiency do not present any evident aging phenotype (*68*). The importance of farnesylation in the pathogenesis of HGPS was corroborated by the generation of *Lmna*$^{csmHG/csmHG}$ and *Lmna*$^{nPLAO/nPLAO}$ mouse models expressing nonfarnesylated progerin and prelamin A, respectively, which did not exhibit a progeroid phenotype (*69, 70*). Furthermore, treatment with farnesyl transferase inhibitors (FTIs) reverted the nuclear defects in progerin-expressing cells (*56, 71*), and prolonged the lifespan of *Zmpste24*$^{-/-}$and *Lmna*$^{HG/+}$ mice (*57, 72*). FTIs also prevented CVD in progeroid G608G BAC transgenic mice (*73*).

It was subsequently demonstrated that prelamin A and progerin can undergo alternative prenylation by geranylgeranyltransferase upon farnesyltransferase inhibition (*74*). Thus, inhibition of both farnesylation and geranylgeranylation with a combination of statins and aminobisphosphonates was found to ameliorate the progeriod phenotype and extend survival in *Zmpste24*$^{-/-}$ mice (*74*). Based on all the above findings, a clinical trial with HGPS patients was conducted targeting farnesylation with an FTI (lonafarnib) alone or in combination with a statin (pravastatin) and a bisphosphonate (zoledronate) (*75-77*). Monotherapy with lonafarnib improved vascular stiffness, bone structure, and audiological status in some patients, and was estimated to extend survival by 1.6 years (*75, 76*). Triple-drug therapy with lonafarnib, pravastatin and zoledronate had an additional beneficial effect on bone mineral density, but no cardiovascular improvement was detected when compared with lonafarnib monotherapy (*77*).

Prenylation (farnesylation and geranylgeranylation) is not the only detrimental effect of progerin, since the aforementioned combination treatment provided some therapeutic benefits but not a cure for HGPS. Supported by the observation that unfarnesylated progerin forms aggregates at the nuclear membrane, akin to the farnesylated form, Kalinowski *et al.* recently suggested that increased

electrostatic interactions and aggregation are also responsible for progerin association with the nuclear inner membrane (*78*). In addition, Qin *et al.* showed that progerin has a less heterogeneous and a more compact tail compared with normal lamin A, and this may affect its interaction with DNA and other proteins (*79*). Accumulating evidence shows that progerin may also elicit toxic effects through altered protein structure due to the deletion of 50 amino acids at the C terminus. Abnormal interactions of progerin with other nuclear components result in changes in nuclear shape (so-called nuclear blebbing), increased thickness and stiffness of the lamina, heterochromatin mislocalization, and alterations in nuclear pore complexes (*80, 81*). Lee *et al.* showed that progerin exhibits strong binding affinity for lamin A/C and this interaction induced nuclear abnormalities (*82*). Importantly, pharmacological therapy to disrupt the progerin-lamin A/C binding reduced nuclear aberrations and prevented cell senescence *in vitro*, and also ameliorated progeroid features and extended lifespan in $Lmna^{G609G/G609G}$ mice (*82*).

A recent study by Ibrahim *et al.* revealed that methylation of progerin by ICMT might also play a role in premature aging syndromes (*83*). They showed that hypomorphic $Zmpste24^{-/-}Icmt^{hm/hm}$ mice with 70-90% lower expression and activity of ICMT present improvement in body weight, grip strength and bone structure, and exhibit extended survival when compared with $Zmpste24^{-/-}Icmt^{+/+}$ littermates. This diminished activity of ICMT leads to mislocalization of prelamin A in the nucleus and activates AKT-mammalian target of rapamycin (mTOR) signaling, which in turn delays cell senescence. However, these findings are not completely in accord with the results of Cao *et al.* and Graziotto *et al.*, who showed that treatment with the mTOR inhibitor rapamycin activates autophagic clearance of progerin and reduces nuclear abnormalities (*84, 85*). These results clearly show that ICMT and mTOR are implicated in premature aging, but the precise mechanism and relationship between them awaits further investigation.

I.6. Mechanisms underlying CVD in progeria

I.6.1. VSMC loss

Progressive VSMC loss was reported both in HGPS patients (*20-22*) and in various progeria mouse models (*58, 59, 61*), indicating its importance in the pathogenesis of the premature vascular disease. Depletion of VSMCs in the media has also been described in physiological aging (*86*), although not as severe as is seen in HGPS.

VSMCs in the blood vessels are subjected to high mechanical stress related to the blood flow. In normal conditions, cells respond to increased shear stress by increasing the expression of A-type lamins and changing their distribution within the nucleus (*63, 87, 88*). This response to physical stress is perturbed in progerin-expressing cells (*81, 89*) and may lead to cell damage and death. This premise is supported by the work of Verstraeten *et al.,* showing reduced viability and increased apoptosis of HGPS fibroblasts under repetitive mechanical strain (*90*). One possible explanation for the progerin-induced increase in mechanosensitivity relates to changes in the expression of proteins controlling cytoskeleton organization, mechanotransduction and extracellular matrix production (*91, 92*). Song *et al.* showed that the ascending aorta of G608G BAC transgenic mice exhibits reduced expression of vimentin (*91*), a cytoskeletal protein attached to the nucleus, endoplasmic reticulum, and mitochondria that is important for maintaining cellular integrity (*93*). This correlation between downregulation of mechanotransduction proteins and high shear stress in progerin-expressing VSMCs might partially explain their loss in HGPS.

To elucidate how progerin leads to VSMC death, various groups established an *in vitro* model of human smooth muscle cells (SMCs) differentiated from HGPS induced pluripotent stem cells (iPSCs). Liu *et al.* showed that iPSC-derived progerin-expressing SMCs exhibit premature senescence associated with vascular aging, and they identified DNA-dependent protein kinase catalytic subunit (DNA-PKcs) as a binding partner of progerin (*94*). DNA-PKcs, which is a catalytic subunit of a nuclear DNA-PK, participates in the non-homologous end joining (NHEJ) pathway of DNA repair. Recently, Kinoshita *et al.* analyzed the interactome of lamin A mutant forms and they found that progerin, unlike wild-type lamin A, cannot bind to proteins related to DNA damage response, including DNA-PK holoenzyme (*95*). They also reported that progerin expression in VSMCs, but not in endothelial cells (ECs), induces DNA-PK activation and growth arrest, leading to cell senescence. Given that the results of Liu *et al.* and Kintoshita *et al.* are somewhat contradictory, the interaction between progerin and DNA-PK and its subunits should be further defined.

Zhang *et al.* found that HGPS iPSC-derived SMCs exhibit severe proliferative defects triggered by a caspase-independent mechanism (*96*). They also reported that progerin expression in SMCs is associated with inhibition of poly(ADP-ribose) polymerase 1, an important regulator of DNA repair, and induces the activation of the error-prone NHEJ response. The subsequent prolonged mitosis results in mitotic catastrophe, leading to SMC death. Similar to progerin, prelamin A induces DNA damage and increases DNA damage response in aged VSMCs (*97, 98*). This response might be the consequence of impaired recruitment of 53 binding protein-1 (53BP1) to the sites of DNA damage due to a defective

import of 53BP1 to the nucleus, related to mislocalization of nucleoporin 153 (*99*). Defective DNA damage repair has been also described in non-vascular HGPS cells and in progeria mouse models (*100-102*). All of the above findings confirm the contribution of DNA damage response to progerin-driven VSMC death. Interestingly, DNA damage plays an important role in normal aging (*103*).

I.6.2. Vascular calcification

HGPS patients exhibit excessive aortic and valvular calcification (*20, 31, 32, 104*), which is also a hallmark of physiological aging (*105*). Likewise, vascular calcification is observed in progeroid transgenic G608G BAC and knock-in *Lmna*$^{G609G/+}$ mice (*58, 60*). Villa-Bellosta *et al.* (*60*) found abnormally high expression of the osteogenic markers bone morphogenetic protein 2 (*Bmp2*) and Run-related transcription factor-2 (*Runx2*) in calcified aortas from *Lmna*$^{G609G/+}$ mice, without alterations in the anti-calcification agents matrix Gla-protein and fetuin A. Moreover, *Lmna*$^{G609G/+}$-derived primary VSMCs showed a reduced capacity to inhibit calcium deposition *in vitro*, which was associated with a decreased amount of extracellular inorganic pyrophosphate (ePPi), the major endogenous inhibitor of vascular calcification. The diminished level of ePPi was related to an impairment in ePPi synthesis due to decreased ATP production (the main substrate for ePPi synthesis) and an upregulation of tissue-nonspecific alkaline phosphatase (the main enzyme involved in PPi hydrolysis) and ectonucleoside triphosphatase diphosphohydrolase 1 (the enzyme that hydrolyzes ATP to release Pi). Accordingly, plasma concentrations of ePPi and ATP were found to be lower in *Lmna*$^{G609G/+}$ mice than in *Lmna*$^{+/+}$ littermates. Moreover, injection of exogenous PPi prevented vascular calcification in *Lmna*$^{G609G/G609G}$ mice.

The diminished capacity of progerin-expressing VSMCs to prevent calcification might be related to a switch from a contractile to an osteochondrocytic phenotype. This notion is supported by the work of Liu *et al.*, who showed that prelamin A accumulation in VSMCs interferes with DNA damage repair leading to osteogenic differentiation (*98*). These findings are of special interest because, similar to progerin, prelamin A accumulates with age in medial VSMCs and atherosclerotic lesions, and has been proposed as a novel biomarker of VSMC aging (*97*). Prelamin A activates DNA damage-related ataxia telangiectasia mutated /ataxia telangiectasia and Rad3-related signaling, and induces senescence-associated secretory phenotype in VSMCs (*98*). Prelamin A-expressing senescent VSMCs release pro-calcification factors, such as BMP2, which may trigger calcification both locally and at remote sites.

A recent study also demonstrated that VSMCs cultured in calcifying medium show higher expression of lamin A and prelamin A, accompanied by upregulated gene expression of relevant regulators of calcification, such as *Runx2*, osteocalcin and osteopontin, and increased calcium deposition (*106*). Remarkably, human mesenchymal stems cells expressing progerin also show elevated levels of osteopontin and exhibit enhanced osteogenic differentiation (*107*). In summary, lamin A and its mutant or unprocessed forms participate in osteoblastic differentiation and vascular calcification, indicating a further need to examine the role of progerin and prelamin A in premature and physiological aging.

I.6.3. Endothelial dysfunction

EC dysfunction is an essential event in atherosclerosis development, which is the life-threatening component of HGPS. It has been well established that aortic regions subjected to turbulent blood flow and high shear stress, such as the ascending aorta, are more susceptible to atheroma plaque formation (*108, 109*). ECs can sense and respond to different types of blood flow. Song *et al.* observed that ECs in the ascending aorta of G608G BAC mice form an intact monolayer in the zones with an almost complete loss of VSMCs (*91*). Moreover, these ECs showed a greater than 8-fold increase in vimentin levels compared with ECs in zones with preserved VSMCs. An elevated level of vimentin in progerin-expressing ECs might augment their resistance to increased shear stress, thus explaining the presence of well-preserved endothelium in HGPS vessels (*20*).

A recent study showed that accumulation of prelamin A in ECs, through blocking lamin A maturation, induces cell senescence and promotes intercellular adhesion molecule 1-dependent monocyte adhesion to ECs (*110*). Since monocyte adhesion to ECs and extravasation is an important step in the initiation of the atheroma plaque formation, further studies are needed to unravel the relationship between progerin and prelamin A expression in ECs and atheroma build-up.

I.6.4. Cardiac electrical alterations

Previous studies in HGPS patients revealed repolarization abnormalities, such as ST segment depression/elevation and negative and biphasic T waves, which were especially evident at advanced stages of the disease (*17, 30*). Progeriod *Zmpste24*$^{-/-}$ mice show similar alterations manifesting as T-wave flattening (*30*). Although progerin-expressing *Lmna*$^{G609G/G609G}$ and prelamin A-expressing

Zmpste24$^{-/-}$ mice develop severe bradycardia as they age, HGPS patients present cardiac rhythm that remains within the normal range; yet, the heart rate seemed to be slower in older patients (*30, 59*). Moreover, 18-20-week-old *Zmpste24*$^{-/-}$ animals showed prolonged PQ interval and QRS complex, indicating defective cardiac conduction (*30*). These alterations were accompanied by mislocalization of the gap junction protein connexin 43, which was also evident in heart tissue from HGPS patients (*30*). Intercellular connectivity defects might therefore underlie cardiac electrical defects in progeria. Taken together, these findings suggest that cardiac alterations in HGPS patients and progeroid mice are a characteristic of progeria that could increase the risk of arrhythmias and lead to premature death.

I.7. Endoplasmic reticulum (ER) stress and the unfolded protein response (UPR)

Aging has been linked to the capacity of an organism to cope with stress stimuli (*111, 112*). Organisms have a wide variety of stress response mechanisms that can act at the cellular or organelle-specific level to restore homeostasis, including heat shock response, autophagy, mitochondrial and ER stress responses, remodeled proteasome, and the DNA damage response (*112*). These stress responses involve recognition of the damage, transmission of the stress signal to the nucleus, production of stress-related proteins and their translocation to the site of damage. Impaired responses to stress are believed to contribute to age-related tissue damage, but compromised stress response can also accelerate aging.

Alterations in the ER stress response have been linked to some age-associated diseases such as diabetes, heart disease and neurodegenerative disorders (*113-115*). In response to certain stress stimuli, such as free cholesterol, oxidized lipids, high glucose, mitochondrial dysfunction and calcium imbalance, unfolded proteins accumulate within the ER, leading to ER stress (*116, 117*). In an attempt to reestablish homeostasis, ER stress triggers several adaptive mechanisms, which together are known as the UPR (*116, 118*). UPR activation leads to diminished misfolded or unfolded protein load by reducing the influx of proteins into the ER, synthesizing proteins responsible for folding and quality control in the ER, and increasing the ER membrane size (*119-122*). However, under persistent stress conditions, UPR fails to restore homeostasis and triggers programmed cell death (*123*).

Three classes of ER stress sensors are known to mediate UPR activation: inositol-requiring enzyme 1 (IRE1), protein kinase RNA-like ER kinase (PERK), and activating transcription factor 6 (ATF6) (*118*) (**Fig. 2**). These transmembrane receptors are maintained in an inactive form through binding to the ER chaperone 78 kDa glucose-regulated protein (GRP78), also known as

immunoglobulin heavy chain-binding protein. In the presence of high levels of misfolded or unfolded proteins, GRP78 dissociates from IRE-1, PERK and ATF6, enabling their activation (*124*).

During the early stages of the UPR, protein synthesis is inhibited by blocking translation in a process mediated by the PERK-dependent phosphorylation of eukaryotic translation initiator factor 2α (eIF2α) (*125*). Moreover, regulated IRE1-dependent decay leads to degradation of specific mRNAs that code for ER-located proteins (*126-128*). ER stress also stimulates autophagy though the IRE1-JUN N-terminal kinase pathway, in order to eliminate damaged ER and aberrant protein aggregates (*129*). Generally, these first-line responses aim to reduce protein influx into the ER and facilitate adaptive and repair mechanisms that restore homeostasis.

During the middle stages of the UPR, the transcription factors ATF6 fragment (ATF6f), spliced X box-binding protein 1 (XBP1s) and ATF4 are activated to restore ER function and promote survival. Under ER stress, ATF6 dissociates from GRP78 and translocates to the Golgi apparatus, where it is cleaved (*130, 131*). The resulting cytosolic fragment ATF6f enters the nucleus and stimulates transcription of the ER-associated protein degradation (ERAD) constituents and XBP1 (*132, 133*).

Dimerization and autotransphosphorylation of IRE1 upon ER stress results in the activation of its cytosolic RNase domain (*134*). Active IRE1 excises 26 nucleotides from the mRNA coding for XBP1, leading to a shift in the reading frame and the production of an active and stable transcription factor called XBP1s (s for “spliced”) (*133, 135, 136*). Subsequently, XBP1s enters the nucleus and activates the transcription of genes that encode proteins involved in ERAD and protein folding (*137, 138*). XBP1s also regulates phospholipid synthesis, leading to the ER membrane expansion upon ER stress (*139*). By contrast, XBP1, which is the protein product of unspliced XBP1 mRNA, is unstable and inhibits UPR target gene transcription (*135*).

Although PERK activation leads to the attenuation of translation, it upregulates the expression of some proteins, including ATF4 and GRP78 (*140, 141*). ATF4 regulates genes responsible for amino acid metabolism, redox balance, protein folding and autophagy (*122, 142*). Moreover, it also promotes eIF2α dephosphorylation and translation recovery by increasing the expression of growth arrest and DNA damage-inducible gene 34 (*143*).

Although UPR is a pro-survival mechanism, it can lead to cell death in situations of acute or chronic ER stress. The central factor orchestrating the ER stress-related apoptosis is DNA damage-inducible transcript 3 protein (DDIT3), also called growth arrest and DNA damage-inducible protein or CCAAT/enhancer-binding protein homologous protein (*144*). Under normal conditions, the amount

of DDIT3 in the cell is low; however, the protein level of DDIT3 increases via IRE1-, PERK- and ATF6- pathways upon ER stress activation (although ATF4 plays the main role in the activation of *DDIT3* gene expression). In turn, DDIT3 upregulates tumor necrosis factor-related apoptosis-inducing ligand (TRAIL) receptors, leading to activation of the extrinsic apoptotic pathway (*145*). In addition to DDIT3, other factors mediating ER stress-related apoptosis have been proposed, including IRE1 and caspase 12 (*122*).

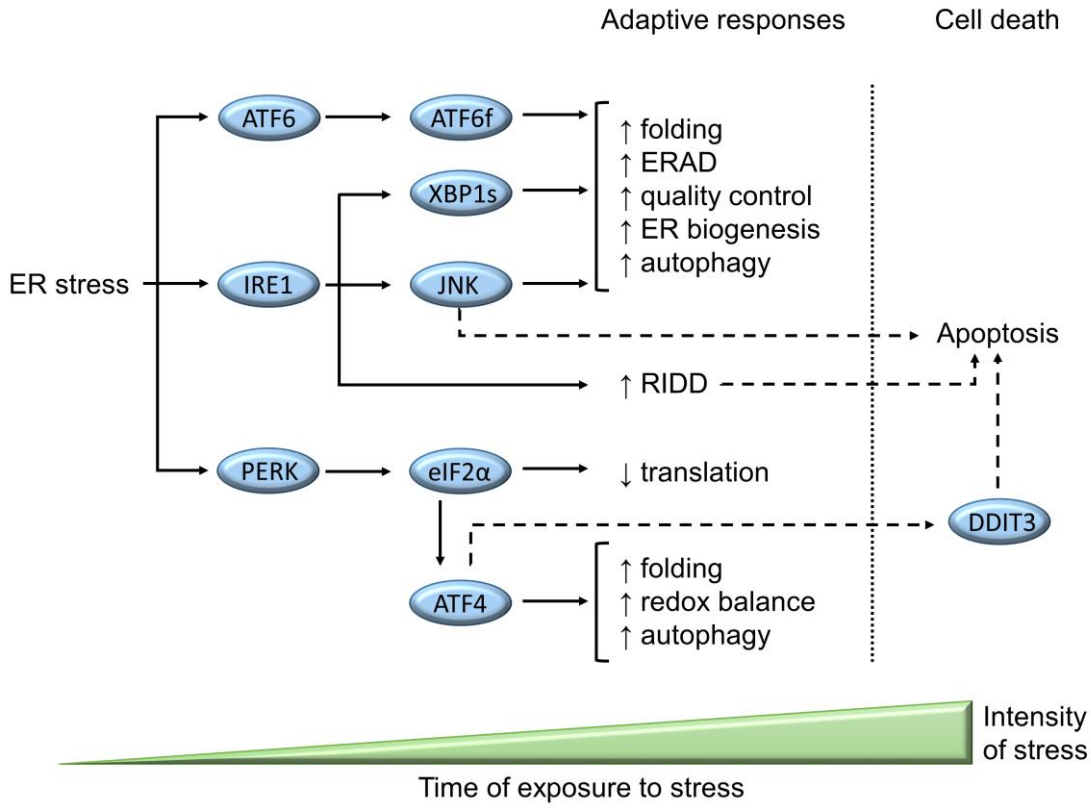

Figure 2. A simplified scheme of endoplasmic reticulum (ER) stress and the unfolded protein response (UPR) activation. Three UPR-related molecules are activated upon ER stress: activating transcription factor 6 (ATF6), inositol-requiring enzyme 1 (IRE1), and protein kinase RNA-like ER kinase (PERK). At the early stages of the UPR, protein translation is diminished through PERK-mediated phosphorylation of eukaryotic translation initiator factor 2α (eIF2α). Moreover, initiation of regulated IRE1- dependent decay (RIDD) leads to decay of some mRNAs. In parallel, autophagy is activated via the IRE1α–JUN N-terminal kinase (JNK) pathway. At the middle stages of the UPR, three transcription factors (activating transcription factor 6 cytosolic fragment (ATF6f), spliced X box-binding protein 1 (XBP1s) and ATF4) promote various adaptive responses in order to reestablish ER function and promote cell survival. However, unresolved ER stress triggers apoptosis via different pathways, with DNA damage-inducible transcript 3 protein (DDIT3; also known as C/EBP-homologous protein) being the key transcription factor regulating this process. Dashed lines indicate events promoting apoptosis. ERAD: ER-associated protein degradation.

II. OBJECTIVES

Since the discovery in 2003 of the HGPS-causing mutation in the *LMNA* gene, much progress has been made in unraveling the mechanisms underlying progerin-induced premature aging and death. However, few studies have investigated the molecular alterations triggered by progerin accumulation in VSMCs, major players in atherosclerosis development (*60, 94-96, 146*). Moreover, the mechanisms through which progerin accelerates atherosclerosis remain largely undefined, in part due to the lack of adequate mouse models.

Ongoing HGPS clinical trials are testing FTIs, either as monotherapy or in combination with bisphosphonates and statins (*75-77*). These strategies are clearly not curative since most HGPS symptoms persist in treated patients, including CVD and premature death. Further research is therefore needed to identify new disease mechanisms and to develop more efficient therapies to inhibit atherosclerosis development, the main cause of death in HGPS patients.

The main objectives of this thesis were the following:

1. To generate the first progeroid mouse model exhibiting progerin-induced acceleration of atherosclerosis that phenocopies the main vascular alterations observed in HGPS patients.
2. To assess the relative contribution of macrophages and VSMCs to progerin-driven atherosclerosis.
3. To identify the molecular mechanisms underlying progerin-induced atherosclerosis.
4. To test new treatments to prevent cardiovascular events and extend lifespan of progeric mice that could be used in HGPS patients.

III. MATERIALS AND METHODS

III.1. Mice

All experimental and other scientific procedures with animals conformed to EU Directive 2010/63EU and Recommendation 2007/526/EC, enforced in Spanish law under Real Decreto 53/2013. Animal protocols were approved by the local ethics committees and the Animal Protection Area of the Comunidad Autónoma de Madrid (PROEX76/14, PROEX78/14, PROEX167/16).

All mice used in this study were male on the C57BL/6J genetic background. Apolipoprotein E-deficient (*Apoe*$^{-/-}$, The Jackson Laboratory, stock no: 002052), *Lmna*$^{G609G/+}$ (*59*), *Lmna*$^{LCS/+}$ (*59*), *SM22αCre* (*Tagln*-Cre, The Jackson Laboratory, stock no: 017491), and *LysMCre* (*147*) mice were purchased or kindly provided by collaborators. These lines were used to generate atherosclerosis-susceptible mouse models with ubiquitous progerin expression (*Apoe*$^{-/-}$*Lmna*$^{G609G/G609G}$), VSMC-specific progerin expression (*Apoe*$^{-/-}$*Lmna*$^{LCS/LCS}$*SM22αCre*), macrophage (myeloid)-specific progerin expression (*Apoe*$^{-/-}$*Lmna*$^{LCS/LCS}$*LysMCre*), and their corresponding controls expressing normal lamin A/C (*Apoe*$^{-/-}$*Lmna*$^{+/+}$) or lamin C only (*Apoe*$^{-/-}$*Lmna*$^{LCS/LCS}$). Moreover, to compare the atherosclerosis-prone (*Apoe*$^{-/-}$) and atherosclerosis-resistant (*Apoe*$^{+/+}$) backgrounds, we bred *Lmna*$^{LCS/LCS}$*SM22αCre*, *Lmna*$^{LCS/LCS}$, *Lmna*$^{G609G/G609G}$ and *Lmna*$^{+/+}$ mice. With the exception of longevity studies, animals on the *Apoe*$^{-/-}$ background were sacrificed at 8, 16, 21-23, 27 or 51 weeks of age (indicated in the figure legends). *Lmna*$^{LCS/LCS}$*SM22αCre* and *Lmna*$^{LCS/LCS}$ mice were sacrificed at 38 week of age.

III.2. Longevity study

Beginning at 4 weeks of age, animals were weighed and inspected for health and survival at least once per week (checks were more frequent for *Apoe*$^{-/-}$*Lmna*$^{G609G/G609G}$ mice). Diseased animals were examined by a specialized veterinarian blinded to genotype. Animals that met humane endpoint criteria were euthanized and the deaths recorded. Animals sacrificed due to hydrocephalus, malocclusion, inter-male aggression or other reasons unconnected to phenotype, were excluded from the analysis (normally at a very early stage of the study).

III.3. High-fat diet (HFD) experiments

For diet-induced atherosclerosis studies, animals were maintained for 8 weeks on a HFD (10.7% total fat, 0.75% cholesterol, S9167-E010, Ssniff), beginning at 8 weeks of age. Mice were sacrificed at 16 weeks of age after an overnight fast.

III.4. Hematology and serum biochemical analysis

Animals were fasted overnight for all blood analyses, which were performed by specialized staff from the CNIC Animal Unit. For hematology, blood samples were collected in Microvette 100 EDTA tubes (Sarstedt) and analyzed using a PENTRA 80 hematology analyzer (Horiba). For biochemical analysis, blood samples were collected in plastic tubes, incubated at room temperature (RT) for 2-3 hours to allow clotting, and centrifuged at 2000 × *g* for 5 minutes. Serum was stored at -80°C until samples from all experiments were collected. Because of volume limitations, serum samples were pooled from approximately 2-3 animals of the same experimental group. Specimens with overt hemolysis were excluded from testing. Biochemical variables were analyzed using a Dimension RxL Max Integrated Chemistry System (Siemens Healthineers).

III.5. Blood pressure measurement

Blood pressure and heart rate measurements were performed in conscious mice using the BP2000 noninvasive automated tail-cuff system (Visitech Systems). All experiments were performed in the morning to avoid variability related to circadian oscillations in the blood pressure (*148, 149*). Animals were trained during five consecutive days (first week) and then experimental data was collected during 5 consecutive days (second week). For each mouse, at least 10 measurements of blood pressure and heart rate were registered each day. Final measurements were preceded by 10 preliminary measurements to allow the animals to settle. Values that were equal to 0 (which arose from equipment error or animal movements) were excluded from the analysis. For each day, the median was calculated for the heart rate, systolic and diastolic blood pressure. The mean from 5 days was used for further analysis.

III.6. ECG

Mice were anesthetized with 1.5-2% isoflurane and four ECG electrodes were inserted subcutaneously into the limbs. ECG was recorded in the morning (to account for circadian variations) using the MP36R system (Biopac Systems). ECG data were analyzed using AcqKnowledge software by specialized staff blinded to the genotype.

III.7. Treatment

Tauroursodeoxycholic acid (TUDCA, 580549, Calbiochem) was dissolved in phosphate-buffered saline (PBS) and passed through a 0.22 µm filter. After genotyping, mice were randomized into treatment and control groups (an equal or similar number of animals from each litter was assigned to each group). TUDCA (400 mg/kg) or PBS was administered intraperitoneally 3 times a week, beginning at 6 weeks of age in the case of *Apoe*$^{-/-}$*Lmna*$^{G609G/G609G}$ mice and at 8 weeks of age in the case of *Apoe*$^{-/-}$*Lmna*$^{LCS/LCS}$*SM22αCre* mice. Atherosclerosis experiments included PBS- or TUDCA-treated *Apoe*$^{-/-}$*Lmna*$^{+/+}$ and *Apoe*$^{-/-}$*Lmna*$^{LCS/LCS}$ control mice.

III.8. Quantification of atherosclerosis burden

Mouse aortas were fixed with 4% formaldehyde/PBS, cleaned of fatty tissue, and stained with 0.2% Oil Red O (ORO, O0625, Sigma). The thoracic aorta or/and aortic arch was then incised longitudinally and pinned out flat, intimal side up, for computer-assisted planimetric analysis. Images were taken with a digital camera (OLYMPUS UC30) mounted on a stereo microscope (OLYMPUS SZX3). The percentage of lesion area (ORO-stained) was quantified using SigmaScan Pro 5 software (Systat Software Inc.) by an observer blinded to genotype.

III.9. Histology and immunofluorescence

For all mice on the *Apoe*$^{-/-}$ background, formaldehyde-fixed aortic arches were cleaned of fatty tissue, incubated in 30% sucrose in PBS overnight at 4°C, and embedded in Tissue-Tek® OCT compound (SAKURA, Netherlands) for cryostat sectioning. Serial 8-µm sections were stained with ORO, hematoxylin-eosin (H&E), and Masson's trichrome. For immunofluorescence, sections were blocked and permeabilized for 1 hour at RT in PBS containing 0.3% Triton X-100 (9002-93-1, Sigma), 5% bovine serum albumin (BSA, A7906, Sigma), and 5% normal goat serum (005-000-001, Jackson ImmunoResearch). Next, sections were incubated overnight at 4°C with the following antibodies: anti-smooth muscle α-actin (Sma-Cy3, C6198, Sigma, 1:200), anti-CD68 (MCA1957, Serotec, 1:200), and anti-progerin/lamin A (sc-20680, Santa Cruz, 1:100) diluted in PBS containing 0.3% Triton X-100 and 2.5% normal goat serum. Samples were incubated with corresponding secondary antibodies (Alexa Fluor, Invitrogen) and the nucleic acid stain Hoechst 33342 (B2261, Sigma) for 2 hours at RT, and mounted using Fluoromount G imaging medium (4958-02, Affymetrix eBioscience).

Aortic arches of *Lmna*$^{LCS/LCS}$*SM22αCre* and *Lmna*$^{LCS/LCS}$ mice were fixed in 4% formaldehyde in PBS, cleaned of fatty tissue, dehydrated to xylene and embedded in paraffin. Thoracic aortas used for atherosclerosis burden quantification (from TUDCA-treatment experiments) were also embedded in paraffin. Serial 4-µm sections were deparaffinized, rehydrated, and stained with H&E, and Masson's trichrome. For immunofluorescence, antigen retrieval was performed using 10 mM sodium citrate buffer (pH 6). Then, samples were blocked with PBS containing 5% BSA and 5% normal goat serum for 1 hour at RT. Sections were incubated for 2 hours at RT with an anti-smooth muscle α-actin antibody (Sma-Cy3, C6198, Sigma, 1:200) and Hoechst 33342 stain diluted in PBS with 2.5% normal goat serum, and mounted using Fluoromount G imaging medium.

Mouse hearts were fixed in 4% formaldehyde in PBS, divided into two parts (apex and upper part containing aortic root with aortic valve), dehydrated to xylene and embedded in paraffin. Heart (apex) sections from 6 different levels were prepared. The aortic root was sectioned throughout the aortic valve. Serial 4-µm sections were deparaffinized, rehydrated, and stained with H&E, and Masson's trichrome.

ORO-, H&E- and Masson's trichrome-stained sections were scanned with a NanoZoomer-RS scanner (Hamamatsu), and images were exported using NDP.view2. Immunofluorescence images were acquired with the Zeiss LSM 700 confocal microscope. Images were analyzed using NDP.view2 and ImageJ Fiji software by an observer blinded to genotype. Aortic media and adventitia thickness, collagen and lipid medial content, and VSMC content were analyzed in approximately 3 sections (for aortic arch) and/or 4 (for thoracic aorta) per animal, and the mean was used for the statistical analysis. Atherosclerotic plaque area, plaque collagen and VSMC content were quantified in 3 different zones of the aortic valve (beginning, middle, and end) per animal, and the mean was used for the statistical analysis.

III.10. Sample collection and preparation for RNAseq

Eight-week-old mice (*Apoe*$^{-/-}$*Lmna*$^{G609G/G609G}$, *Apoe*$^{-/-}$*Lmna*$^{+/+}$, *Apoe*$^{-/-}$*Lmna*$^{LCS/LCS}$*SM22αCre* and *Apoe*$^{-/-}$*Lmna*$^{LCS/LCS}$) were sacrificed by CO_2 inhalation, and thoracic aortas were extracted, cleaned of fatty tissue and digested with 2 mg/ml collagenase (CLS-2, Worthington) for 10 minutes at 37°C to separate medial and adventitial tissue. Medial aortas from 3-4 mice of the same genotype were pooled and snap frozen. Samples were disrupted using TissueLyser (Qiagen), and total RNA was isolated with

QIAzol (Qiagen). RNA integrity was confirmed by RNA electrophoresis and with an Agilent 2100 Bioanalyzer.

III.11. RNAseq library preparation, sequencing, and generation of FastQ files

Total RNA (500 ng) was used to generate barcoded RNAseq libraries using the TruSeq RNA Sample Preparation Kit v2 (Illumina). Briefly, poly A+ RNA was purified using poly-T oligo-attached magnetic beads through two rounds of purification, followed by fragmentation and first and second cDNA strand synthesis. Next, cDNA 3' ends were adenylated and the adapters were ligated, followed by PCR library amplification. Finally, library size was checked using the Agilent 2100 Bioanalyzer DNA 1000 chip and concentration was determined in a Qubit® fluorometer (Life Technologies). Libraries were sequenced on a HiSeq2500 sequencer (Illumina) to generate 60-base single reads. FastQ files for each sample were obtained using CASAVA v1.8 (Illumina). NGS experiments were performed in the CNIC Genomics Unit. RNAseq data were deposited in the NCBI SRA, accession number: SRP099105.

III.12. Differential expression analysis

Sequencing reads were pre-processed by means of a pipeline that used FastQC (*150*) to assess read quality, and Cutadapt (*151*) to trim sequencing reads and eliminate Illumina adaptor sequences, and to discard reads that were shorter than 30 base pairs. The number of reads obtained per sample was in the range of 8 to 14 million. The resulting reads were mapped against the mouse transcriptome (GRCm38, release 76; aug2014 archive) and quantified using RSEM v1.17 (*152*). The percentage of aligned reads was in the range of 79 to 82%. Data were then processed with a differential expression analysis pipeline that used the Bioconductor package EdgeR (*153*) for normalization and differential expression testing. Only genes with at least 1 count per million in at least 4 samples (13,664 genes) were considered for statistical analysis. Three comparisons were made to identify differentially expressed genes in our models: 1) *Apoe*$^{-/-}$*Lmna*$^{G609G/G609G}$ vs *Apoe*$^{-/-}$*Lmna*$^{+/+}$; 2) *Apoe*$^{-/-}$*Lmna*$^{LCS/LCS}$*SM22αCre* vs *Apoe*$^{-/-}$*Lmna*$^{LCS/LCS}$; and 3) *Apoe*$^{-/-}$*Lmna*$^{LCS/LCS}$ vs *Apoe*$^{-/-}$*Lmna*$^{+/+}$. The lists of genes detected as differentially expressed in the 3 comparisons were subjected to a series of bioinformatic analyses. The list of 240 genes shared between comparisons 1 and 2 was extracted and the logFC values (base-2 logarithm of fold change) for those genes were plotted against each other

using Microsoft Excel to check for correlation. Differential expression analysis was performed in the CNIC Bioinformatics Unit. Area-proportional Venn diagrams were generated using BioVenn (*154*) to visualize the overlap between data sets.

III.13. Pathway analysis

Ingenuity Pathway Analysis (IPA, Qiagen) was used for more comprehensive RNAseq data analysis. Briefly, core analyses were performed for the 3 comparisons to visualize pathways altered by progerin expression as well as by the lack of lamin A. Benjamini-Hochberg correction of the *P* value was applied to extract the most significant pathways and stacked bar charts were exported. A comparison analysis was performed to compare results obtained with ubiquitous and VSMC-specific progeroid models. Heatmaps showing canonical pathways and upstream regulators were exported. For more detailed information about IPA tools (Global Canonical Pathways, Upstream regulators and Comparative analysis), see www.ingenuity.com.

III.14. RNA extraction and cDNA preparation

Tissues were homogenized using TissueLyser (Qiagen), and total RNA was extracted with QIAzol reagent (Qiagen). The RNA pellet was dissolved in RNase-free water and concentration was measured in a NanoDrop spectrophotometer (Wilmington). RNA (2 µg) was transcribed to cDNA using the High Capacity cDNA Reverse Transcription Kit (Applied Biosystems).

III.15. PCR detection of lamin A and progerin

Lamin A and progerin mRNA levels were quantified according to a protocol adapted from Yang *et al.* (*155*). cDNA (100 ng for medial aortas and 200 ng for other organs) was amplified by PCR using DNA polymerase (Biotools, Spain). PCR products were separated on a 2% agarose gel containing ethidium bromide. Images were taken with a Molecular Imager® Gel Doc™ XR+ System (BioRad) and analyzed with Image Lab™ (BioRad).

III.16. Quantitative real-time PCR

qPCR reactions were prepared using *Power* SYBR® Green PCR Master Mix (Applied Biosystems). PCR reaction mixes were loaded on 384-well plates (Applied Biosystems) and run on a 7900-FAST-384 thermal cycler (Applied Biosystems). All reactions were performed in triplicate. Primers used in this study are as follows: *Calr* (F: 5′-CCAGAAATTGACAACCCTGAA-3′, R: 5′-CCTTAAGCCTCTGCTCCTCAT-3′), *Ddit3* (F: 5′-ATATCTCATCCCCAGGAAACG-3′, R: 5′-CTCCTGCTCCTTCTCCTTCAT-3′), *Dnajb9* (F: 5′-AGAATTAATCCTGGCCTCCAA-3′, R: 5′-GGCATCCGAGAGTGTTTCATA-3′), *Hspa5* (F: 5′-GTGGGAGGAGTCATGACAAAA-3′, R: 5′-TTCAGCTGTCACTCGGAGAAT-3′), *Hsp90b1* (F: 5′-AGTGGAAGAGGACCTGGGTAA-3′, R: 5′-AGCGAGTGCATTTTCATCAGT-3′), *Pdia4* (F: 5′-TCCTGAAGGATGGAGATGATG-3′, R: 5′-ACCTGGGCTCATACTTGGACT-3′), *Gusb* (F: 5′-GAGTATGGAGCAGACGCAATC-3′, R: 5′-TCCGACCACGTATTCTTTACG-3′), and *Hprt* (F: 5′-AGGCCAGACTTTGTTGGATTT-3′, R: 5′-GGCTTTGTATTTGGCTTTTCC-3′).

III.17. Statistical analysis

Experimental data are presented as mean (error bars indicate standard error of the mean (SEM)) for parametric data, or median with interquartile range (error bars indicate minimum and maximum) for non-parametric data. For small sample sizes, data were plotted as independent points (dot plots). Based on all experiments, distribution of a variable (lesion size, nucleus count, etc.) was assessed using the Kolmogorov-Smirnov and D'Agostino-Pearson normality tests. If the distribution was normal in most of the experiments, a two-tailed *t*-test was used, except for the validation of RNAseq data by qPCR and VSMC content quantification after TUDCA treatment where a one-tailed *t*-test was used. If the distribution of a variable was skewed, the two-tailed Mann-Whitney test was used, except for the adventitia-to-media ratio quantification after TUDCA treatment where a one-tailed Mann-Whitney test was used. To compare multiple groups, one-way ANOVA with Tukey´s *post hoc* test was used for both parametric and non-parametric data because this approach is resistant to normality violations with similar sized groups. A log-rank (Mantel-Cox) test was used for Kaplan-Meier survival curves. Differences were considered significant at $P < 0.05$. Statistical analysis was performed with GraphPad Prism 5.

IV. RESULTS AND DISCUSSION

IV.1. Ubiquitous progerin expression aggravates atherosclerosis in HFD-fed *Apoe*$^{-/-}$ mice

Among the available HGPS-like mouse models, *Lmna*$^{G609G/G609G}$ knock-in mice ubiquitously expressing progerin recapitulate most of the clinical manifestations of HGPS, including growth impairment, bone abnormalities, lipodystrophy, vascular calcification, and reduced survival (average lifespan: ≈15 weeks) (*59, 60*). However, we did not observe atherosclerosis in aortas of *Lmna*$^{G609G/G609G}$ mice even when 8-week-old animals were challenged with HFD for 8 weeks (**Fig. 3**). This finding is consistent with the observation that, unlike humans, mice are extremely resistant to atherosclerosis development, due in part to differences in cholesterol and lipoprotein metabolism (*156*).

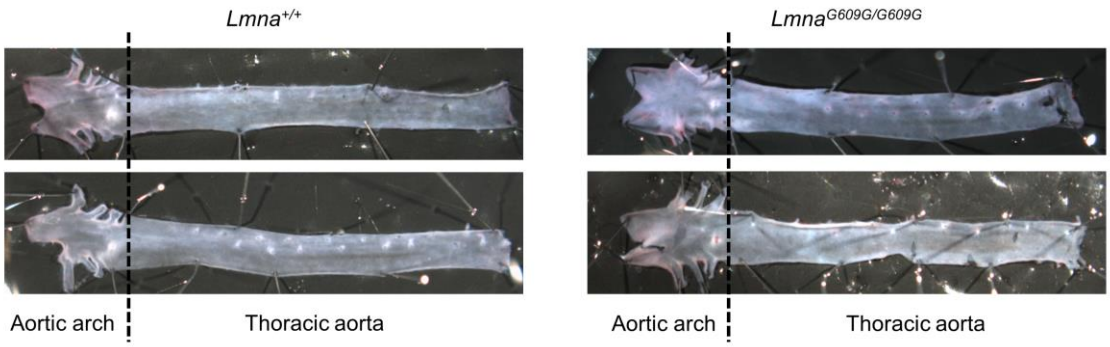

Figure 3. *Lmna*$^{G609G/G609G}$ mice do not show any signs of atherosclerosis development. *Lmna*$^{G609G/G609G}$ and *Lmna*$^{+/+}$ mice were fed high-fat diet for 8 weeks starting at 8 weeks of age. Mice were sacrificed at 16 weeks (close to their maximum survival) and aortas were stained with Oil Red O to visualize lipid-rich atheroma plaques. No red staining was observed indicating absence of atherosclerosis.

To circumvent this limitation, we generated an atherosclerosis-prone mouse model of HGPS by crossing *Lmna*$^{G609G/+}$ mice with *Apoe*$^{-/-}$ mice, a widely-used model of atherosclerosis (*156*). As expected, *Apoe*$^{-/-}$*Lmna*$^{G609G/G609G}$ mice showed decreased body weight and a shortened life span (median survival: 18.5 weeks) as compared with *Apoe*$^{-/-}$*Lmna*$^{+/+}$ littermates with normal *Lmna* gene expression (median survival: 117.6 weeks) (**Fig. 4**). Notably, the *Apoe*$^{-/-}$*Lmna*$^{G609G/G609G}$ phenotype, including survival and body weight curves, was similar to that of *Lmna*$^{G609G/G609G}$ mice (*59*).

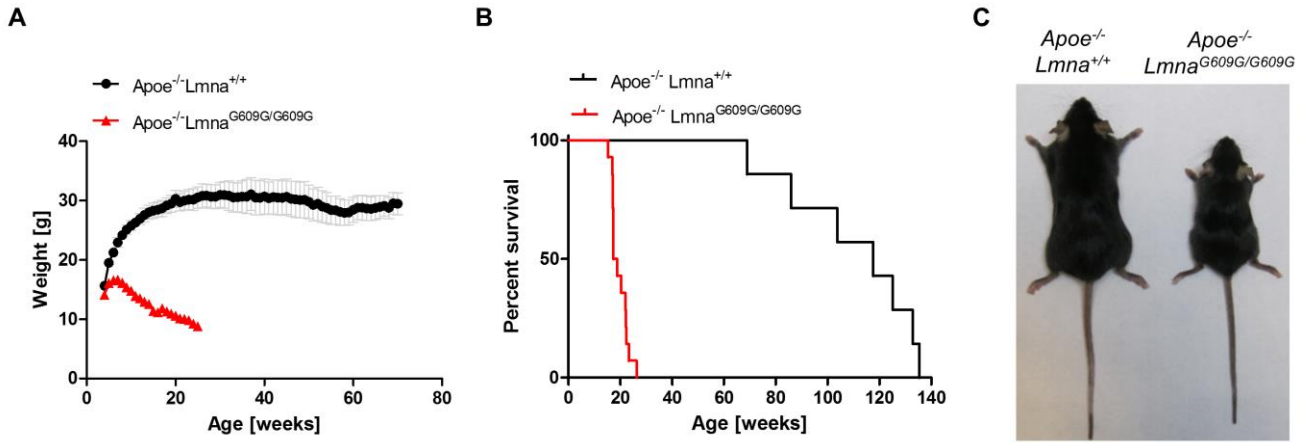

Figure 4. Ubiquitous progerin expression in *Apoe*$^{-/-}$*Lmna*$^{G609G/G609G}$ mice impairs postnatal growth and reduces lifespan. (A) Postnatal body weight curves for *Apoe*$^{-/-}$*Lmna*$^{+/+}$ mice (n=7) and *Apoe*$^{-/-}$*Lmna*$^{G609G/G609G}$ mice (n=14). **(B)** Kaplan-Meier survival curves. Median survival = 18.5 weeks for *Apoe*$^{-/-}$*Lmna*$^{G609G/G609G}$ mice (n=14) and 117.6 weeks for *Apoe*$^{-/-}$*Lmna*$^{+/+}$ mice (n=7); $P<0.001$. **(C)** Representative photograph of 16-week-old males. Data are presented as mean ± SEM in **A**. Statistical analysis was performed by log-rank test in **B**.

To study the influence of progerin on atherosclerosis development, 8-week-old mice were challenged for 8 weeks with HFD. Pre-HFD fasting serum lipid levels, including total cholesterol, free cholesterol, LDL and HDL, were indistinguishable between experimental groups (**Fig. 5A**). However, post-HFD levels were significantly lower in *Apoe*$^{-/-}$*Lmna*$^{G609G/G609G}$ mice than in *Apoe*$^{-/-}$*Lmna*$^{+/+}$ controls (**Fig. 5B**), probably due to a reduced food intake related to premature aging and associated disease progression in progeric mice. Nevertheless, despite the lower serum lipid levels, atherosclerosis burden assessed by ORO staining was 1.8-fold higher in the aortic arch and 3.1-fold higher in the thoracic aorta of HFD-fed *Apoe*$^{-/-}$*Lmna*$^{G609G/G609G}$ mice (**Fig. 5C**). Both groups had focal aortic lesions, but the aortic surface of progeroid *Apoe*$^{-/-}$*Lmna*$^{G609G/G609G}$ mice was covered with lipid deposits, which were not seen in control *Apoe*$^{-/-}$*Lmna*$^{+/+}$ mice (**Fig. 5C**).

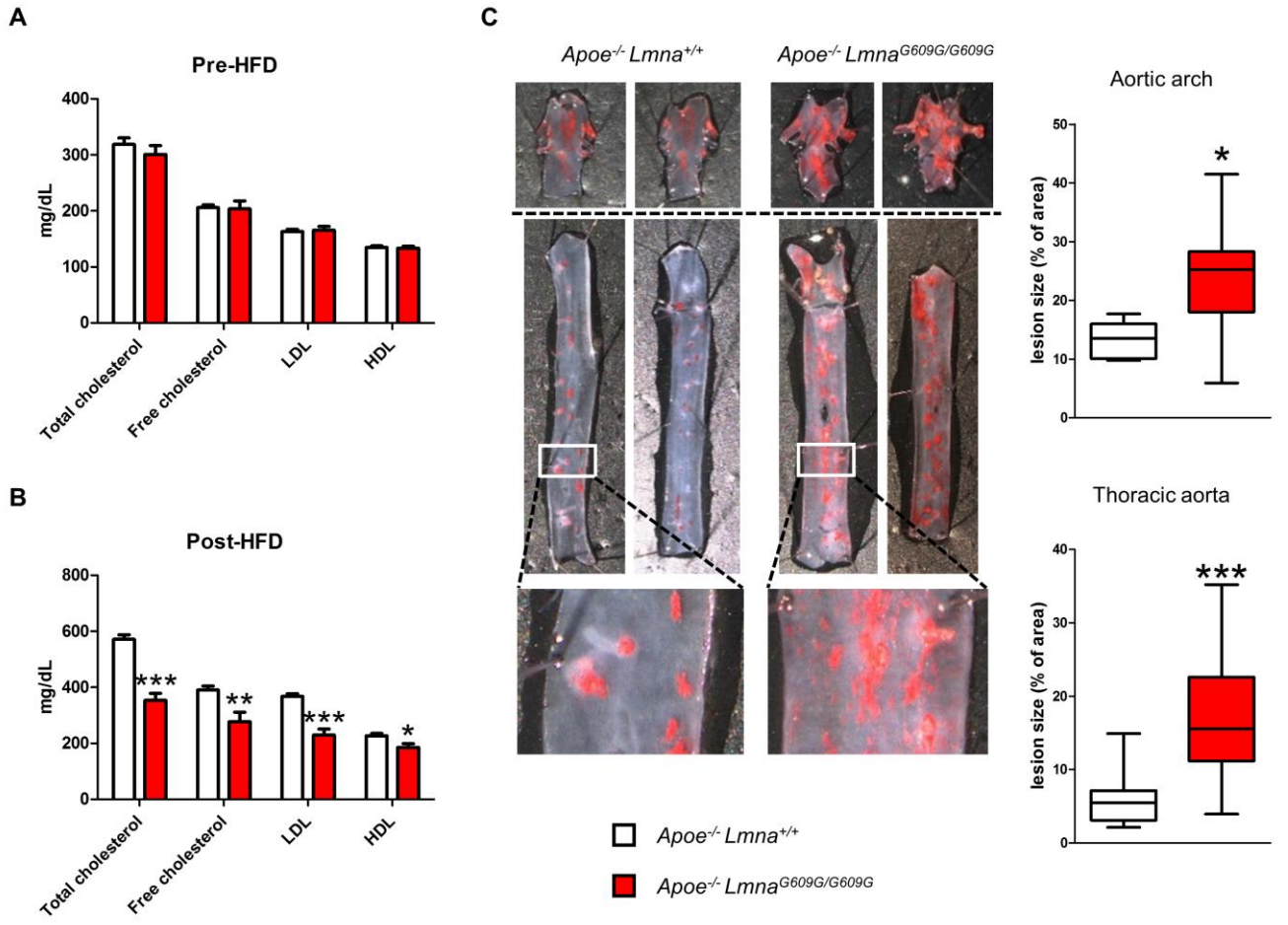

Figure 5. Ubiquitous progerin expression in *Apoe*$^{-/-}$*Lmna*$^{G609G/G609G}$ mice accelerates atherosclerosis upon high-fat diet (HFD). Mice were fed HFD for 8 weeks starting at 8 weeks of age. **(A)** Fasting serum pre-HFD levels of total cholesterol, free cholesterol, low-density lipoprotein (LDL), and high-density lipoprotein (HDL) in 8-week-old *Apoe*$^{-/-}$*Lmna*$^{G609G/G609G}$ mice (n=5) and *Apoe*$^{-/-}$*Lmna*$^{+/+}$ mice (n=7). **(B)** Fasting serum post-HFD levels of total cholesterol, free cholesterol, LDL, and HDL in 16-week-old *Apoe*$^{-/-}$*Lmna*$^{G609G/G609G}$ mice (n=6) and *Apoe*$^{-/-}$*Lmna*$^{+/+}$ mice (n=8). **(C)** Representative aortic arches (top) and thoracic aortas (middle and bottom) stained with Oil Red O; graphs show quantification of atherosclerosis burden in *Apoe*$^{-/-}$*Lmna*$^{G609G/G609G}$ mice (n=6 aortic arches; n=12 thoracic aortas) and *Apoe*$^{-/-}$*Lmna*$^{+/+}$ mice (n=9 aortic arches; n=13 thoracic aortas). Data are shown as mean ± SEM in **A** and **B**, and as median with interquartile range and minima and maxima in **C**. Statistical differences were analyzed by two-tailed *t*-test in **A** and **B** and by two-tailed Mann-Whitney test in **C**. **P*<0.05, ***P*<0.01, ****P*<0.001.

Histology revealed that this abnormality was due to excessive lipid accumulation in the aortic tunica media in atheroma-free zones of *Apoe*$^{-/-}$*Lmna*$^{G609G/G609G}$ aorta (**Fig. 6A, B**). These lipid deposits typically corresponded to the medial regions, with an almost complete loss of VSMCs (**Fig. 6A**). As in human HGPS arteries, VSMC depletion in *Apoe*$^{-/-}$*Lmna*$^{G609G/G609G}$ mice was accompanied by increased collagen content in the media and abnormal elastin structure (**Fig. 6A, B**). Importantly, *Apoe*$^{-/-}$*Lmna*$^{G609G/G609G}$ mice developed adventitial thickening and inflammation (**Fig. 6A, B**), a relevant feature of HGPS. Some of the pathologies described above have been observed in other progeroid

mouse models, such as VSMC depletion in knock-in *Lmna*$^{G609G/G609G}$ and transgenic G608G BAC mice (*58*, *59*), but not as early and as severe as in the model described here (**Fig. 6C**).

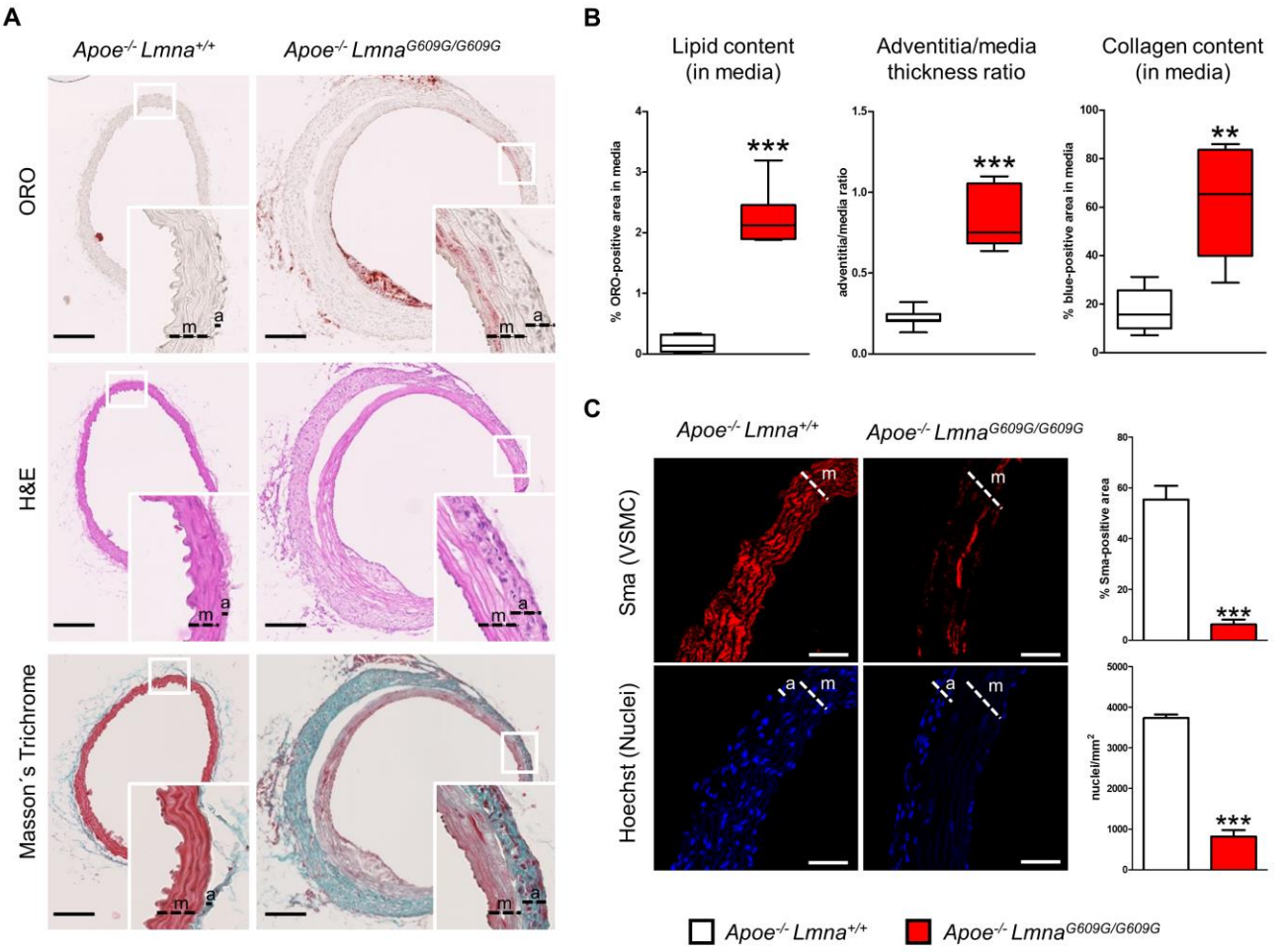

Figure 6. Ubiquitous progerin expression in *Apoe*$^{-/-}$*Lmna*$^{G609G/G609G}$ mice produces severe vascular pathology, including lipid retention in the media, vascular smooth muscle cell (VSMC) loss, adventitial thickening, and increased collagen content upon high-fat diet (HFD). Mice were fed HFD for 8 weeks starting at 8 weeks of age. **(A)** Representative staining of aorta sections with Oil Red O (ORO), hematoxylin & eosin (H&E), and Masson's Trichrome. **(B)** Graphs show quantification of lipid content in atheroma-free zones of the media (as % of ORO-positive area), adventitia-to-media thickness ratio, and collagen content in the media (% of blue staining); n=6-8. Scale bar, 200 µm. **(C)** Representative immunofluorescence images of aortas stained with anti-smooth muscle actin (Sma) antibody (red) and Hoechst3442 (blue); graphs show quantification of VSMC content in the media as either % of Sma-positive area (*top*) or nucleus count (*bottom*); n=6-8. Scale bar, 50 µm. Box and whisker plots in **B** show medians, interquartile range, and minima and maxima; data in **C** are mean ± SEM. Statistical analysis was performed by two-tailed Mann-Whitney test in **B**, and two-tailed *t*-test in **C**. ***P*<0.01, ****P*<0.001. m: media, a: adventitia.

Apoe$^{-/-}$*Lmna*$^{G609G/G609G}$ mice also showed significant hematological alterations in leukocyte subpopulations, including lower pre- and post-HFD lymphocyte and monocyte counts (**Fig. 7 and 8**). Since hematological analysis is based on the size and granularity of the cell, some of these measurements may be compromised because progerin affects nuclear shape. These findings should

therefore be confirmed by flow cytometry using specific cell surface marker antibodies to precisely define changes in circulating leukocyte subpopulations of *Apoe*$^{-/-}$*Lmna*$^{G609G/G609G}$ mice.

Although HGPS patients have increased platelet count (*17*), we did not find significantly higher amount of platelets in the blood of *Apoe*$^{-/-}$*Lmna*$^{G609G/G609G}$ mice as compared with *Apoe*$^{-/-}$*Lmna*$^{+/+}$ controls. This progerin-driven alteration could be masked by the *Apoe* deficiency, because atherosclerosis-resistant *Lmna*$^{G609G/G609G}$ mice with an intact *Apoe* gene have a higher platelet count than *Lmna*$^{+/+}$ littermates (data not shown).

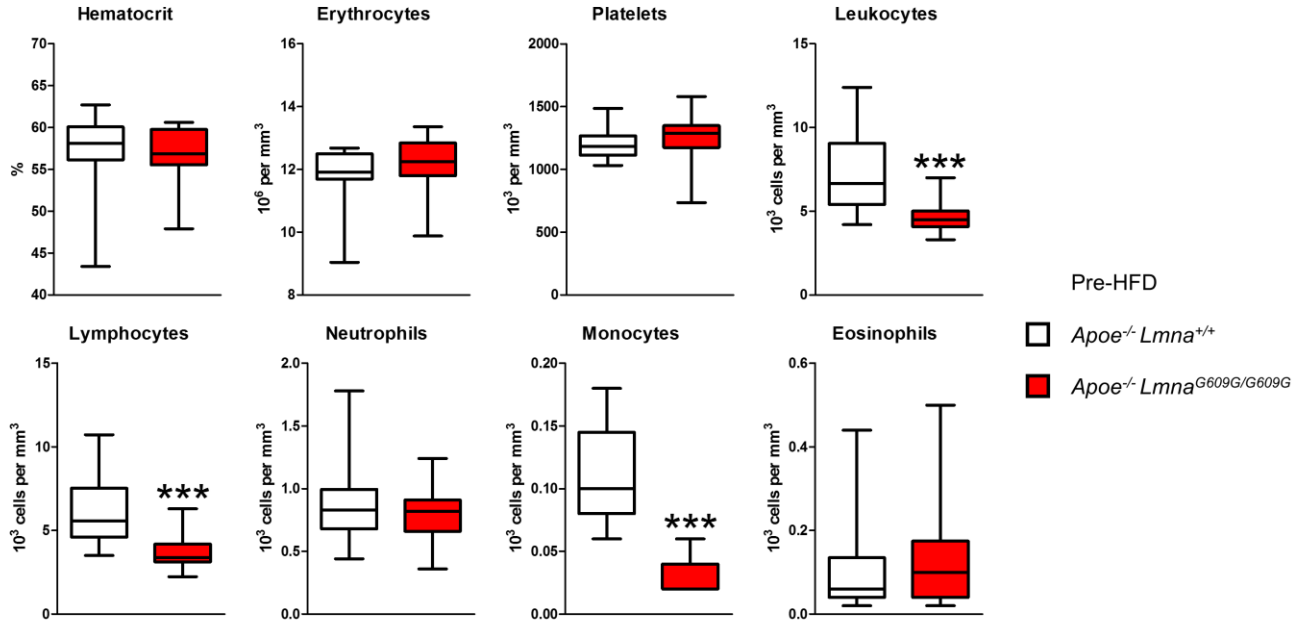

Figure 7. *Apoe*$^{-/-}$*Lmna*$^{G609G/G609G}$ mice have lower leukocyte, lymphocyte and monocyte counts pre-high fat diet (HFD). Pre-HFD (fasting) hematology results for 8-week-old *Apoe*$^{-/-}$*Lmna*$^{G609G/G609G}$ mice (n=18) and *Apoe*$^{-/-}$*Lmna*$^{+/+}$ *mice* (n=18). Data are shown as median with interquartile range and minima and maxima. Statistical differences were analyzed by two-tailed Mann-Whitney test. ****P*<0.001.

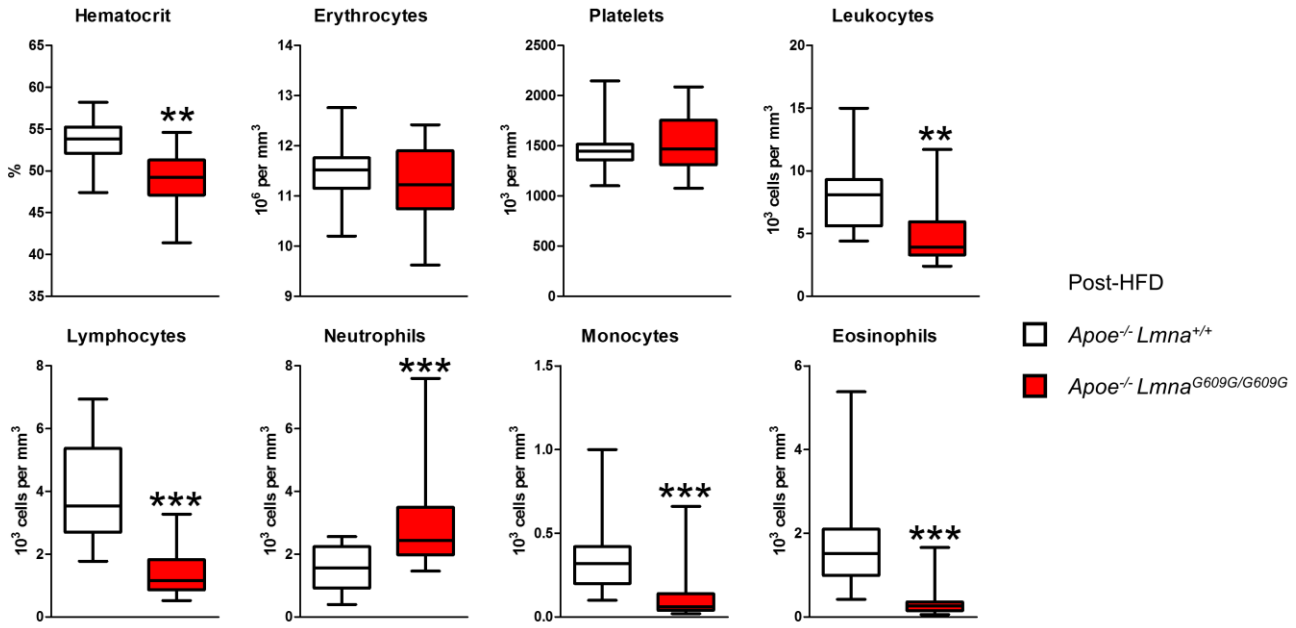

Figure 8. *Apoe*$^{-/-}$*Lmna*$^{G609G/G609G}$ mice show higher neutrophil and lower leukocyte, lymphocyte, monocyte, and eosinophil counts post-high fat diet (HFD). Post-HFD (fasting) hematology results for 16-week-old *Apoe*$^{-/-}$ *Lmna*$^{G609G/G609G}$ mice (n=17) and *Apoe*$^{-/-}$*Lmna*$^{+/+}$ mice (n=17). Data are shown as median with interquartile range and minima and maxima. Statistical differences were analyzed by two-tailed Mann-Whitney test. ***P*<0.01, ****P*<0.001.

In this study, we have generated the first mouse model of progerin-induced acceleration of atherosclerosis, a pathological process that leads to myocardial infarction- or stroke-related death in most children with HGPS. As our *Apoe*$^{-/-}$*Lmna*$^{G609G/G609G}$ mice faithfully recapitulate most of the aspects of the human disease, they are a valuable tool to investigate the molecular and cellular mechanisms underlying premature CVD and death in HGPS.

IV.2. VSMC-specific progerin expression in HFD-fed *Apoe*$^{-/-}$ mice aggravates atherosclerosis and shortens lifespan

Atherosclerosis is a complex process involving many cell types, including VSMCs and macrophages (*157*). Immunohistopathological characterization of atherosclerotic plaques in HGPS patients suggests that both cell types contribute to progerin-driven atherogenesis (*20*). Since *Apoe*$^{-/-}$ *Lmna*$^{G609G/G609G}$ mice showed medial VSMC depletion and decreased numbers of circulating monocytes (which give rise to macrophages in atheromata), we generated mice with specific progerin expression in VSMCs or macrophages to study the relative contribution of these cell types in progeria.

To this end, we used knock-in *Lmna*$^{LCS/LCS}$ (LaminC-STOP) mice expressing only lamin C (*59*). The *Lmna*^{LCS} allele consists of a modified *Lmna* gene in which a neomycin resistance gene flanked with two *loxP* sequences was introduced after exon 10 to abolish lamin A production (**Fig. 9**). Additionally, an HGPS-equivalent point mutation (c.1827C>T; p.G609G) was inserted in exon 11. Excision of the neomycin resistance cassette in the presence of Cre recombinase enables progerin production (as well as lamin C and some residual lamin A). *Lmna*$^{LCS/LCS}$ mice expressing lamin C and lacking lamin A are apparently normal, but are slightly heavier and longer-lived than wild-type controls, and show decreased energy metabolism (*158*).

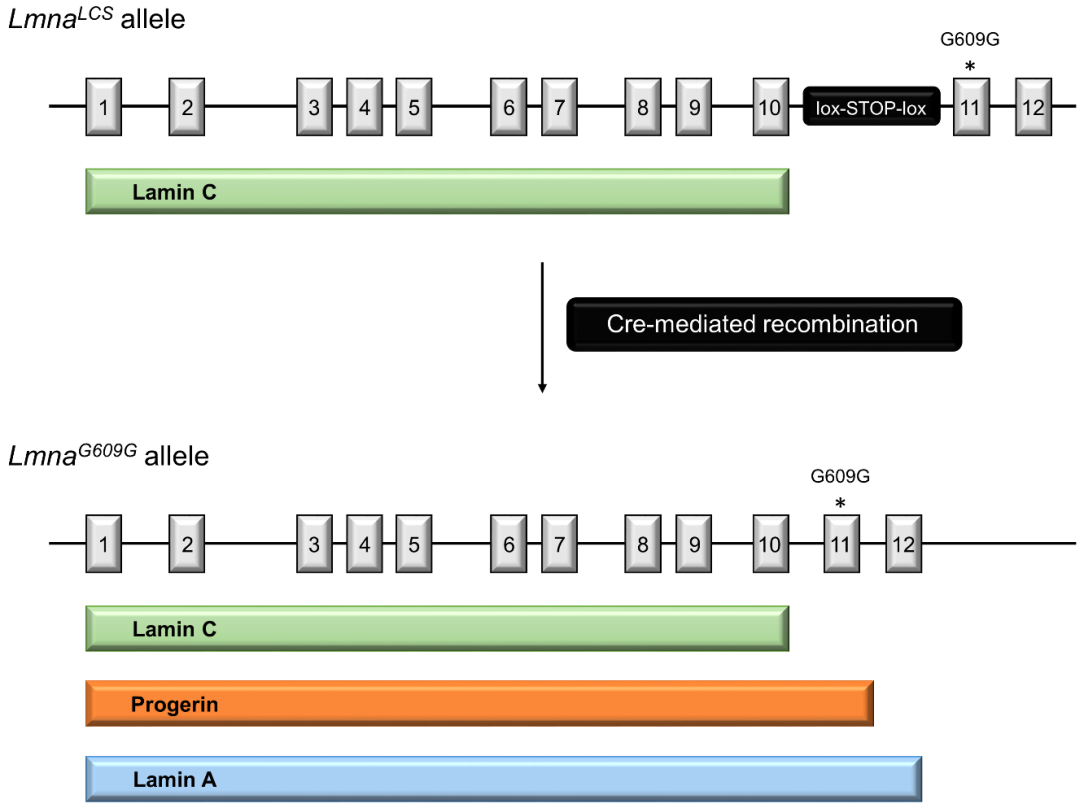

Figure 9. Schematic representation of *Lmna*^{LCS} allele before and after Cre-mediated recombination. The *Lmna*^{LCS} allele carries an HGPS-causing mutation (p.G609G, indicated with an asterisk) in exon 11. However, the only product of the *Lmna*^{LCS} allele is lamin C due to the insertion of a neomycin resistance gene after exon 10 which disables production of lamin A. In the presence of *Cre* recombinase, the neomycin resistance cassette, which is flanked with *loxP* sequences, is excised and three proteins are produced via alternative splicing: lamin C, progerin and lamin A.

We first performed pilot studies to assess whether the absence of lamin A may aggravate atherosclerosis. To do this, we generated *Apoe*$^{-/-}$*Lmna*$^{LCS/LCS}$ mice and analyzed atheroma plaque formation in 16-week-old mice challenged for 8 weeks with HFD (beginning at 8 weeks of age). No

significant differences in atherosclerosis burden, serum lipid levels, and hematological parameters were found between control *Apoe*$^{-/-}$*Lmna*$^{+/+}$ and *Apoe*$^{-/-}$*Lmna*$^{LCS/LCS}$ mice (**Fig. 10**).

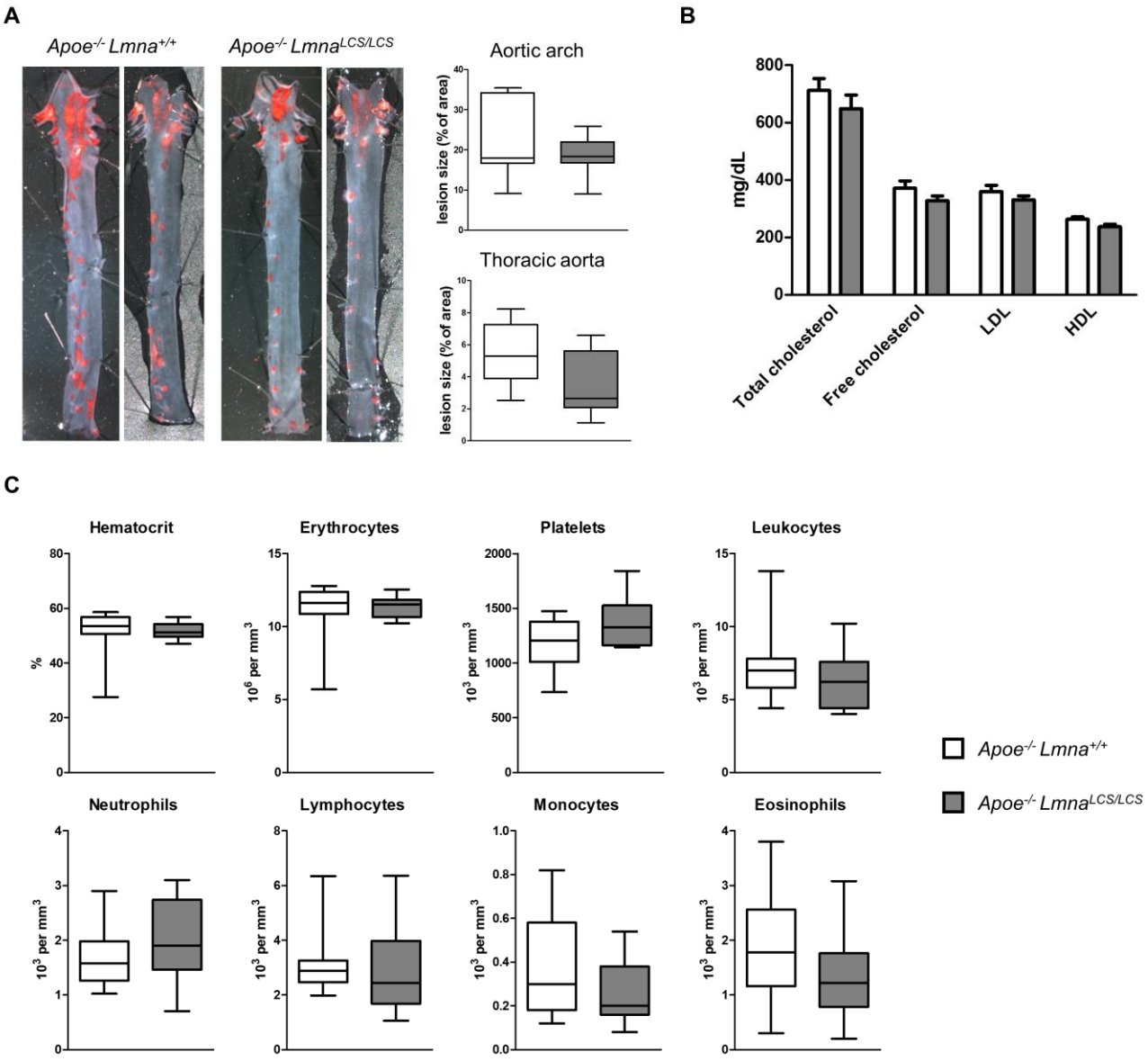

Figure 10. Fat-fed *Apoe*$^{-/-}$*Lmna*$^{LCS/LCS}$ mice expressing only lamin C do not show more atherosclerosis than *Apoe*$^{-/-}$*Lmna*$^{+/+}$ control mice expressing wild-type lamin A/C. Mice were fed high-fat diet (HFD) for 8 weeks starting at 8 weeks of age. **(A)** Representative examples of aortas stained with Oil Red O and quantification of atherosclerosis burden in *Apoe*$^{-/-}$*Lmna*$^{LCS/LCS}$ mice (n=8 aortic arches, n=11 thoracic aortas) and *Apoe*$^{-/-}$*Lmna*$^{+/+}$ mice (n=7 aortic arches, n=11 thoracic aortas). **(B)** Post-HFD fasting serum levels of total cholesterol, free cholesterol, low-density lipoprotein (LDL), and high-density lipoprotein (HDL) in *Apoe*$^{-/-}$*Lmna*$^{LCS/LCS}$ (n=6) and *Apoe*$^{-/-}$*Lmna*$^{+/+}$ (n=7) mice. **(C)** Post-HFD (fasting) hematology results for 16-week-old *Apoe*$^{-/-}$*Lmna*$^{LCS/LCS}$ mice (n=11) and *Apoe*$^{-/-}$*Lmna*$^{+/+}$ mice (n=11). Data are shown as median with interquartile range and minima and maxima in **A** and **C** and as mean ± SEM in **B**. Statistical differences were analyzed by two-tailed Mann-Whitney test in **A** and **C** and by two-tailed *t*-test in **B**.

The above result allowed *Apoe*$^{-/-}$*Lmna*$^{LCS/LCS}$ mice to serve as controls for the cell-type-specific models *Apoe*$^{-/-}$*Lmna*$^{LCS/LCS}$*LysMCre* (macrophage-specific) and *Apoe*$^{-/-}$*Lmna*$^{LCS/LCS}$*SM22αCre* (VSMC-specific). Progerin expression was verified by immunofluorescence in atheroma-containing aorta and by PCR in other organs. These studies confirmed that control *Apoe*$^{-/-}$*Lmna*$^{LCS/LCS}$ mice did not express progerin in any organ tested (**Fig. 11 and 12**). By contrast, *Apoe*$^{-/-}$*Lmna*$^{LCS/LCS}$*SM22αCre* mice abundantly expressed progerin in medial VSMCs and to a lesser extent in the adventitia (**Fig. 12**), as well as in heart (**Fig. 11**). Progerin expression in *Apoe*$^{-/-}$*Lmna*$^{LCS/LCS}$*LysMCre* mice was detected in intimal macrophages (**Fig. 12**), but was either absent or negligible in other organs (**Fig. 11**).

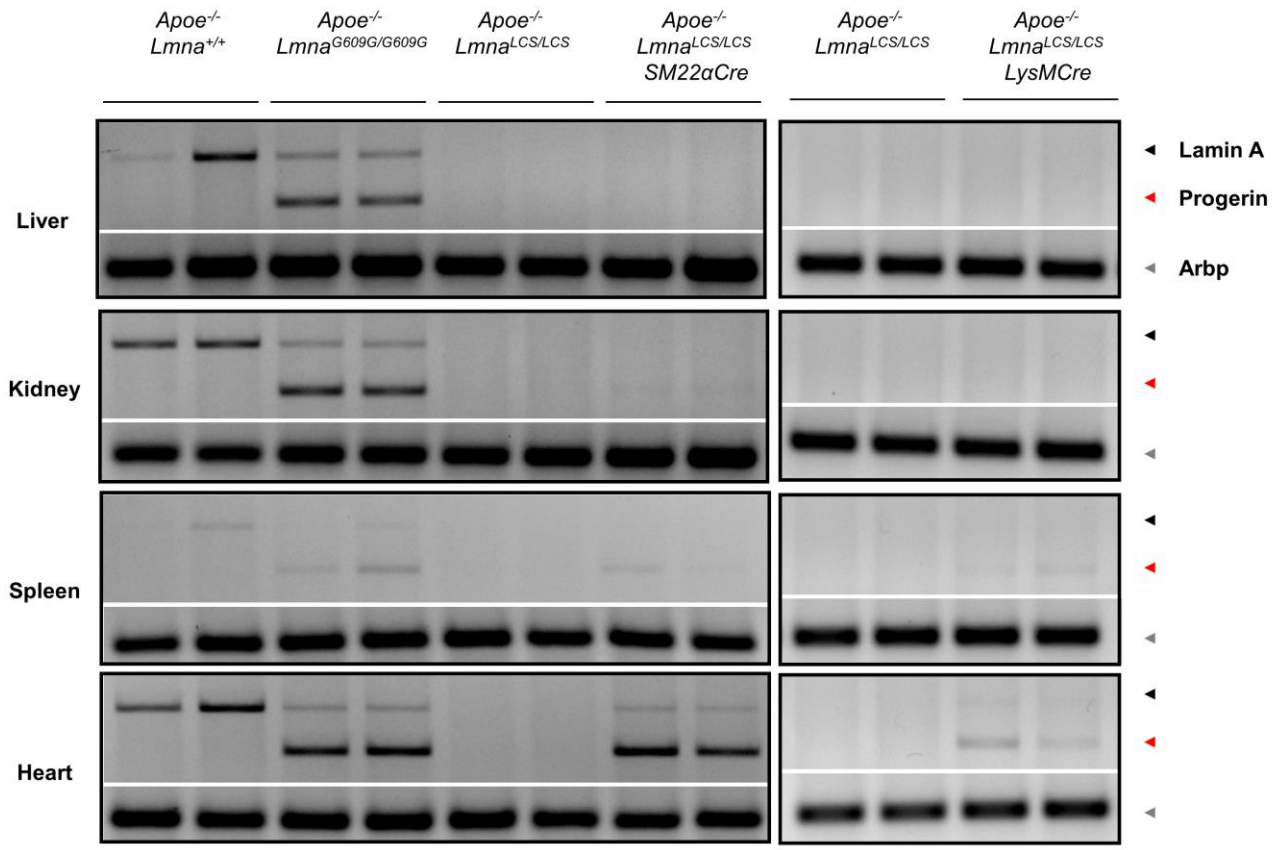

Figure 11. Progerin expression in different organs of progeroid and control mice. Representative images of PCR products showing lamin A and progerin mRNA expression in liver, kidney, spleen, and heart of 8-week-old mice of the indicated genotypes. Lamin A but not progerin was expressed in all organs from *Apoe*$^{-/-}$*Lmna*$^{+/+}$ mice, and progerin was detected in all organs from *Apoe*$^{-/-}$*Lmna*$^{G609G/G609G}$ mice (which also expressed low levels of lamin A). Lamin A and progerin were undetectable or negligible in all organs of *Apoe*$^{-/-}$*Lmna*$^{LCS/LCS}$, *Apoe*$^{-/-}$*Lmna*$^{LCS/LCS}$*SM22αCre*, and *Apoe*$^{-/-}$*Lmna*$^{LCS/LCS}$*LysMCre* mice, with the exception of *Apoe*$^{-/-}$*Lmna*$^{LCS/LCS}$*SM22αCre* heart, which expressed both progerin and lamin A. *Arbp* was used as an endogenous control.

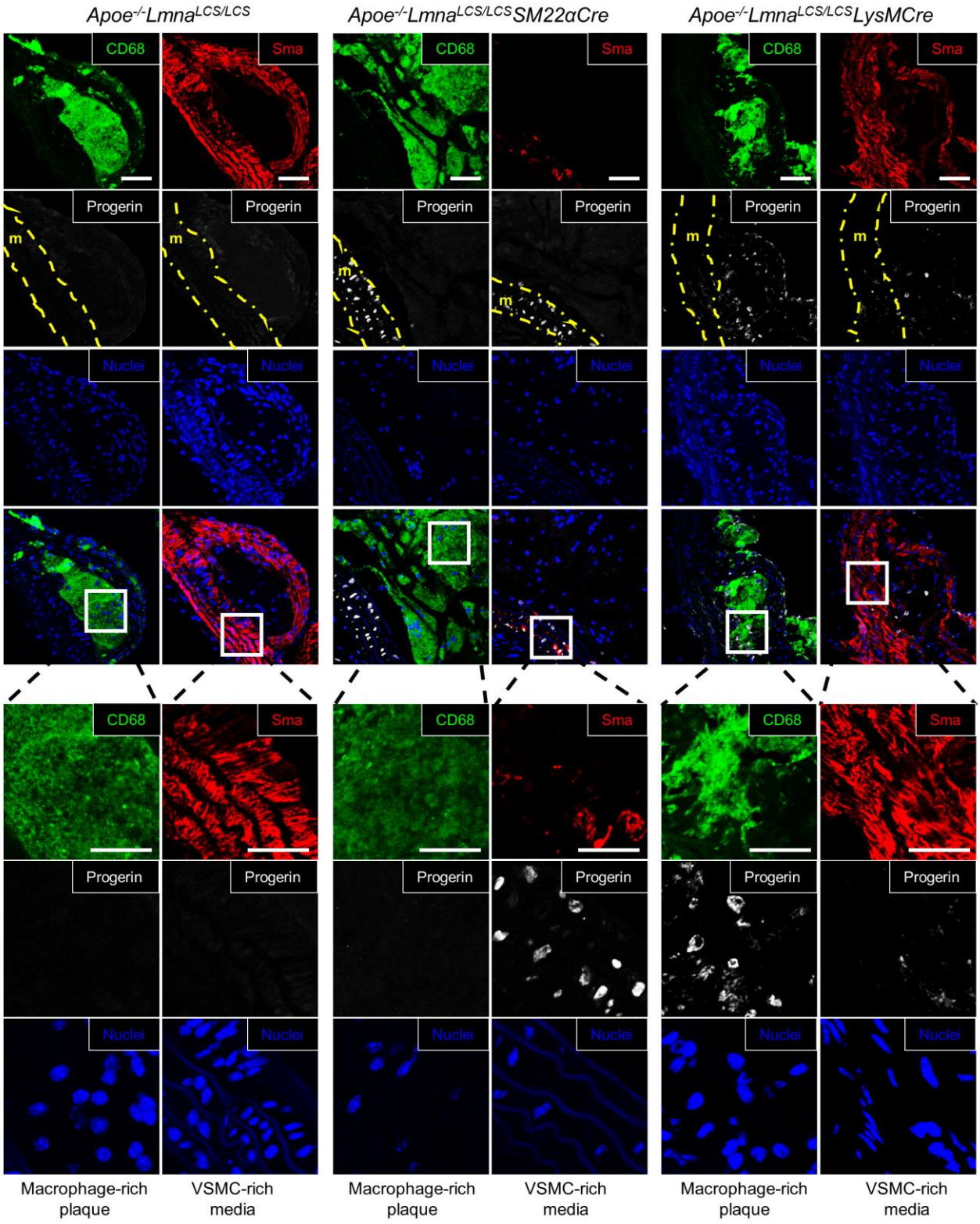

Figure 12. Progerin is expressed specifically in vascular smooth muscle cells (VSMCs) of *Apoe*$^{-/-}$*Lmna*$^{LCS/LCS}$*SM22αCre* aorta and in macrophages of *Apoe*$^{-/-}$*Lmna*$^{LCS/LCS}$*LysMCre* aorta. Representative images of atheroma-containing aortas from 16-week-old mice fed a high-fat diet for 2 months starting at 8 weeks of age. Progerin was visualized in white, macrophages were detected with anti-CD68 antibody (green), and VSMCs with anti-Sma antibody (red). Nuclei were stained with Hoechst3442 (blue). Scale bar, 50µm. Amplified images show VSMC-rich media and a macrophage-rich atherosclerotic plaque.

Apoe$^{-/-}$*Lmna*$^{LCS/LCS}$*LysMCre* mice with macrophage-specific progerin expression showed no significant differences in body weight, longevity and organ size relative to controls (**Fig. 13 and 14**). *Apoe*$^{-/-}$*Lmna*$^{LCS/LCS}$*SM22αCre* mice with VSMC-specific progerin expression appeared normal early in life, but stopped gaining weight after approximately 20 weeks of age and died at a median age of 34.3 weeks (**Fig. 13 and 14**).

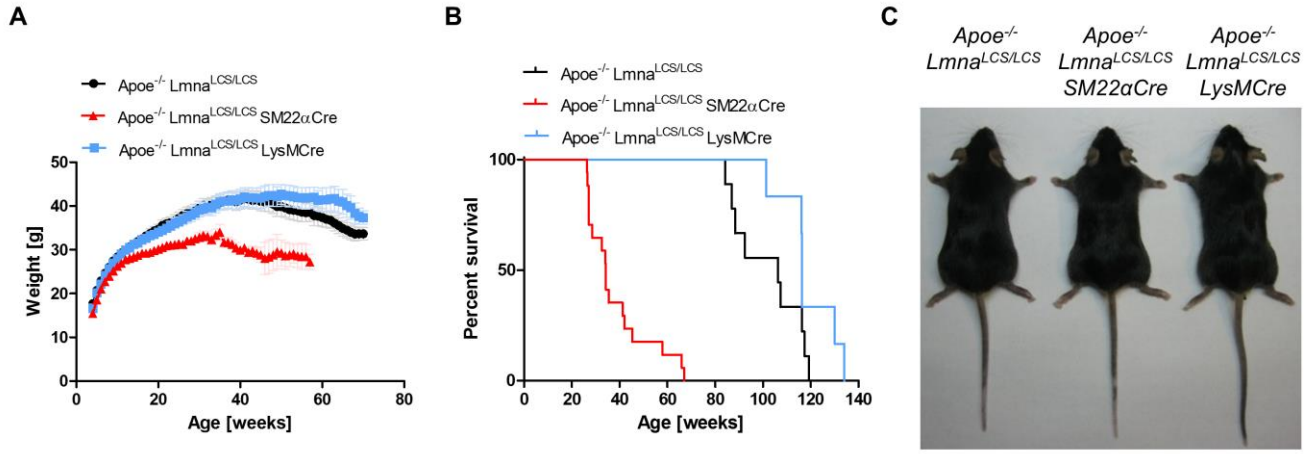

Figure 13. Vascular smooth muscle cell (VSMC)-specific progerin expression in *Apoe*$^{-/-}$*Lmna*$^{LCS/LCS}$*SM22αCre* mice reduces lifespan. (A) Postnatal body weight curves for *Apoe*$^{-/-}$*Lmna*$^{LCS/LCS}$ mice (n=9), *Apoe*$^{-/-}$*Lmna*$^{LCS/LCS}$*SM22αCre* mice (n=12), and *Apoe*$^{-/-}$*Lmna*$^{LCS/LCS}$ *LysMCre* mice (n=6). The weight curve for *Apoe*$^{-/-}$*Lmna*$^{LCS/LCS}$*SM22αCre* mice is shown up to the time when approximately 90% of the animals were dead. Data are presented as mean ± SEM. **(B)** Kaplan-Meier survival curves. Median survival = 34.3 weeks for *Apoe*$^{-/-}$*Lmna*$^{LCS/LCS}$*SM22αCre* mice (n=17), 106.3 weeks for *Apoe*$^{-/-}$ *Lmna*$^{LCS/LCS}$ mice (n=9), and 116.3 weeks for *Apoe*$^{-/-}$*Lmna*$^{LCS/LCS}$*LysMCre* mice (n=6). $P<0.0001$ for *Apoe*$^{-/-}$ *Lmna*$^{LCS/LCS}$*SM22αCre* mice vs *Apoe*$^{-/-}$*Lmna*$^{LCS/LCS}$ controls. Statistical analysis was performed by log-rank test. **(C)** Representative photograph of 16-week-old males.

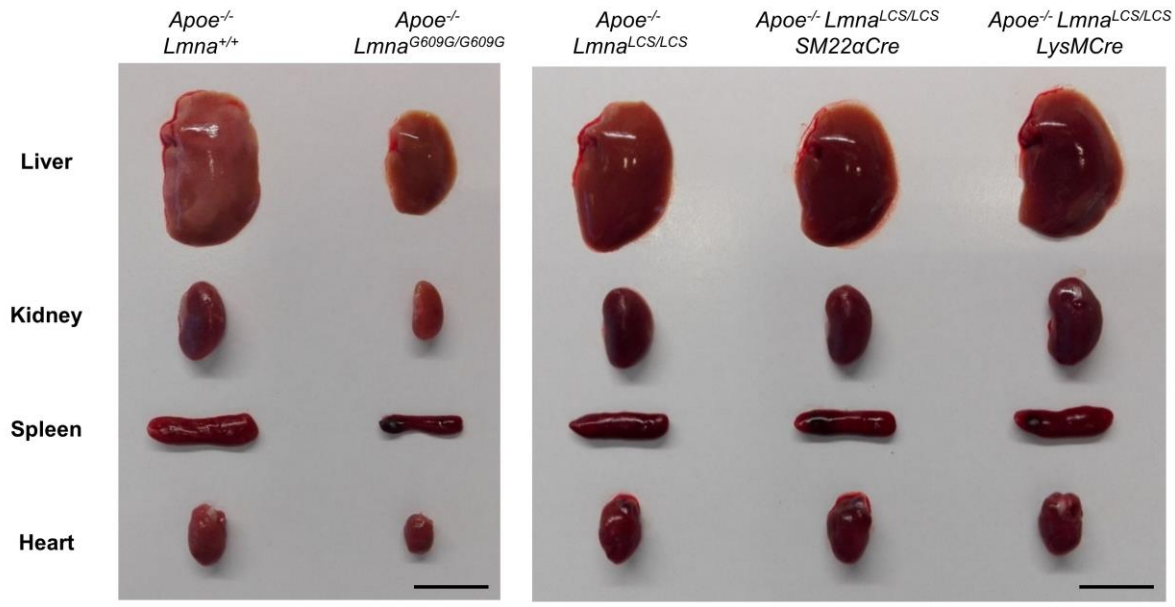

Figure 14. *Apoe*$^{-/-}$*Lmna*$^{LCS/LCS}$*SM22αCre* and *Apoe*$^{-/-}$*Lmna*$^{LCS/LCS}$ *LysMCre* mice, unlike *Apoe*$^{-/-}$*Lmna*$^{G609G/G609G}$, show normal organ size. Representative images of liver, kidney, spleen, and heart of 16-week-old mice of the indicated genotypes. Scale bar 1 cm.

We next studied atherosclerosis development in the cell type-specific models following the same protocol as that used for the ubiquitous progerin-expressing *Apoe*$^{-/-}$*Lmna*$^{G609G/G609G}$ mice. The three experimental groups showed no inter-group differences in fasting serum lipid levels or hematological parameters, either pre- or post-HFD (**Fig. 15 and 16**).

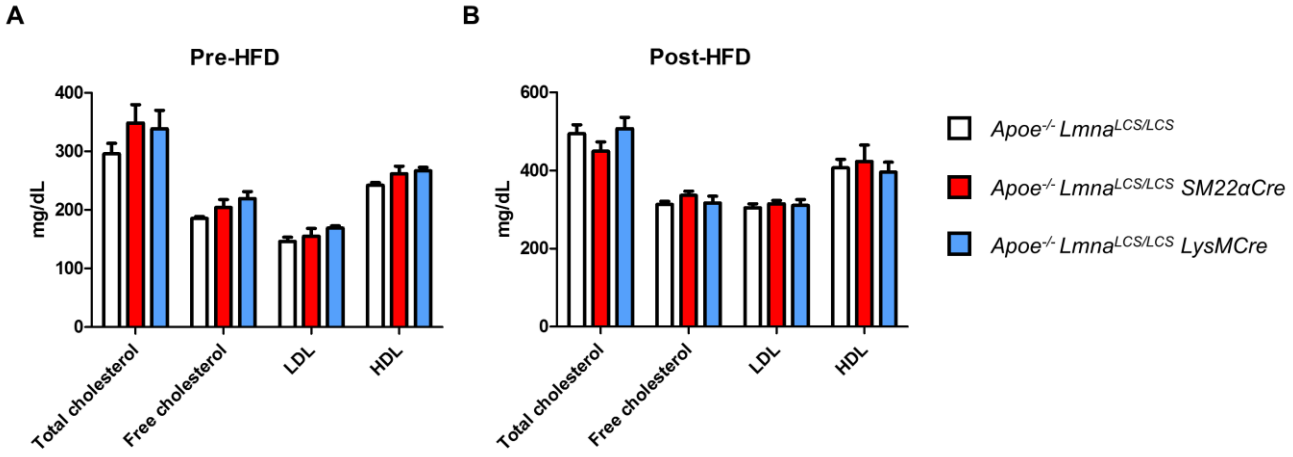

Figure 15. *Apoe*$^{-/-}$*Lmna*$^{LCS/LCS}$*SM22αCre* and *Apoe*$^{-/-}$*Lmna*$^{LCS/LCS}$*LysMCre* mice have normal serum cholesterol levels. Mice were fed high-fat diet (HFD) for 8 weeks starting at 8 weeks of age. **(A)** Pre-HFD fasting serum levels of total cholesterol, free cholesterol, low-density lipoprotein (LDL), and high-density lipoprotein (HDL) in 8-week-old *Apoe*$^{-/-}$*Lmna*$^{LCS/LCS}$ mice (n=5), *Apoe*$^{-/-}$*Lmna*$^{LCS/LCS}$*SM22αCre* mice (n=4), and *Apoe*$^{-/-}$*Lmna*$^{LCS/LCS}$*LysMCre* mice (n=6). **(B)** Post-HFD fasting serum levels of total cholesterol, free cholesterol, LDL, and HDL in 16-week-old *Apoe*$^{-/-}$*Lmna*$^{LCS/LCS}$ mice (n=10), *Apoe*$^{-/-}$*Lmna*$^{LCS/LCS}$*SM22αCre* mice (n=7), and *Apoe*$^{-/-}$*Lmna*$^{LCS/LCS}$*LysMCre* mice (n=7). Data are shown as mean ± SEM. Statistical differences were analyzed by one-way ANOVA with Tukey´s post hoc test.

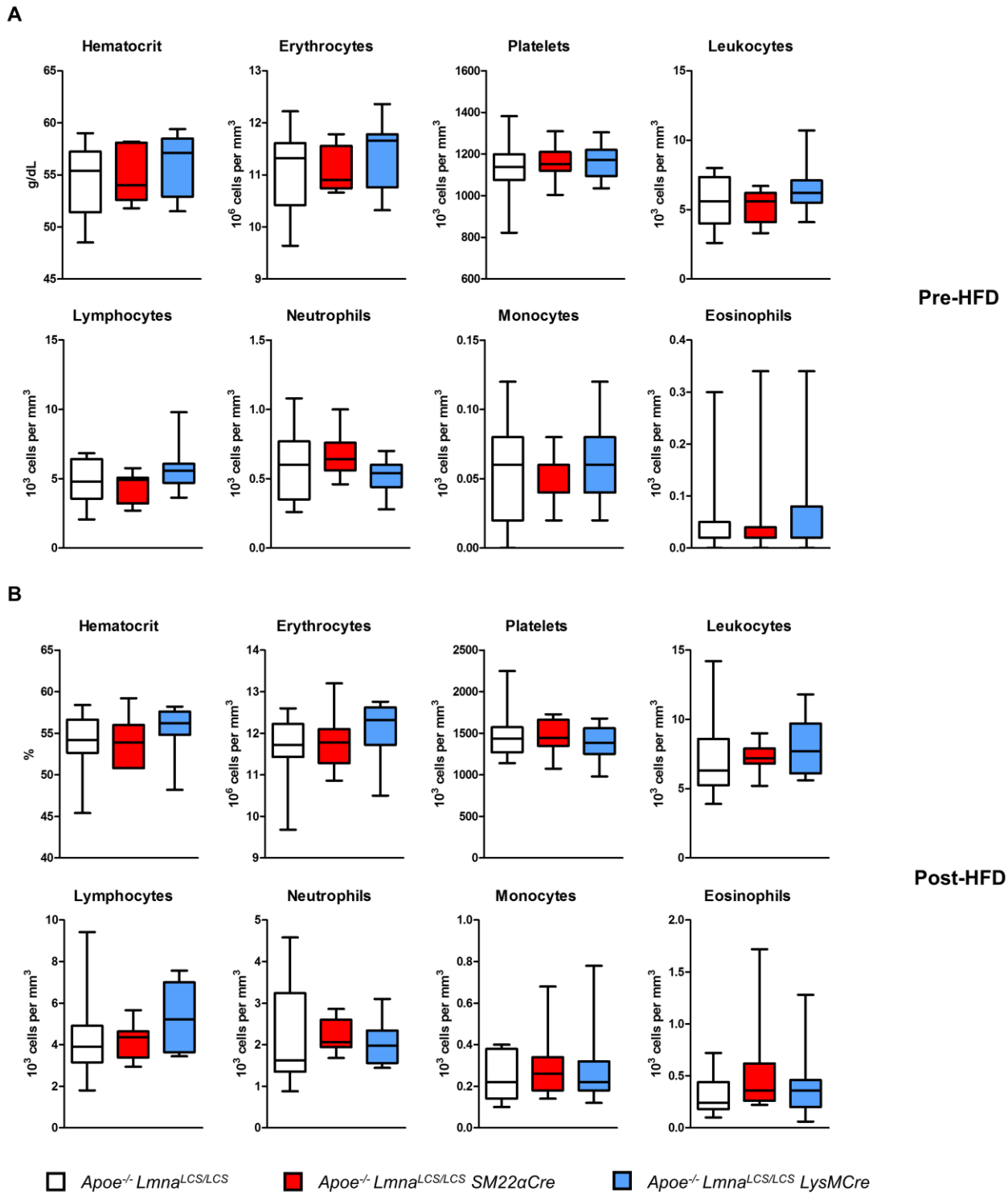

Figure 16. *Apoe*$^{-/-}$*Lmna*$^{LCS/LCS}$*SM22αCre* and *Apoe*$^{-/-}$*Lmna*$^{LCS/LCS}$*LysMCre* mice show normal hematological parameters. Mice were fed high-fat diet (HFD) for 8 weeks starting at 8 weeks of age. **(A)** Pre-HFD (fasting) hematology results for 8-week-old *Apoe*$^{-/-}$*Lmna*$^{LCS/LCS}$ mice (n=17), *Apoe*$^{-/-}$*Lmna*$^{LCS/LCS}$*SM22αCre* mice (n=11), and *Apoe*$^{-/-}$*Lmna*$^{LCS/LCS}$*LysMCre* mice (n=11). **(B)** Post-HFD (fasting) hematology results for 16-week-old *Apoe*$^{-/-}$*Lmna*$^{LCS/LCS}$ mice (n=17), *Apoe*$^{-/-}$*Lmna*$^{LCS/LCS}$*SM22αCre* mice (n=11), and *Apoe*$^{-/-}$*Lmna*$^{LCS/LCS}$*LysMCre* mice (n=11). Data are shown as median with interquartile range and minima and maxima. Statistical differences were analyzed by one-way ANOVA with Tukey´s post hoc test.

Atherosclerosis burden in the thoracic aorta was similar between *Apoe*$^{-/-}$*Lmna*$^{LCS/LCS}$*LysMCre* and *Apoe*$^{-/-}$*Lmna*$^{LCS/LCS}$ mice. By contrast, lesion burden in *Apoe*$^{-/-}$*Lmna*$^{LCS/LCS}$*SM22αCre* mice was 3.7-fold higher (**Fig. 17A**). Moreover, histological analysis of *Apoe*$^{-/-}$*Lmna*$^{LCS/LCS}$*SM22αCre* mice revealed the same marked aortic phenotype as observed in the ubiquitous progeroid model, including massive VSMC loss, adventitial thickening, elastin structure changes, and medial lipid accumulation (**Fig. 17B, C**).

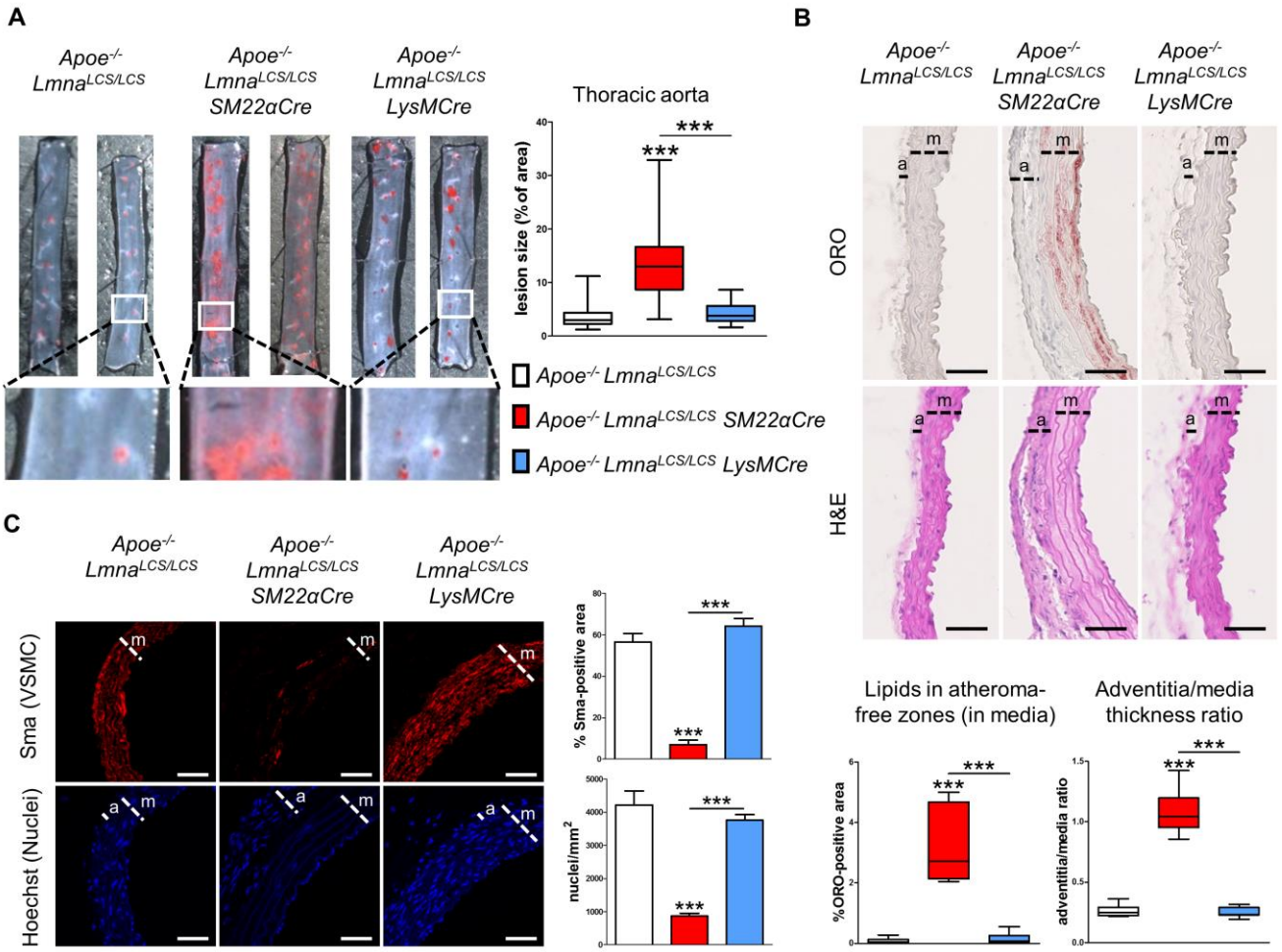

Figure 17. Vascular smooth muscle cell (VSMC)-specific progerin expression in fat-fed *Apoe*$^{-/-}$*Lmna*$^{LCS/LCS}$*SM22αCre* mice triggers severe vascular pathology, including atherosclerosis, VSMC loss, lipid retention in the media and adventitial thickening. Mice were fed high-fat diet (HFD) for 8 weeks starting at 8 weeks of age. **(A)** Representative examples of thoracic aortas stained with Oil Red O (ORO); the graph shows quantification of atherosclerosis burden in *Apoe*$^{-/-}$*Lmna*$^{LCS/LCS}$ mice (n=24) *Apoe*$^{-/-}$*Lmna*$^{LCS/LCS}$*SM22αCre* mice (n=17), and *Apoe*$^{-/-}$*Lmna*$^{LCS/LCS}$*LysMCre* mice (n=19). **(B)** Representative staining of aorta sections with ORO and hematoxylin & eosin (H&E); graphs show quantification of lipid content in atheroma-free zones of the media (% of ORO-positive area) and adventitia-to-media thickness ratio; n=6-8. Scale bar, 50 µm. **(C)** Representative immunofluorescence images of aortas stained with anti-smooth muscle actin (Sma) antibody (red) and Hoechst3442 (blue); graphs show quantification of VSMC content in the media as either % of Sma-positive area (*top*) or nucleus count (*bottom*); n=6-8. Scale bar, 50 µm. Box and whisker plots in **A** and **B** show medians, interquartile range, and minima and maxima; data in **C** are mean ± SEM. Statistical analysis was performed by one-way ANOVA with Tukey´s post hoc test in **A**, **B**, and **C**. ***P<0.001, m: media, a: adventitia.

The above results provide the first direct evidence that restricting progerin expression to VSMCs is sufficient to accelerate atherosclerosis and reduce lifespan, offering the possibility to study CVD independently of other premature aging symptoms. Another advantage of *Apoe*$^{-/-}$ *Lmna*$^{LCS/LCS}$*SM22αCre* animals is the lack of overt growth defects, which may permit diagnostic techniques and interventional strategies that are unattainable in the undersized *Apoe*$^{-/-}$*Lmna*$^{G609G/G609G}$ model.

IV.3. Progerin triggers plaque vulnerability

Previous studies have shown that loss of VSMCs in the tunica media may lead to changes in the composition and stability of atherosclerotic plaques (*159*). We therefore performed a more in-depth analysis of atheromata in the aortic root of *Apoe*$^{-/-}$*Lmna*$^{G609G/G609G}$ and *Apoe*$^{-/-}$*Lmna*$^{LCS/LCS}$*SM22αCre* mice and their respective controls. Three different zones of the aortic root were analyzed, at the beginning, in the middle, and at the end of the aortic valve. Consistent with our previous results in the aorta (**Fig. 5 and 17**), we observed a higher atherosclerosis burden in both progeria models than in the respective controls, and this was accompanied by fibrosis and inflammation of the adjacent cardiac tissue (**Fig. 18A, B**). Moreover, a greater percentage of the aortic surface was affected by the atherosclerosis process in both *Apoe*$^{-/-}$*Lmna*$^{G609G/G609G}$ and *Apoe*$^{-/-}$*Lmna*$^{LCS/LCS}$*SM22αCre* mice (**Fig. 18A, B**). Importantly, all *Apoe*$^{-/-}$*Lmna*$^{G609G/G609G}$ and *Apoe*$^{-/-}$*Lmna*$^{LCS/LCS}$*SM22αCre* mice exhibited coronary VSMC loss (**Fig. 18C, D**), and some of them developed coronary atherosclerosis (data not shown). In addition, we observed aortic valve degeneration and plaque formation on the aortic valve leaflets in *Apoe*$^{-/-}$*Lmna*$^{G609G/G609G}$ and *Apoe*$^{-/-}$*Lmna*$^{LCS/LCS}$*SM22αCre* mice, pathologies that were absent in control mice (**Fig. 18A, B**, and data not shown).

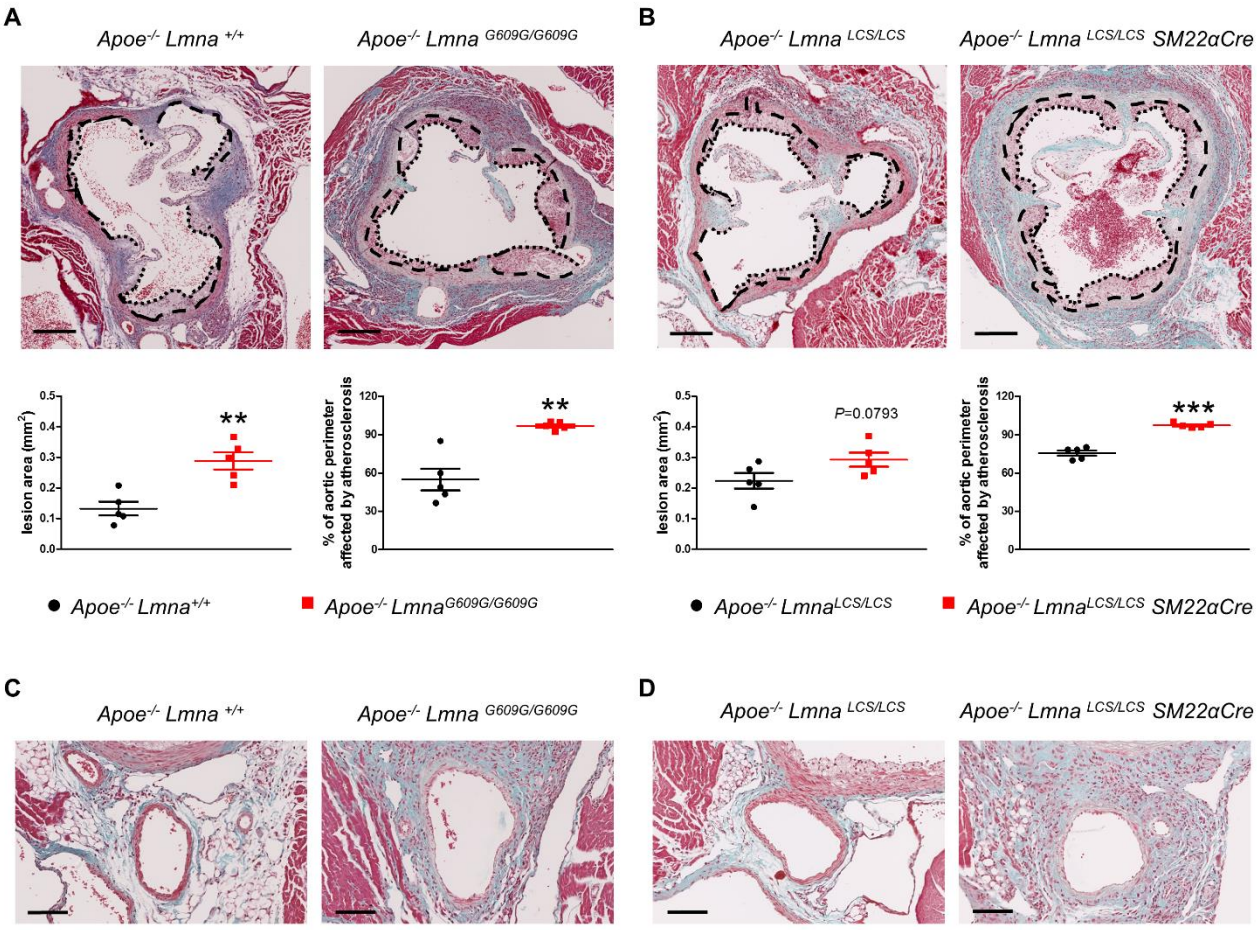

Figure 18. Fat-fed *Apoe*$^{-/-}$*Lmna*$^{G609G/G609G}$ and *Apoe*$^{-/-}$*Lmna*$^{LCS/LCS}$*SM22αCre* mice exhibit increased atherosclerosis in the aortic root together with inflammation of the adjacent cardiac tissue and coronary alterations (including vascular smooth muscle cell (VSMC) loss and thickening and inflammation of the adventitia). Mice were fed high-fat diet (HFD) for 8 weeks starting at 8 weeks of age. Serial sections of the aortic root were made and 3 different regions were stained with Masson's Trichrome. **(A, B)** Representative photographs of atheroma plaque in the aortic root of *Apoe*$^{-/-}$*Lmna*$^{G609G/G609G}$ **(A)** and *Apoe*$^{-/-}$*Lmna*$^{LCS/LCS}$*SM22αCre* mice **(B)**, and their corresponding controls; graphs show quantification of plaque area, with each point representing mean from three different aortic root regions (n=5). Scale bar, 200 μm. Dashed lines indicate medial perimeter (the last layer of elastin), dotted lines indicate the luminal surface of the atheroma plaque. **(C, D)** Representative photographs of coronary artery of *Apoe*$^{-/-}$*Lmna*$^{G609G/G609G}$ **(C)** and *Apoe*$^{-/-}$*Lmna*$^{LCS/LCS}$*SM22αCre* mice **(D)**, and their corresponding controls. Scale bar, 100 μm. Data in **A** and **B** are shown as mean ± SEM. Statistical analysis was performed by two-tailed *t*-test in **A** and **B**. ***P*<0.01, ****P*<0.001.

Importantly, *Apoe*$^{-/-}$*Lmna*$^{G609G/G609G}$ and *Apoe*$^{-/-}$*Lmna*$^{LCS/LCS}$*SM22αCre* atheromata showed features of vulnerable plaques. Accordingly, plaques of *Apoe*$^{-/-}$*Lmna*$^{G609G/G609G}$ and *Apoe*$^{-/-}$*Lmna*$^{LCS/LCS}$*SM22αCre* mice contained erythrocytes, indicating healed plaque fissure (**Fig. 19A, B, *top***), and some animals showed hemorrhage in the aortic valve itself (**Fig. 19A, *bottom***). We also found evidence of thrombus formation (**Fig. 19B, *bottom***), which might be related to plaque erosion.

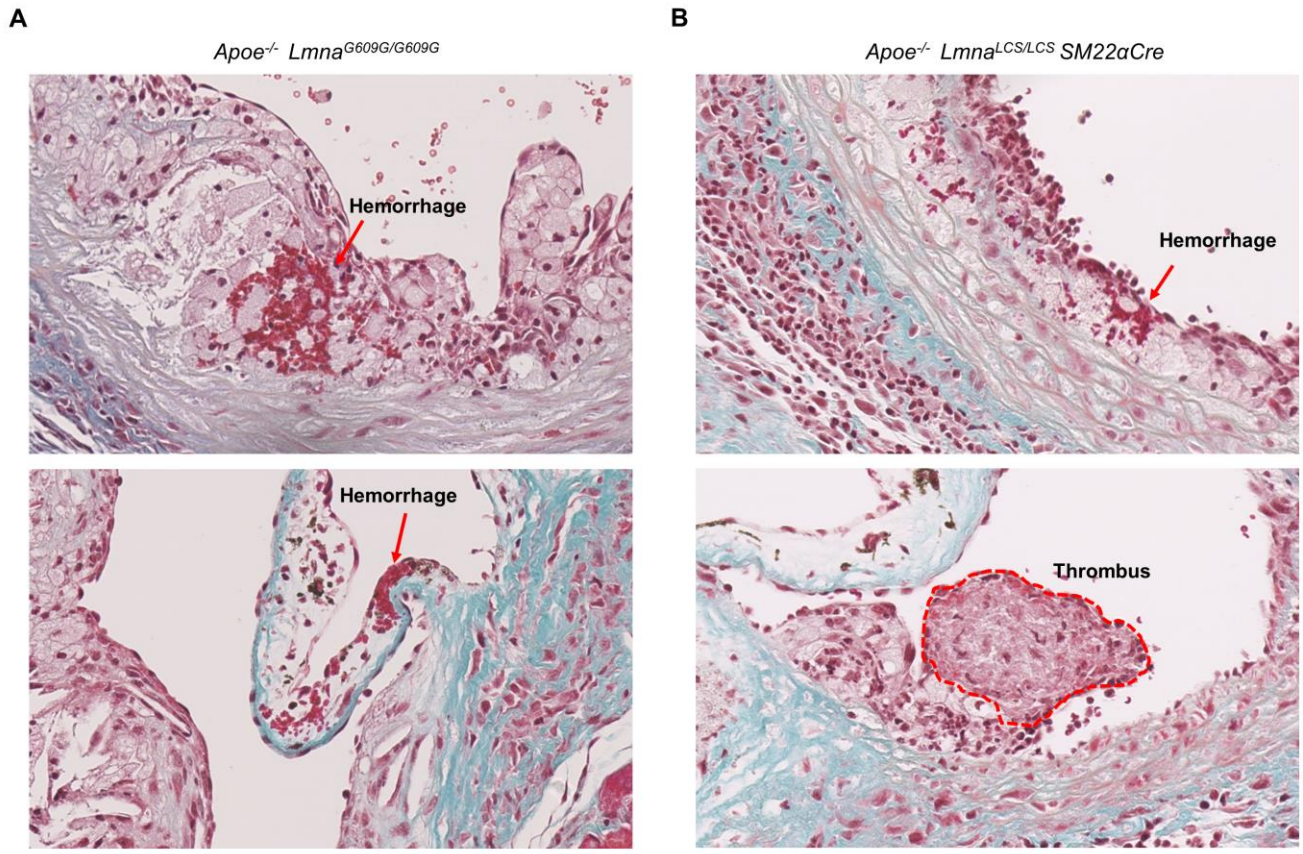

Figure 19. Atherosclerotic plaques of fat-fed *Apoe*$^{-/-}$*Lmna*$^{G609G/G609G}$ and *Apoe*$^{-/-}$*Lmna*$^{LCS/LCS}$*SM22αCre* mice show evidence of disruption. Mice were fed high-fat diet (HFD) for 8 weeks starting at 8 weeks of age. Serial sections of the aortic root were made and 3 different regions were stained with Masson's Trichrome. **(A)** An example of intraplaque (*top*) and intravalve hemorrhage (*bottom*) in *Apoe*$^{-/-}$*Lmna*$^{G609G/G6090G}$ mice. **(B)** An example of intraplaque hemorrhage (*top*) and thrombus formation (*bottom*) in *Apoe*$^{-/-}$*Lmna*$^{LCS/LCS}$*SM22αCre* mice.

IV.4. Progerin expression accelerates atherosclerosis in *Apoe*$^{-/-}$ mice fed normal chow

To gain insight into the kinetics of progerin-induced atherogenesis and to assess the role of cholesterol in this process, we performed experiments in mice fed normal chow. Histological examination of aortas from young, 8-week-old mice revealed no differences between the progeroid models and their controls, with tissue almost free of atherosclerosis and no obvious structural alterations (**Fig. 20A, C, E**). By contrast, atherosclerosis was evident in the thoracic aorta of 16-week-old *Apoe*$^{-/-}$*Lmna*$^{G609G/G609G}$ and *Apoe*$^{-/-}$*Lmna*$^{LCS/LCS}$*SM22αCre* mice, as well as regions with VSMC loss and increased collagen content (**Fig. 20B, D, E**). Notably, *Apoe*$^{-/-}$*Lmna*$^{LCS/LCS}$*SM22αCre* mice presented a marginally more pronounced vascular phenotype than *Apoe*$^{-/-}$*Lmna*$^{G609G/G609G}$ mice, with lipid retention in the media and adventitial thickening (data not shown), probably due to normal food intake and the consequent cholesterol level similar to that of the control mice.

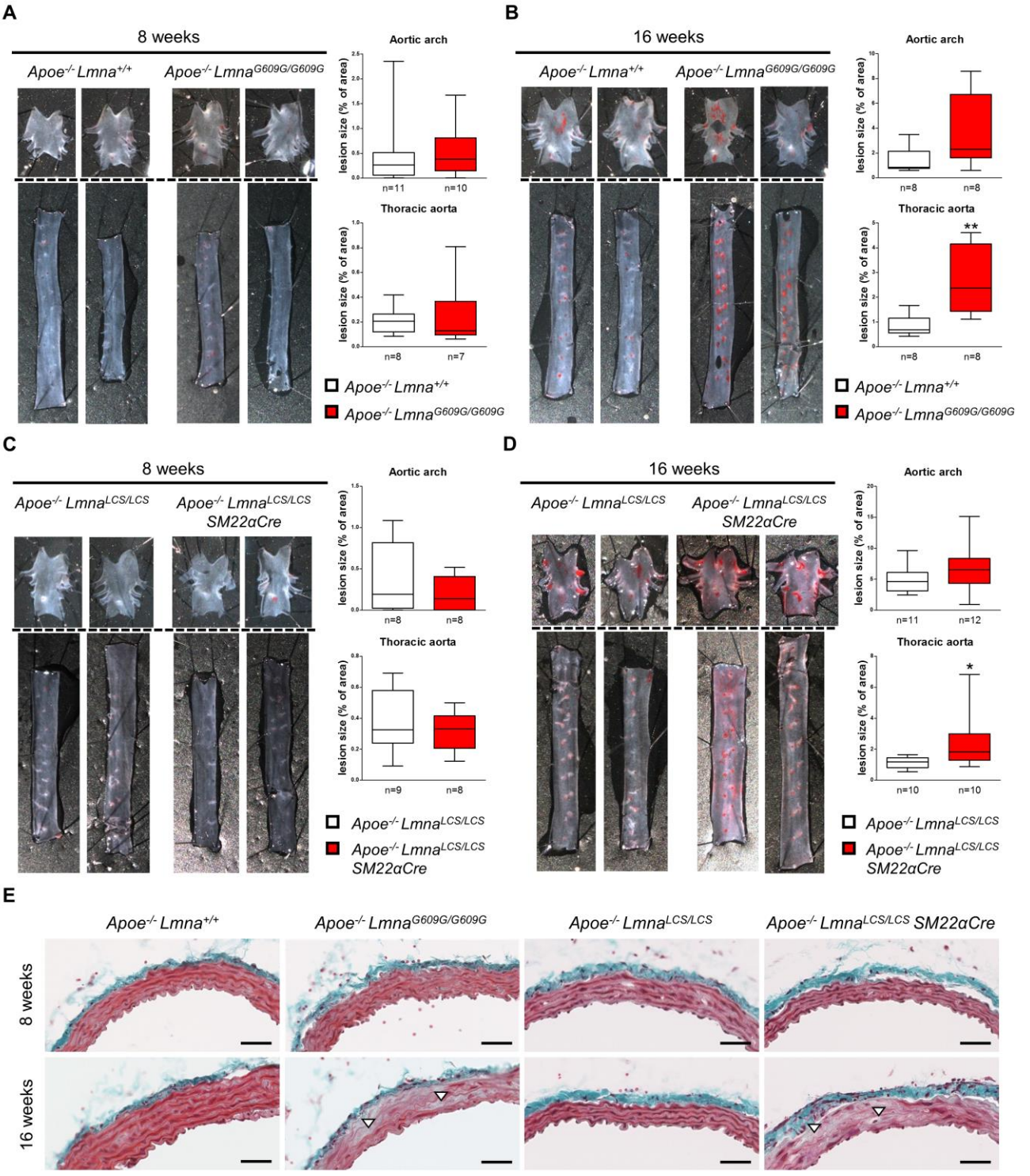

Figure 20. Vascular disease in 16-week-old but not 8-week-old *Apoe*$^{-/-}$*Lmna*$^{G609G/G609G}$ and *Apoe*$^{-/-}$*Lmna*$^{LCS/LCS}$*SM22αCre* mice fed normal chow. (A-D) Representative images of thoracic aortas stained with Oil Red O and quantification of atherosclerosis burden in mice of the indicated ages and genotypes. Controls for *Apoe*$^{-/-}$*Lmna*$^{G609G/G609G}$ and *Apoe*$^{-/-}$*Lmna*$^{LCS/LCS}$*SM22αCre* mice were *Apoe*$^{-/-}$*Lmna*$^{+/+}$ and *Apoe*$^{-/-}$*Lmna*$^{LCS/LCS}$, respectively. The number of mice is indicated below each graph. **(E)** Representative histology sections of Masson´s Trichrome-stained aortic arches extracted from mice of the indicated ages and genotypes fed normal chow diet. White arrowheads indicate regions with vascular smooth muscle cell loss. Scale bar, 50 μm. Data in **A-D** are shown as median with interquartile range and minima and maxima. Statistical differences were analyzed by the two-tailed Mann-Whitney test. **P*<0.05, ***P*<0.01.

Our findings in both the ubiquitous and the VSMC-specific progeric mouse models fed either normal chow or HFD indicate that VSMCs are particularly sensitive to progerin accumulation, which leads to cell damage and death that is accelerated in the presence of other stress stimuli, including high cholesterol (**Fig. 21**). Mechanical stress also seems to play an important role in this process because VSMC loss differs between distinct aortic regions and positively correlates with high shear stress (e.g., VSMC loss is higher in the aortic arch than in the thoracic aorta, data not shown). Dead VSMCs are replaced by extracellular matrix components, which retain lipids and lipoproteins. Additionally, pro-inflammatory signals from dead cells may activate the vascular endothelium and enhance its permeability for the circulating lipoprotein particles. Cell debris and lipid/lipoprotein deposits trigger inflammation and thickening of the adventitia and accelerate atheroma plaque formation. Finally, vulnerable plaque disruption may lead to cardiovascular events, such as myocardial infarction, and cause premature death.

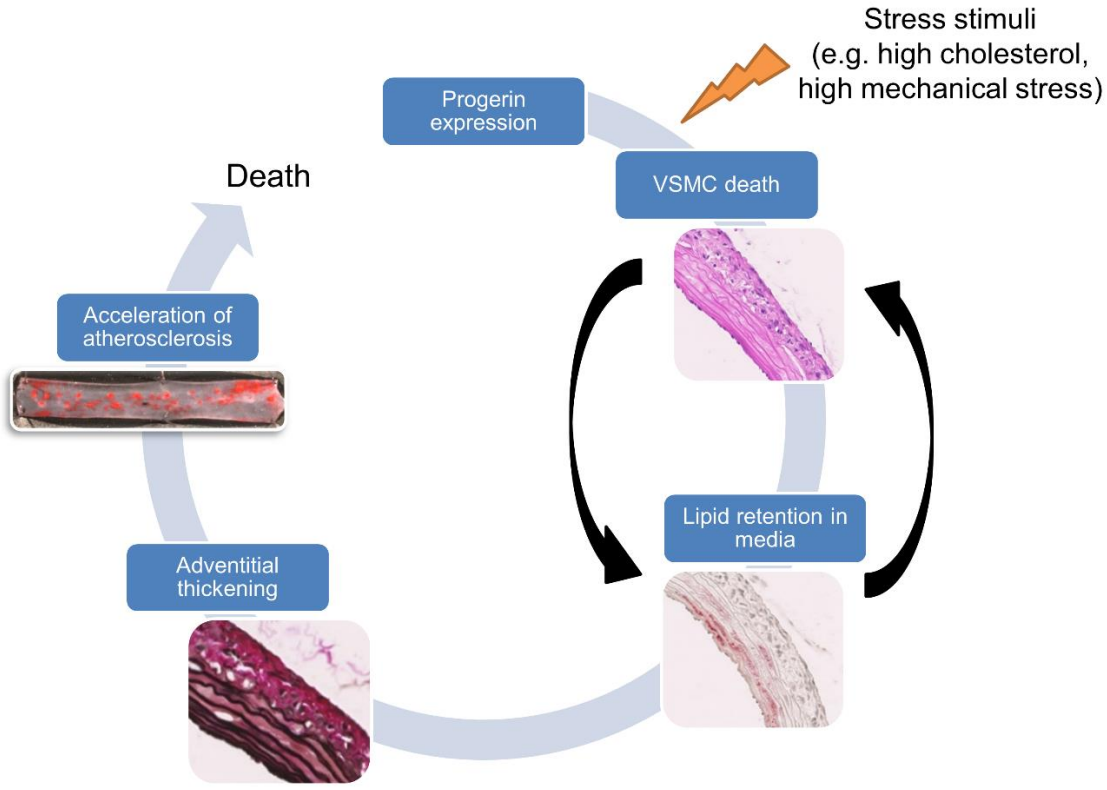

Figure 21. Proposed mechanism of vascular smooth muscle cell (VSMC)-specific progerin toxicity leading to accelerated atherosclerosis and premature death. Progerin expression triggers VSMC death, which is accelerated in the presence of other stress stimuli, such as high cholesterol or high mechanical stress. Dead VSMCs are replaced with extracellular matrix, which retains more lipids and lipoproteins. This may create a vicious circle – the more lipids are accumulated in the media, the more VSMCs die (and *vice versa*). Cell death and lipid/lipoprotein deposits drive inflammation and thickening of the adventitia and accelerate atherosclerosis. Finally, vulnerable plaques lead to death, probably due to a cardiovascular event, such as myocardial infarction.

IV.5. Progerin expression in VSMCs leads to progressive hypotension

The ubiquitous and VSMC-specific models of progeria presented a very similar aortic phenotype, both leading to aortic luminal dilatation and plaque buildup. We therefore hypothesized that progerin expression might affect blood pressure. To address this, mice were fed normal chow and blood pressure was measured at approximately 16 weeks of age during 5 consecutive days. Blood pressure was not different between *Apoe*$^{-/-}$*Lmna*$^{G609G/G609G}$ mice and *Apoe*$^{-/-}$*Lmna*$^{+/+}$ controls (**Fig. 22A**); however, *Apoe*$^{-/-}$*Lmna*$^{G609G/G609G}$ mice developed severe bradycardia (**Fig. 22A**), which has been previously reported for progeroid *Lmna*$^{G609G/G609G}$ and *Zmpste24*$^{-/-}$ mice (*30, 59*). Furthermore, diastolic blood pressure in *Apoe*$^{-/-}$*Lmna*$^{LCS/LCS}$*SM22αCre* mice, which showed more pronounced vasculopathy, was significantly lower than in *Apoe*$^{-/-}$*Lmna*$^{LCS/LCS}$ littermates (**Fig. 22B**). Follow-up of the *Apoe*$^{-/-}$ *Lmna*$^{LCS/LCS}$*SM22αCre* animals showed a further significant decline in both systolic and diastolic blood pressure at 26 weeks of age (**Fig. 22C**).

These results conflict with findings in progeria patients. Specifically, two different studies reported an increased incidence of hypertension in HGPS children (*17, 23*); however, those results could be considered biased. In the first work by Merideth *et al.* only the highest blood pressure readings were reported, although this parameter was measured 6 times during the course of the study (*17*). It is puzzling why the authors elected to report and analyze only the maximum blood pressure values instead of the mean or median, raising concerns about the validity of their conclusions. The second study by Gerhard-Herman *et al.* reported that blood pressure values were increased in around 30% of the patients as compared with age-matched controls (*23*). When height-age standards were applied to account for the growth impairment, systolic and diastolic blood pressures were higher in approximately half of the patients. Nevertheless, the authors did not report how many normotensive and hypotensive children were in the studied cohort. They also did not provide extensive details about experimental design, for example, the number of times that blood pressure was measured and how the data were analyzed. In addition, some published reports describing HGPS phenotypes include as supplementary information all the blood pressure measurements registered during the study and many of these values are below the normal range for age-matched controls (*20*). Based on these observations in patients and our findings in mice, more studies are warranted to elucidate the effect of progerin on blood pressure in children with HGPS, with special emphasis on hypotension and occasional hypertension incidence.

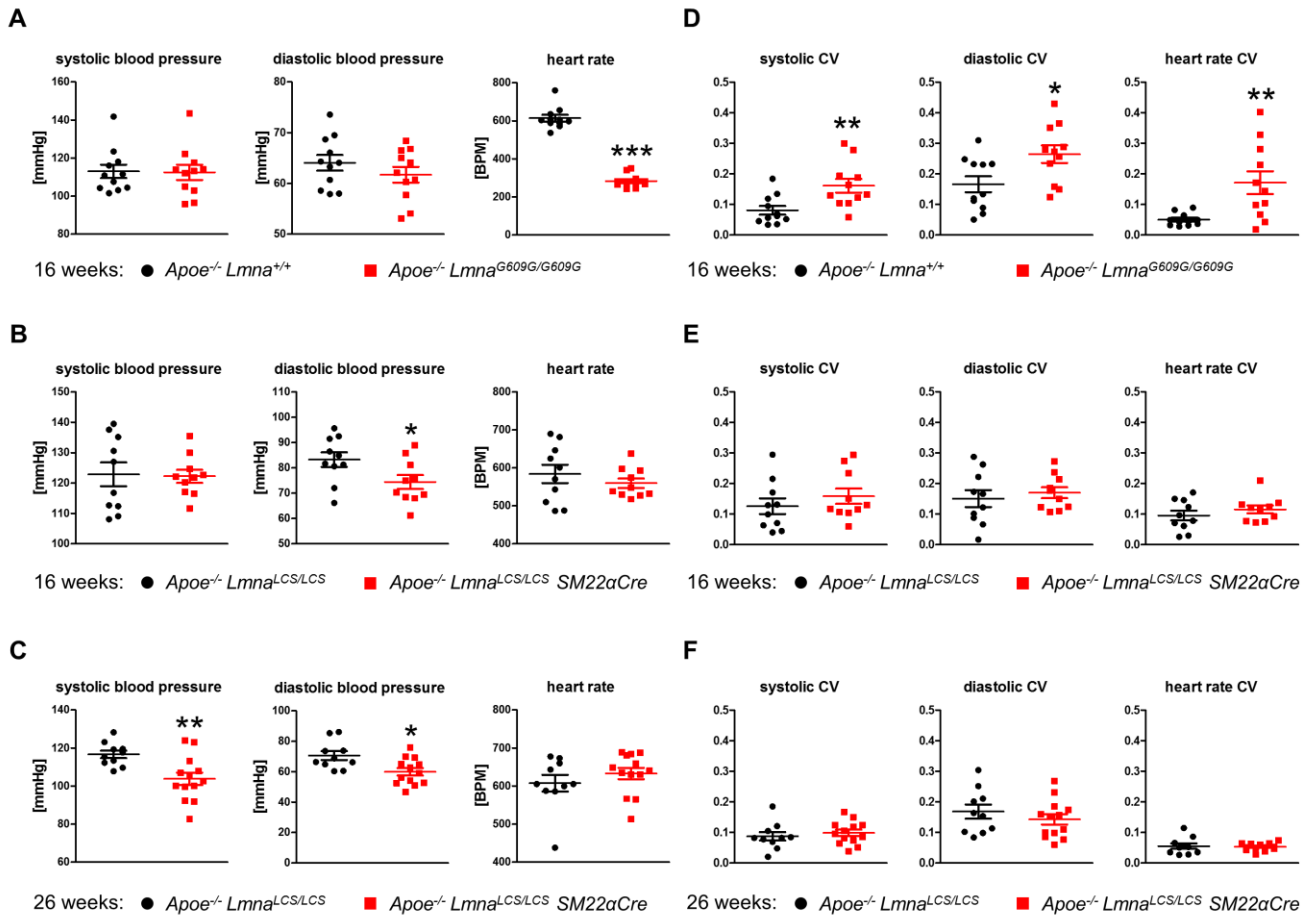

Figure 22. *Apoe*$^{-/-}$*Lmna*$^{LCS/LCS}$*SM22αCre* mice develop progressive hypotension while *Apoe*$^{-/-}$*Lmna*$^{G609G/G609G}$ mice display blood pressure and heart rate variability. Blood pressure and heart rate measurements were performed in conscious 16-week-old (for both progeria models) and 26-week-old (for VSMC-specific progeria model) mice fed normal chow diet. **(A, B, C)** Heart rate, systolic and diastolic blood pressure analysis for *Apoe*$^{-/-}$*Lmna*$^{G609G/G609G}$, *Apoe*$^{-/-}$*Lmna*$^{LCS/LCS}$*SM22αCre*, *Apoe*$^{-/-}$*Lmna*$^{+/+}$ and *Apoe*$^{-/-}$*Lmna*$^{LCS/LCS}$mice. **(C, D, E)** Variability in the heart rate, systolic and diastolic blood pressure for *Apoe*$^{-/-}$*Lmna*$^{G609G/G609G}$, *Apoe*$^{-/-}$*Lmna*$^{LCS/LCS}$*SM22αCre*, *Apoe*$^{-/-}$*Lmna*$^{+/+}$ and *Apoe*$^{-/-}$*Lmna*$^{LCS/LCS}$mice measured as coefficient of variation (CV). n=10-13. Data are presented as mean ± SEM. Statistical analysis was performed by two-tailed *t*-test. **P*<0.05, ***P*<0.01, ****P*<0.001.

Although *Apoe*$^{-/-}$*Lmna*$^{G609G/G609G}$ mice, unlike *Apoe*$^{-/-}$*Lmna*$^{LCS/LCS}$*SM22αCre* mice, did not develop prominent hypotension until 16 weeks of age, we observed a substantial instability and variability in heart rate and blood pressure (**Fig. 22D-F**). Blood pressure variability is defined as changes in blood pressure over time (hours, days, weeks, months etc.), whereas instability refers to transient oscillations in blood pressure, typically in response to pain, stress or change in posture, and adds to total variability. Variability and instability in blood pressure in humans is associated with higher risk of vascular events (such as stoke) related to plaque rupture (*26*, *27*). Thus, blood pressure instability and variability in *Apoe*$^{-/-}$*Lmna*$^{G609G/G609G}$ mice could be linked to intraplaque hemorrhages observed in

those animals upon HFD feeding (see subsection IV.3). However, intraplaque hemorrhages were also present in HFD-fed *Apoe*$^{-/-}$*Lmna*$^{LCS/LCS}$*SM22αCre* mice, which do not show blood pressure variability (at least at the same age). Since blood pressure measurements were performed in animals fed normal chow presenting only moderate vasculopathy, the relationship between plaque disruption and blood pressure variation in progeria mice should be further defined by preforming blood pressure analysis in HFD-fed progeroid mice.

IV.6. *Apoe*$^{-/-}$*Lmna*$^{G609G/G609G}$ mice develop arrhythmias

Blood pressure measurements in conscious *Apoe*$^{-/-}$*Lmna*$^{G609G/G609G}$ mice revealed heart rate instability and variability, suggesting cardiac involvement (**Fig. 22D**). Moreover, a previous study has described electrical cardiac alterations in the *Zmpste24*-deficient (*Zmpste24*$^{-/-}$) progeria mouse model (*30*). Given this information, we performed ECG in both ubiquitous and VSMC-specific progeria models. In accordance with the results from conscious animals (subsection IV.5), 16-week-old anesthetized *Apoe*$^{-/-}$*Lmna*$^{G609G/G609G}$ mice presented severe bradycardia (**Fig. 23A**) together with prolonged QRS, QT and QTc intervals (**Fig. 23A**). Importantly, 3 out of 7 mice showed arrhythmias (**Fig. 23B**), which might explain the blood pressure instability and variability described in the previous subsection. This result is also consistent with the observation that HGPS patients show repolarization abnormalities resulting in an increased risk of arrhythmias and premature death (*30*).

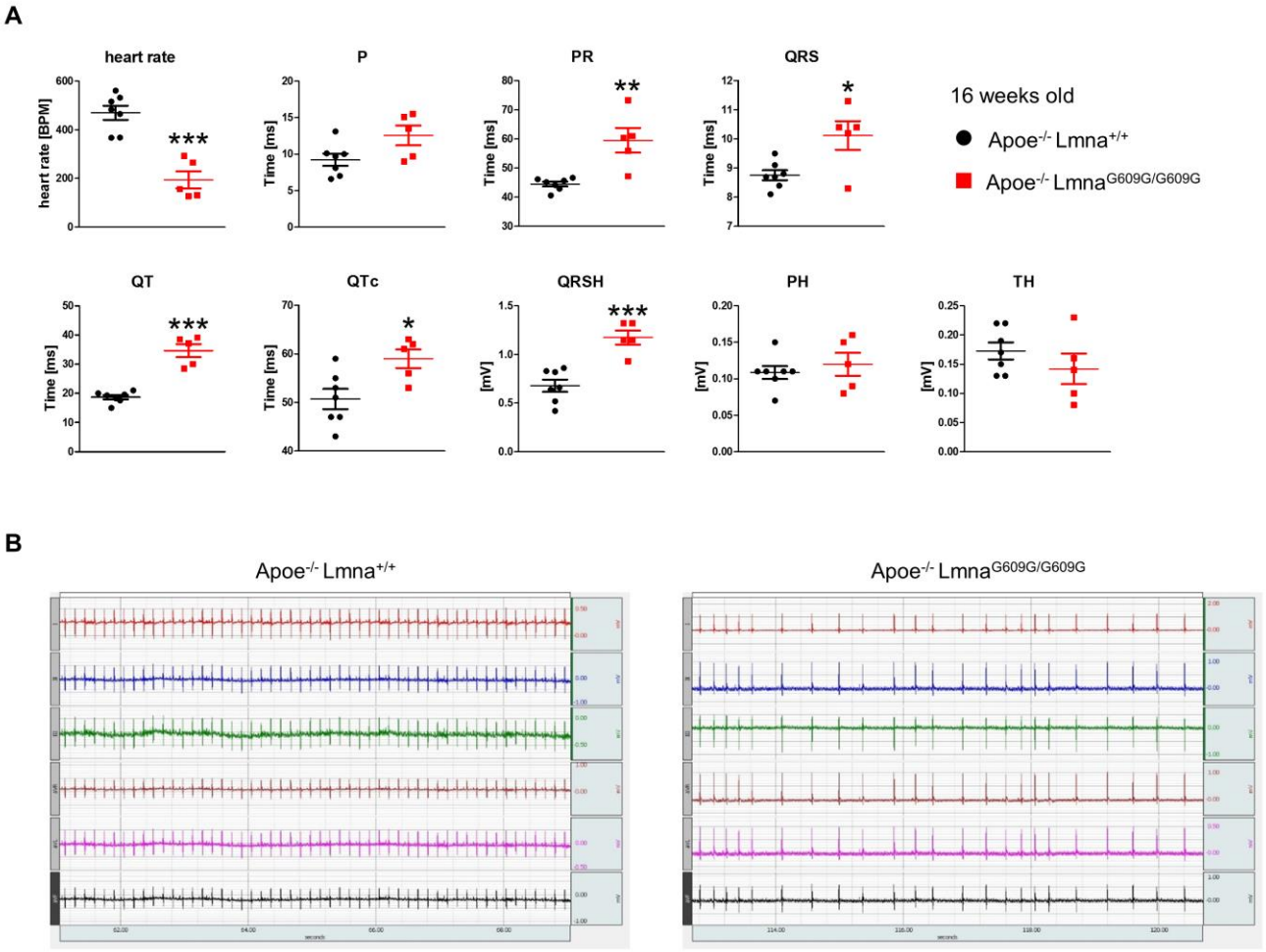

Figure 23. ***Apoe*$^{-/-}$*Lmna*$^{G609G/G609G}$ **mice develop cardiac electrical defects resulting in arrhythmias.** Electrocardiogram (ECG) was performed in isoflurane-anesthetized 16-week-old mice fed normal chow. **(A)** ECG parameters for *Apoe*$^{-/-}$*Lmna*$^{G609G/G609G}$ (n=5) and *Apoe*$^{-/-}$*Lmna*$^{+/+}$ (n=7) mice. **(B)** Representative images of ECG recording for *Apoe*$^{-/-}$*Lmna*$^{+/+}$ (*left*) and *Apoe*$^{-/-}$*Lmna*$^{G609G/G609G}$ (*right*) mice. *Apoe*$^{-/-}$*Lmna*$^{G609G/G609G}$ mice exhibit bradycardia and arrhythmia. QRSH, PH, TH indicate amplitude of QRS complex, PH and TH waves, respectively. Data are presented as mean ± SEM. Statistical analysis was performed by two-tailed *t*-test. **P*<0.05, ***P*<0.01, ****P*<0.001.

In contrast to the findings with *Apoe*$^{-/-}$*Lmna*$^{G609G/G609G}$ mice, 16-week-old *Apoe*$^{-/-}$*Lmna*$^{LCS/LCS}$*SM22αCre* mice did not present any evident ECG alterations (**Fig. 24A**). However, follow-up of these animals revealed low voltage of QRS complex at 26 weeks of age (**Fig. 24B**), which might indicate loss of viable myocardial tissue, for example, due to myocardial infarction. Low QRS voltage on the ECG is a marker of the severity of heart failure, and is a risk factor for adverse outcomes in patients with this condition (*160*). Likewise, many of the *Apoe*$^{-/-}$*Lmna*$^{LCS/LCS}$*SM22αCre* mice exhibited T wave fattening or inversion (**Fig. 24B** and data not shown), further supporting the notion that these animals may have cardiac involvement as they age, probably associated with progressive atherosclerosis. Indeed, acute myocardial ischemia in mice has been related to the inverted T wave on

the ECG (*161*). Remarkably, studies in HGPS patients revealed ST depression/elevation and negative and biphasic T waves, especially evident at advanced stages of the disease (*17*, *30*).

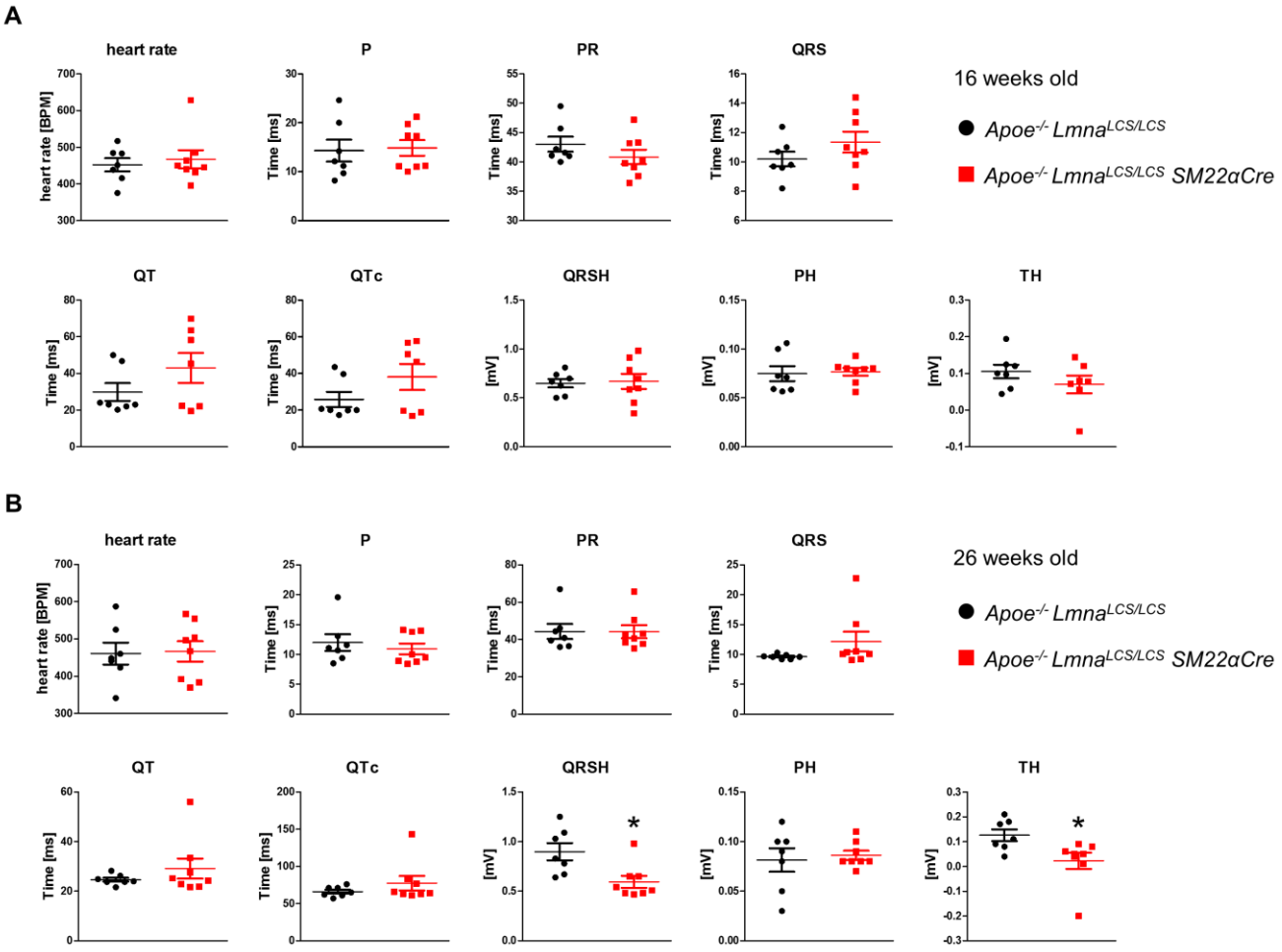

Figure 24. ***Apoe*$^{-/-}$*Lmna*$^{LCS/LCS}$*SM22αCre*** **mice show normal cardiac electrical function at 16 weeks of age and lower voltage of QRS complex and T wave at 26 weeks of age compared with** ***Apoe*$^{-/-}$*Lmna*$^{LCS/LCS}$** **littermates.** Electrocardiogram (ECG) was performed in isoflurane-anesthetized 16- and 26-week-old mice fed normal chow diet. **(A)** ECG parameters for 16-week-old *Apoe*$^{-/-}$*Lmna*$^{LCS/LCS}$*SM22αCre* (n=7) and *Apoe*$^{-/-}$*Lmna*$^{LCS/LCS}$ (n=7) mice. **(B)** ECG parameters for 26-week-old *Apoe*$^{-/-}$*Lmna*$^{LCS/LCS}$*SM22αCre* (n=8) and *Apoe*$^{-/-}$*Lmna*$^{LCS/LCS}$ (n=7) mice. QRSH, PH, TH indicate amplitude of QRS complex, PH and TH waves, respectively. Data are presented as mean ± SEM. Statistical analysis was performed by two-tailed *t*-test. **P*<0.05.

IV.7. *Apoe*$^{-/-}$*Lmna*$^{LCS/LCS}$*SM22αCre* die from atherosclerosis-related causes

Despite an almost identical vascular phenotype, ubiquitous and VSMC-specific atherosclerosis-prone progeria models showed different median survival (18.5 weeks *versus* 34.3 weeks, respectively). *Apoe*$^{-/-}$*Lmna*$^{LCS/LCS}$*SM22αCre* mice, which did not display any overt aging phenotype, died suddenly between 26 and 66 weeks of age. Interestingly, *Lmna*$^{LCS/LCS}$*SM22αCre* mice with an intact *Apoe* gene also presented VSMC loss and aortic adventitial thickening (**Fig. 25A**), but did not develop

atherosclerosis and had a normal life span (**Fig. 25B**). These findings point to progerin-driven atherosclerosis as the main cause of death in *Apoe*$^{-/-}$*Lmna*$^{LCS/LCS}$*SM22αCre* mice. By contrast, *Apoe*$^{-/-}$ *Lmna*$^{G609G/G609G}$ mice progressively lost fat tissue, developed bone problems and muscle weakness, and died between 15 and 24 weeks of age, a median survival very similar to that of atherosclerosis-free *Lmna*$^{G609G/G609G}$ mice. These results strongly suggest that *Apoe*$^{-/-}$*Lmna*$^{G609G/G609G}$ mice and *Lmna*$^{G609G/G609G}$ mice die from the same cause, which is probably independent of atherosclerosis. These observations, together with distinct cardiac alterations present in both atherosclerosis-susceptible progeria models, lead us to hypothesize that the cause of death is different in ubiquitous and VSMC-specific progeria models, at least in the majority of the cases.

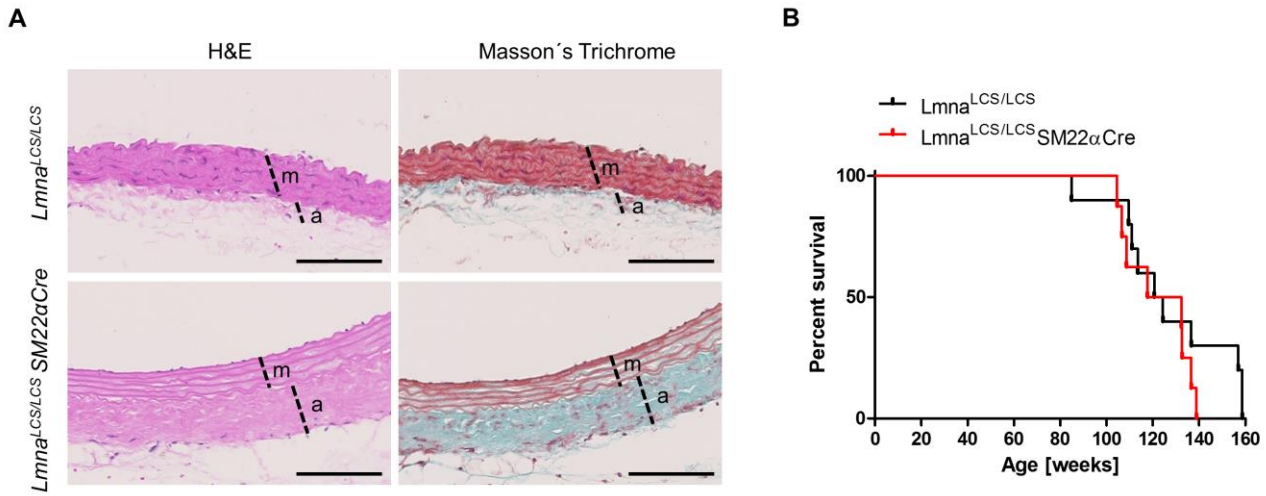

Figure 25. *Lmna*$^{LCS/LCS}$*SM22αCre* mice without atherosclerosis-susceptible background show aortic vascular smooth muscle cell loss and adventitial thickening but have normal lifespan. *Lmna*$^{LCS/LCS}$ mice were used as controls. **(A)** Representative histology sections of aortic arches stained with hematoxylin & eosin (H&E) and Masson´s Trichrome. Mice fed normal chow were sacrificed at 38 weeks of age. m: media, a: adventitia. Scale bar, 100 µm. **(B)** Kaplan-Meier survival curves of *Lmna*$^{LCS/LCS}$*SM22αCre* mice (n=8) and *Lmna*$^{LCS/LCS}$ mice (n=10). Statistical differences in **B** were analyzed using the log-rank test.

To analyze cardiovascular alterations, which may reveal the cause of death, we collected aorta, heart and brain from normal chow-fed *Apoe*$^{-/-}$*Lmna*$^{G609G/G609G}$ and *Apoe*$^{-/-}$*Lmna*$^{LCS/LCS}$*SM22αCre* mice at an age close to their maximum survival (21-23 weeks for ubiquitous and 51 weeks for VSMC-specific model). Atherosclerosis burden in the aortic arch and thoracic aorta was significantly higher in *Apoe*$^{-/-}$*Lmna*$^{G609G/G609G}$ mice than in *Apoe*$^{-/-}$*Lmna*$^{+/+}$ controls (**Fig. 26A**). When *Apoe*$^{-/-}$*Lmna*$^{LCS/LCS}$ and *Apoe*$^{-/-}$*Lmna*$^{LCS/LCS}$*SM22αCre* mice were compared, *Apoe*$^{-/-}$*Lmna*$^{LCS/LCS}$*SM22αCre* mice showed increased lesion formation in the thoracic aorta (**Fig. 26B**); however no significant differences were found in the aortic arch (**Fig. 26B**), likely because this athero-prone aortic region is saturated with

plaques at 51 weeks (1 year) of age. Importantly, vascular pathology was much more severe in *Apoe*$^{-/-}$*Lmna*$^{LCS/LCS}$*SM22αCre* mice than in *Apoe*$^{-/-}$*Lmna*$^{G609G/G609G}$ mice (**Fig. 26C**).

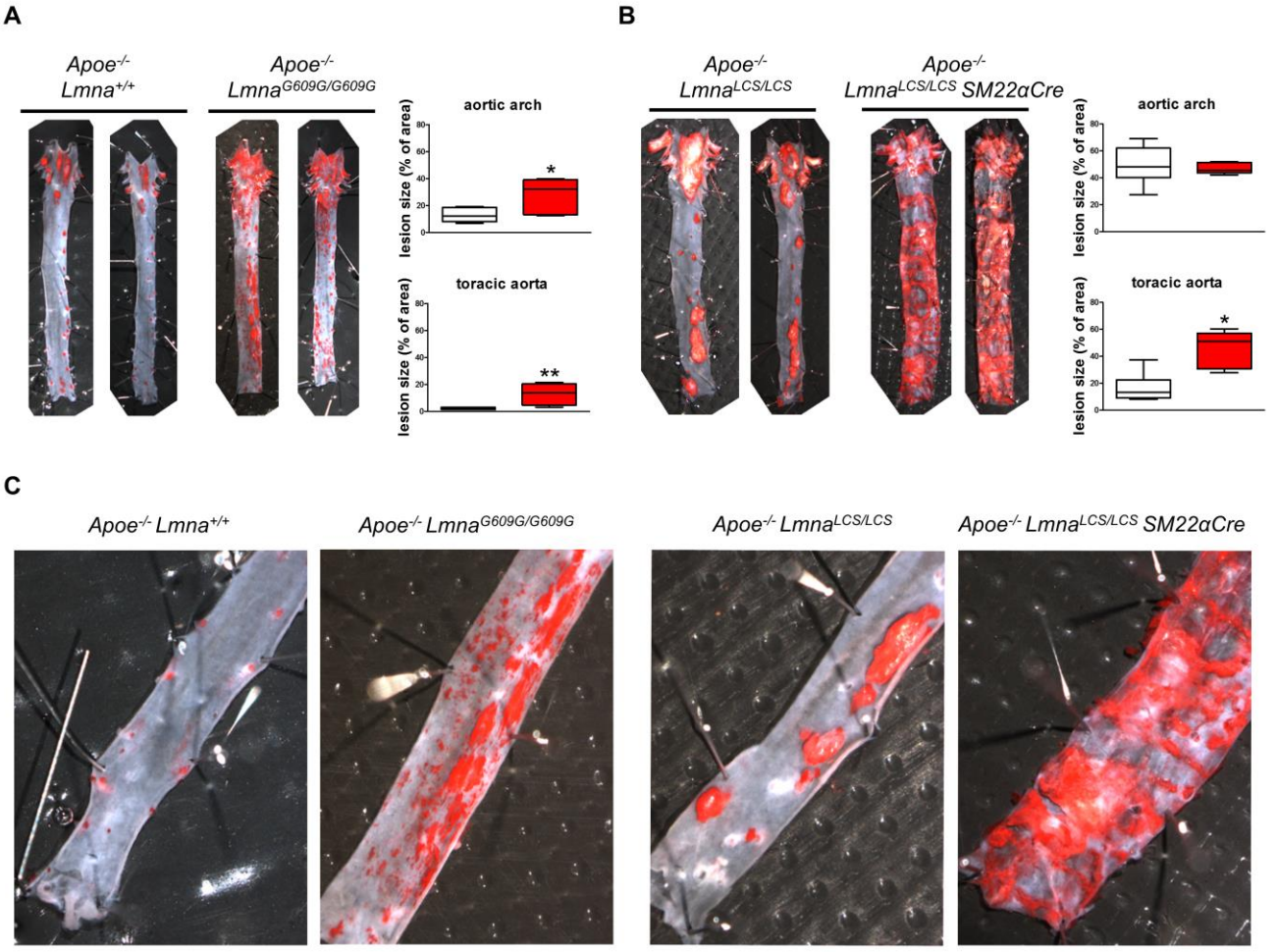

Figure 26. ***Apoe*$^{-/-}$*Lmna*$^{LCS/LCS}$*SM22αCre*** **mice have a more severe vascular phenotype than** ***Apoe*$^{-/-}$*Lmna*$^{G609G/G609G}$****, both at ages close to their maximum survival.** Mice were fed normal chow and sacrificed at 21-23 weeks of age (*Apoe*$^{-/-}$*Lmna*$^{G609G/G609G}$ and control *Apoe*$^{-/-}$*Lmna*$^{+/+}$ mice) and 51 weeks of age (*Apoe*$^{-/-}$*Lmna*$^{LCS/LCS}$*SM22αCre* and control *Apoe*$^{-/-}$*Lmna*$^{LCS/LCS}$ mice). **(A)** Representative aortas of *Apoe*$^{-/-}$*Lmna*$^{G609G/G609G}$ and *Apoe*$^{-/-}$*Lmna*$^{+/+}$ mice stained with Oil Red O (ORO); graphs show quantification of atherosclerosis burden in the aortic arch and thoracic aorta; n=6. **(B)** Representative aortas of *Apoe*$^{-/-}$*Lmna*$^{LCS/LCS}$*SM22αCre* and *Apoe*$^{-/-}$*Lmna*$^{LCS/LCS}$ mice stained with ORO; graphs show quantification of atherosclerosis burden in the aortic arch and thoracic aorta; n=5-6. **(C)** Higher magnification of ORO-stained thoracic aortas of the indicated genotypes. Data are shown as median with interquartile range and minima and maxima. Statistical differences were analyzed by two-tailed Mann-Whitney test. **P*<0.05, ***P*<0.01.

We next performed a more detailed analysis of the atherosclerotic plaques in the aortic root. Both models exhibited aortic valve degeneration characterized by loss of cells and fibrosis (data not shown**)**. *Apoe*$^{-/-}$*Lmna*$^{G609G/G609G}$ plaques were generally immature with intraplaque hemorrhages, which were absent in the age-matched controls (**Fig. 27**). Two out of six *Apoe*$^{-/-}$*Lmna*$^{G609G/G609G}$ animals showed signs of coronary atherosclerosis (data not shown). In *Apoe*$^{-/-}$*Lmna*$^{LCS/LCS}$*SM22αCre* mice,

atheromas were mature, severely calcified, and many of them presented chondroid metaplasia (**Fig. 27**). The atheromas that were not calcified showed thin fibrous caps and large necrotic cores (**Fig 27**), characteristics of vulnerable plaques. The majority of analyzed *Apoe*$^{-/-}$*Lmna*$^{LCS/LCS}$*SM22αCre* mice developed coronary atherosclerosis (data not shown).

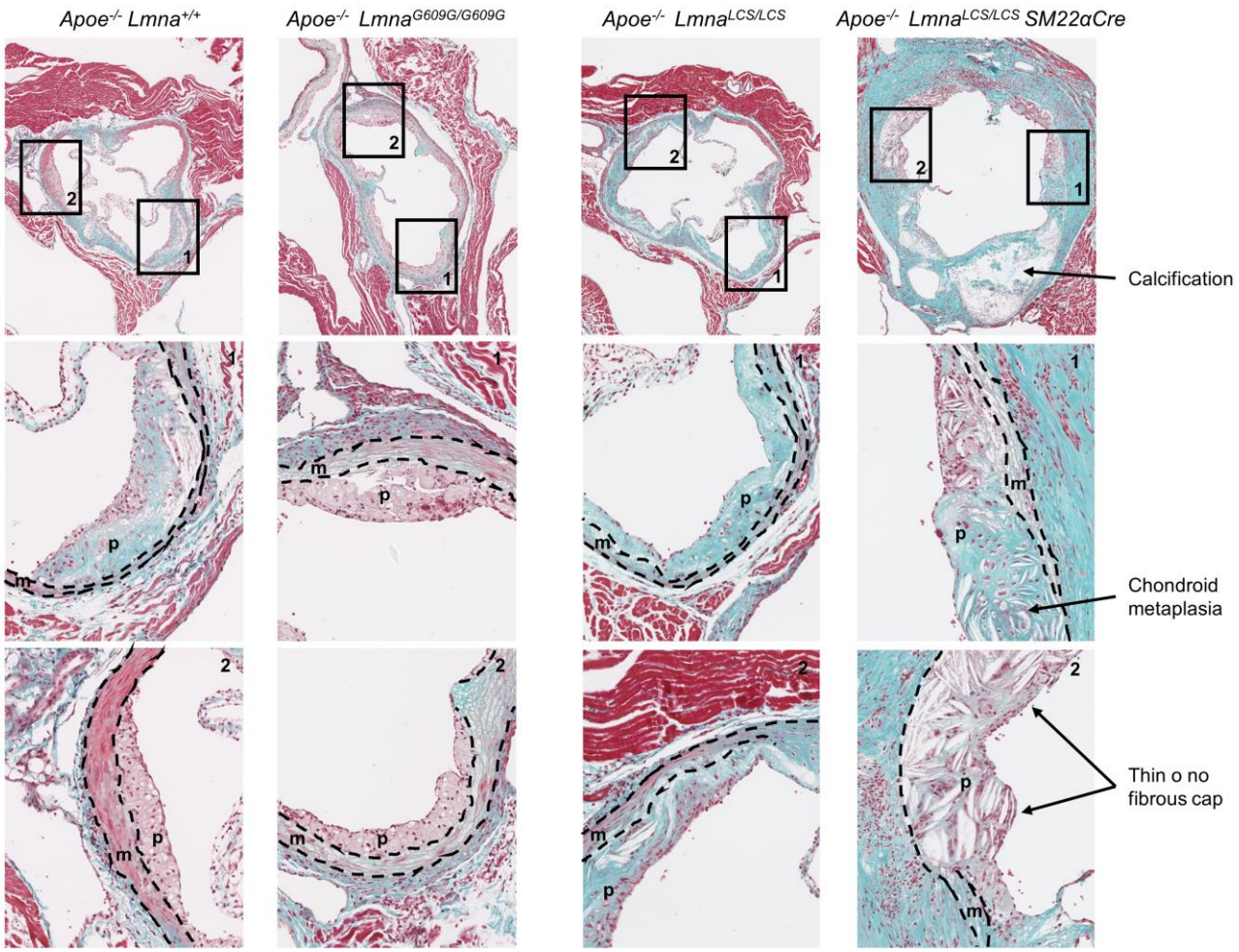

Figure 27. *Apoe*$^{-/-}$*Lmna*$^{LCS/LCS}$*SM22αCre* mice have more severe atherosclerosis in the aortic root than *Apoe*$^{-/-}$*Lmna*$^{G609G/G609G}$, both at ages close to their maximum survival. Mice were fed normal chow and sacrificed at 21-23 weeks of age (*Apoe*$^{-/-}$*Lmna*$^{G609G/G609G}$ and control *Apoe*$^{-/-}$*Lmna*$^{+/+}$ mice) and 51 weeks of age (*Apoe*$^{-/-}$*Lmna*$^{LCS/LCS}$*SM22αCre* and control *Apoe*$^{-/-}$*Lmna*$^{LCS/LCS}$ mice). Representative aortic root sections of *Apoe*$^{-/-}$*Lmna*$^{G609G/G609G}$, *Apoe*$^{-/-}$*Lmna*$^{+/+}$, *Apoe*$^{-/-}$*Lmna*$^{LCS/LCS}$*SM22αCre* and *Apoe*$^{-/-}$*Lmna*$^{LCS/LCS}$ mice stained with Masson´s Trichrome. Middle and bottom panels show higher magnification of atherosclerotic plaques. m: media, p: plaque.

We also performed histopathological evaluation of the heart. *Apoe*$^{-/-}$*Lmna*$^{G609G/G609G}$ hearts were characterized by cardiomyocyte vacuolization that was absent in *Apoe*$^{-/-}$*Lmna*$^{+/+}$, *Apoe*$^{-/-}$*Lmna*$^{LCS/LCS}$*SM22αCre* and *Apoe*$^{-/-}$*Lmna*$^{LCS/LCS}$ mice (**Fig. 28**). This feature was previously described in progeroid *Zmpste24*$^{-/-}$ mice (*43*). Importantly, cardiomyocyte vacuolization is frequently observed in the border zones of infarcted heart tissue and it is a marker of ischemic injury (*162-164*).

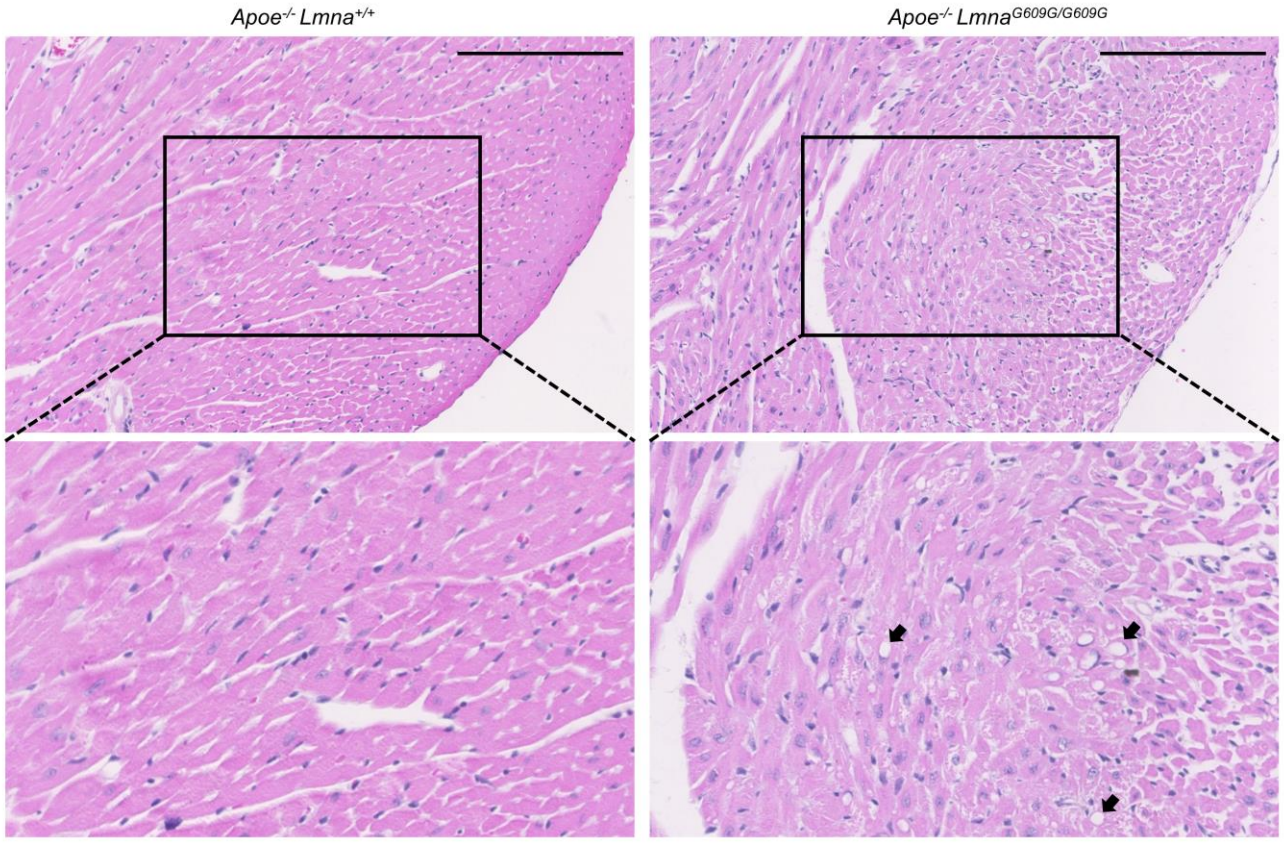

Figure 28. *Apoe*$^{-/-}$*Lmna*$^{G609G/G609G}$ hearts exhibit cardiomyocyte vacuolization. Mice fed normal chow were sacrificed at 21-23 weeks of age (close to their maximum survival). Photographs show hematoxylin & eosin-stained cardiac tissue of *Apoe*$^{-/-}$ *Lmna*$^{+/+}$ (*left*) and *Apoe*$^{-/-}$ *Lmna*$^{G609G/G609G}$ (*right*) mice. Scale bar 200 µm. Black arrows indicate examples of cardiomyocyte vacuolization.

Furthermore, two out of six *Apoe*$^{-/-}$*Lmna*$^{G609G/G609G}$ hearts showed coronary atherosclerosis (**Table 1**) and a collagen scar in the septum, indicative of a non-fatal infarct (**Fig. 29**). Nevertheless, no alterations were detected in half of the animals analyzed (**Table 1**), except for vacuolization of cardiomyocytes.

Genotype	Intimal hyperplasia	Coronary atherosclerosis	Perivascular fibrosis	Interstitial fibrosis	Calcification
Apoe$^{-/-}$*Lmna*$^{+/+}$	1/6	0/6	0/6	0/6	0/6
Apoe$^{-/-}$*Lmna*$^{G609G/G609G}$	3/6	2/6	0/6	2/6	0/6
Apoe$^{-/-}$*Lmna*$^{LCS/LCS}$	2/6	1/6	1/6	0/6	0/6
Apoe$^{-/-}$*Lmna*$^{LCS/LCS}$*SM22αCre*	4/5	4/5	5/5	5/5	2/5

Table 1. *Apoe*$^{-/-}$*Lmna*$^{LCS/LCS}$*SM22αCre* mice exhibit a more severe cardiac phenotype than *Apoe*$^{-/-}$*Lmna*$^{G609G/G609G}$ both at ages close to their maximum survival. Mice fed normal chow were sacrificed at 21-23 weeks of age for *Apoe*$^{-/-}$ *Lmna*$^{G609G/G609G}$ (and control *Apoe*$^{-/-}$*Lmna*$^{+/+}$) and 51 weeks of age for *Apoe*$^{-/-}$*Lmna*$^{LCS/LCS}$*SM22αCre* (and control *Apoe*$^{-/-}$ *Lmna*$^{LCS/LCS}$) mice. Serial sections of the heart (at 6 different levels of the apex) were prepared and stained with hematoxylin & eosin and Masson´s Trichrome. Cardiac pathology was assessed in 5-6 mice per genotype.

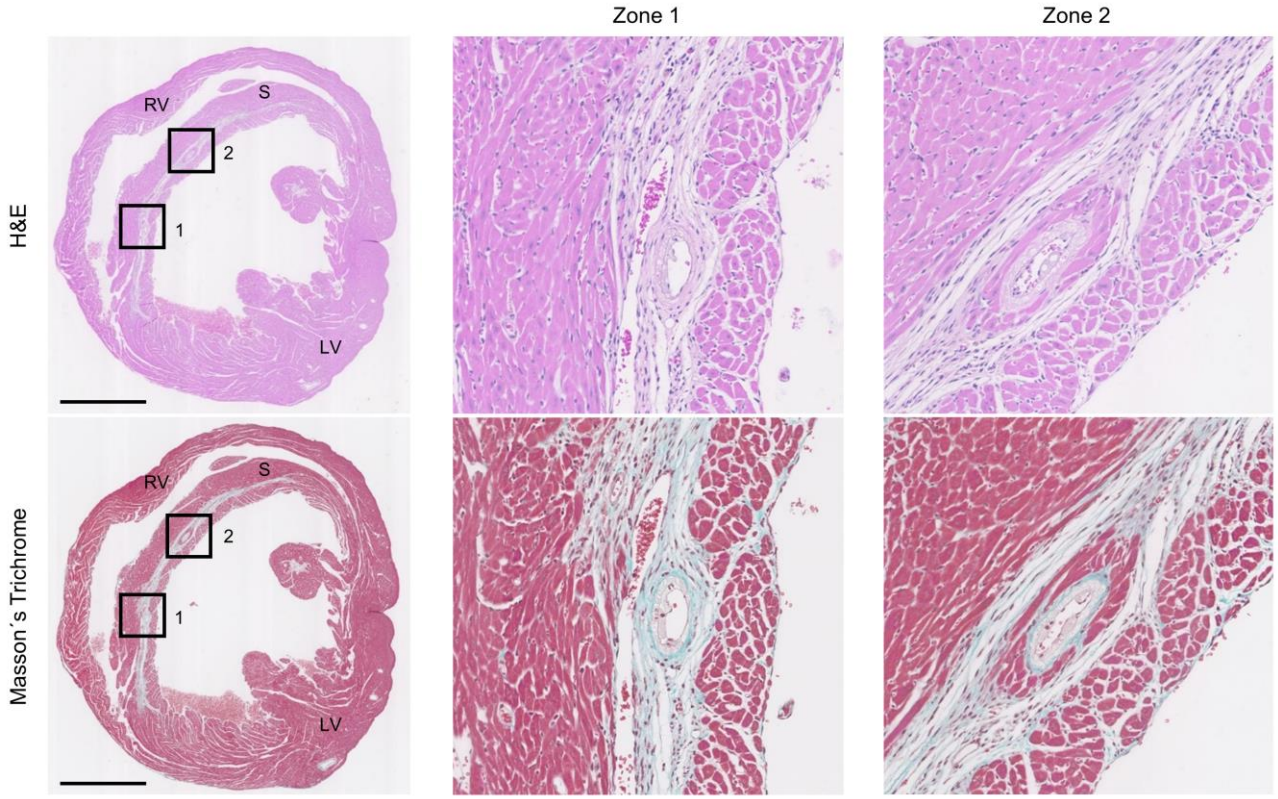

Figure 29. Evidence of coronary atherosclerosis and myocardial infarction in *Apoe*$^{-/-}$ *Lmna*$^{G609G/G609G}$ mice. Mice fed normal chow were sacrificed at 21-23 weeks of age (close to their maximum survival). Photographs show consecutive sections of an *Apoe*$^{-/-}$ *Lmna*$^{G609G/G609G}$ heart stained with hematoxylin & eosin (H&E) and Masson´s trichrome, showing coronary atherosclerosis and infarct in the septum. Scale bar 1mm. RV: right ventricle; S: septum; LV: left ventricle.

Examination of *Apoe*$^{-/-}$*Lmna*$^{LCS/LCS}$*SM22αCre* hearts revealed that the majority presented perivascular and interstitial fibrosis, coronary atherosclerosis and intimal hyperplasia (**Table 1**). We also found calcification of the coronary plaque in some of the animals analyzed (**Table 1**). These pathological alterations in the heart suggest that *Apoe*$^{-/-}$*Lmna*$^{LCS/LCS}$*SM22αCre* animals suffer many small infarcts during their lifetime, similar to HGPS patients. However, no evidence of stroke was found in the brain of *Apoe*$^{-/-}$*Lmna*$^{G609G/G609G}$ and *Apoe*$^{-/-}$*Lmna*$^{LCS/LCS}$*SM22αCre* models (data not shown).

In summary, comparison of mice at ages close to their maximum survival revealed a more severe cardiac phenotype and atherosclerotic disease in *Apoe*$^{-/-}$*Lmna*$^{LCS/LCS}$*SM22αCre* mice than in *Apoe*$^{-/-}$*Lmna*$^{G609G/G609G}$ mice. The histopathological findings in the aorta and heart support our hypothesis that *Apoe*$^{-/-}$*Lmna*$^{LCS/LCS}$*SM22αCre* animals die of atherosclerosis complications, whereas *Apoe*$^{-/-}$*Lmna*$^{G609G/G609G}$ die of atherosclerosis-independent processes. Plaque disruption leading to an infarct and subsequent death may occur in *Apoe*$^{-/-}$*Lmna*$^{G609G/G609G}$ mice only if their survival is close to

26 weeks, the age at which *Apoe*$^{-/-}$*Lmna*$^{LCS/LCS}$*SM22αCre* begin to die. While we cannot rule out the possibility that *Apoe*$^{-/-}$*Lmna*$^{G609G/G609G}$ mice die from heart failure, it is probably related to other complications such as arrhythmias (see subsection IV.6).

IV.8. Progerin expression in VSMCs activates endoplasmic ER stress and the UPR

In an attempt to identify mechanisms underlying the acceleration of atherosclerosis induced by progerin, we conducted a transcriptomic analysis of aortas from the ubiquitous and VSMC-specific progeria models. To identify drivers of disease rather than secondary changes, we collected arteries before the onset of overt disease. The appropriate age for collection was determined based on our previous histopathological analysis in *Apoe*$^{-/-}$*Lmna*$^{G609G/G609G}$ and *Apoe*$^{-/-}$*Lmna*$^{LCS/LCS}$*SM22αCre* mice fed normal chow (subsection IV.4).

Based on these findings and because VSMCs appear to be a major target of progerin, we performed RNA sequencing (RNAseq) on VSMC-rich media of disease-free aortas from 8-week-old *Apoe*$^{-/-}$*Lmna*$^{G609G/G609G}$ and *Apoe*$^{-/-}$*Lmna*$^{LCS/LCS}$*SM22αCre* mice and their corresponding controls (*Apoe*$^{-/-}$*Lmna*$^{+/+}$ and *Apoe*$^{-/-}$*Lmna*$^{LCS/LCS}$, respectively) (**Fig. 30A**). Four pooled samples per genotype were collected, and PCR analysis confirmed proper progerin and lamin A expression (**Fig. 30B**). Differential expression analysis revealed 776 significantly altered genes in the ubiquitous progeroid model and 931 altered genes in the VSMC-specific model (**Fig. 30C**). Of these differentially-regulated genes, 240 were common to both comparisons and had a high correlation ($R^2 \approx 8$, **Fig. 30D**).

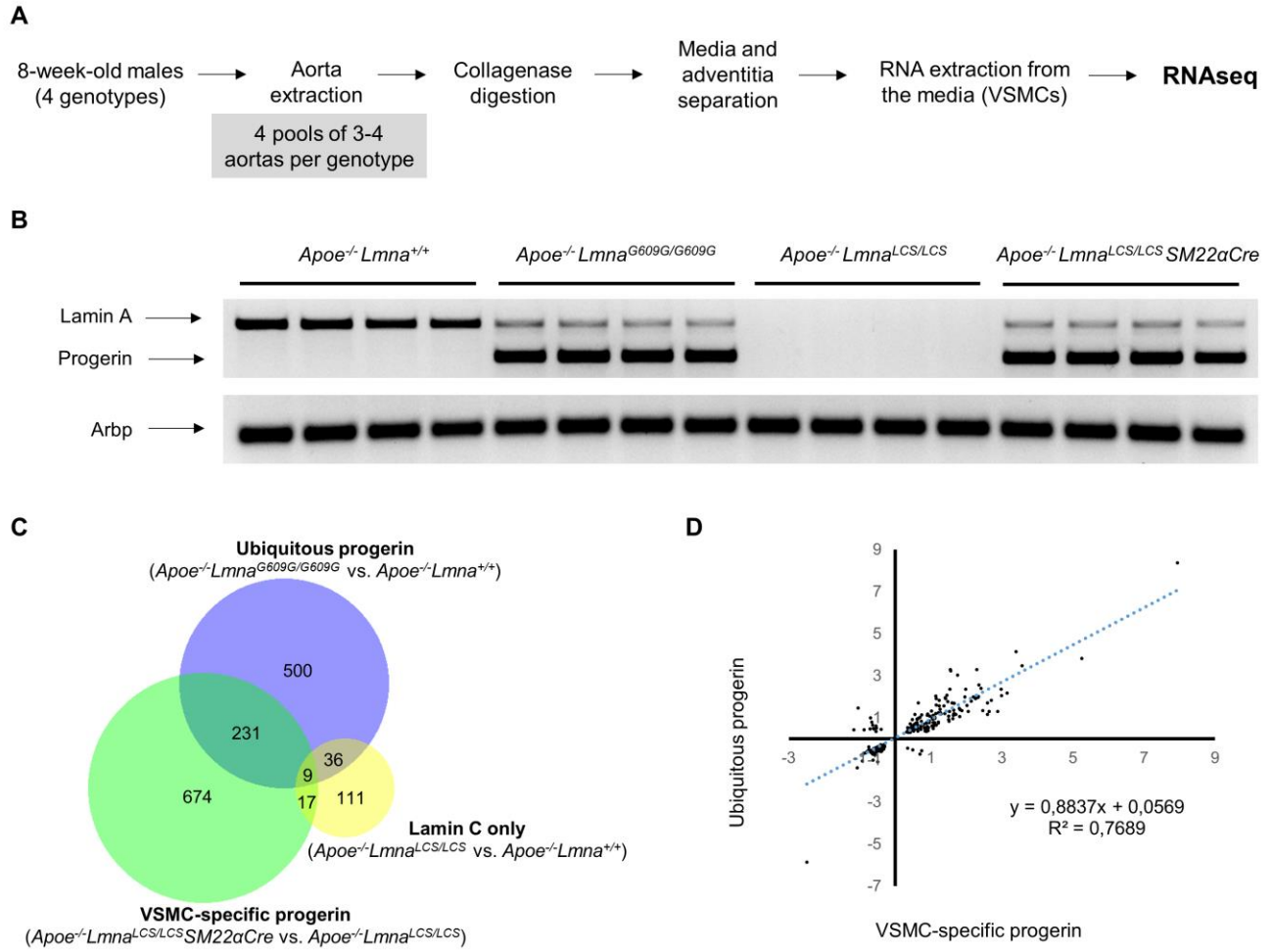

Figure 30. Progerin expression in vascular smooth muscle cells (VSMCs) causes altered gene expression. (A) Sample preparation for RNA sequencing (RNAseq). **(B)** PCR confirmation of proper expression of lamin A and progerin in pooled medial aortas used for RNAseq. Arbp was used as endogenous control. **(C)** Bioinformatic analysis detected 776 differentially expressed genes in medial aortas from *Apoe*$^{-/-}$ *Lmna*$^{G609G/G609G}$ mice with ubiquitous progerin expression compared with *Apoe*$^{-/-}$*Lmna*$^{+/+}$ control mice expressing wild-type lamin A/C and 931 genes in medial aortas from *Apoe*$^{-/-}$ *Lmna*$^{LCS/LCS}$*SM22αCre* mice with VSMC-specific progerin expression compared with *Apoe*$^{-/-}$*Lmna*$^{LCS/LCS}$ control mice expressing lamin C only. There were 176 genes differentially expressed between the two control groups. The Venn diagram shows the overlap between sets of deferentially expressed genes identified in each of the 3 comparisons. **(D)** Correlation between logarithms of fold change calculated for the 240 genes shared between the comparisons "ubiquitous progerin *vs* wild-type lamin A/C" and "VSMC-specific progerin vs lamin C only".

To specifically separate the effect of progerin production from the absence of lamin A, we performed analysis of the two controls, which revealed 176 genes differentially expressed between *Apoe*$^{-/-}$*Lmna*$^{LCS/LCS}$ aortas (expressing lamin C only) and *Apoe*$^{-/-}$*Lmna*$^{+/+}$ aortas (expressing wild-type lamin A/C) (**Fig. 30C**). However, there was hardly any overlap between the gene sets affected by progerin production in *Apoe*$^{-/-}$*Lmna*$^{G609G/G609G}$ and *Apoe*$^{-/-}$*Lmna*$^{LCS/LCS}$*SM22αCre* mice and those influenced by the absence of lamin A in *Apoe*$^{-/-}$*Lmna*$^{LCS/LCS}$ mice (**Fig. 30C**). Likewise, progerin and the absence of lamin A affected different pathways (**Fig. 31**).

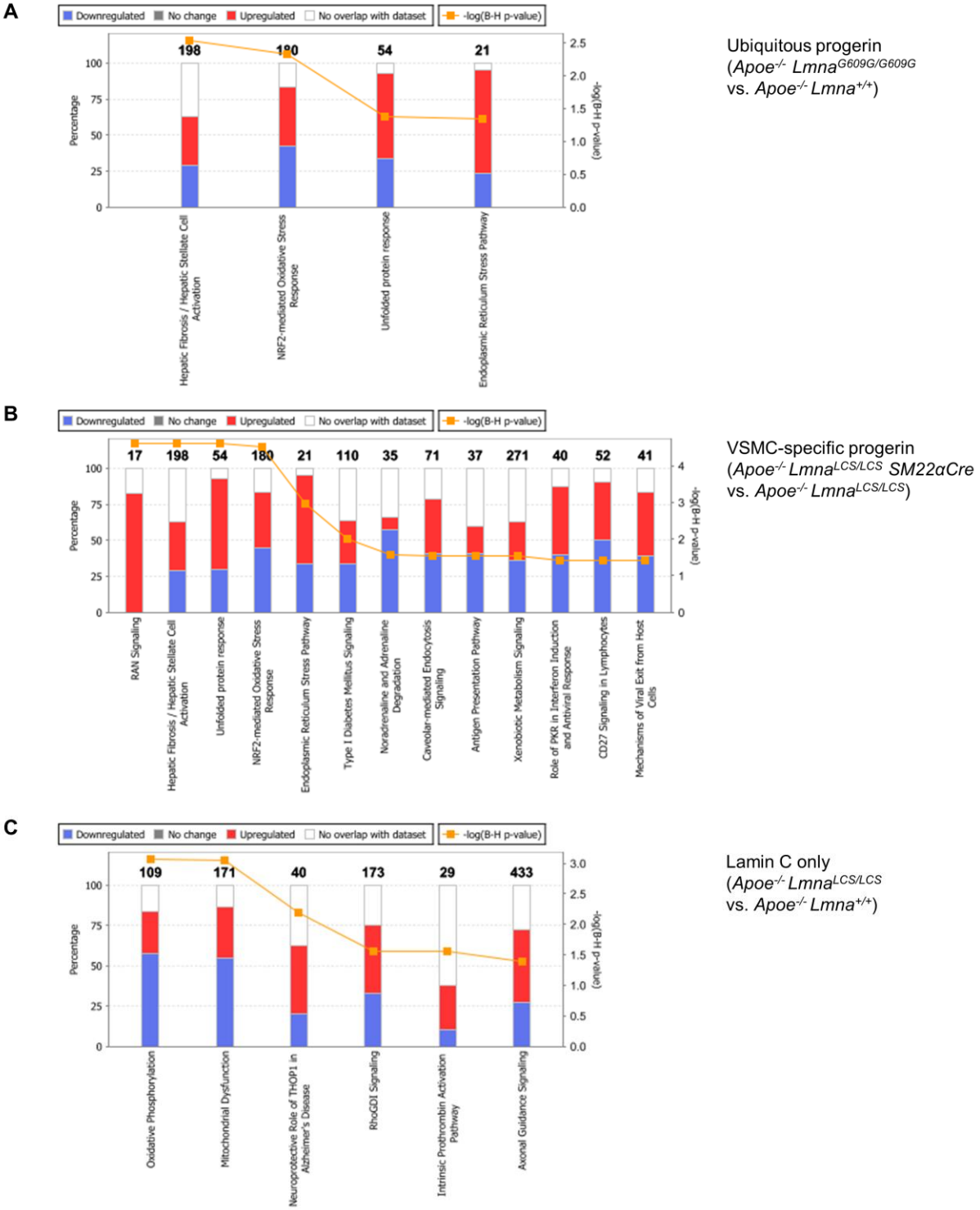

Figure 31. Pathways affected by lack of lamin A do not overlap with those induced by progerin expression. Stacked bar charts representing pathways significantly changed after applying the Benjamini-Hochberg correction for multiple testing in 3 comparisons: **(A)** *Apoe*$^{-/-}$*Lmna*$^{G609G/G609G}$ (ubiquitous progerin) *vs Apoe*$^{-/-}$*Lmna*$^{+/+}$ (ubiquitous lamin A and lamin C), **(B)** *Apoe*$^{-/-}$*Lmna*$^{LCS/LCS}$*SM22αCre* (vascular smooth muscle cell (VSMC)-specific progerin) *vs Apoe*$^{-/-}$*Lmna*$^{LCS/LCS}$ (ubiquitous lamin C, no lamin A), and **(C)** *Apoe*$^{-/-}$*Lmna*$^{LCS/LCS}$ (ubiquitous lamin C, no lamin A) *vs Apoe*$^{-/-}$ *Lmna*$^{+/+}$ (ubiquitous lamin A and lamin C). The numbers of genes in each category (from the Ingenuity Pathway Analysis data base) are indicated above the bars.

Comparison analysis identified four pathways that were significantly altered in both the ubiquitous and the VSMC-specific progeroid models: fibrosis, nuclear factor erythroid 2-like 2 (NRF2)-mediated oxidative stress, the ER stress response, and the UPR (**Fig. 32, *left: Canonical pathways***). We also examined the predicted activation status of upstream regulators based on the expression of their target genes. This analysis revealed that the most differentially regulated factors belong to the ER stress response and ER stress-related UPR, for example, XBP1, ATF4 and DDIT3 (**Fig. 32, *right: Upstream regulators***).

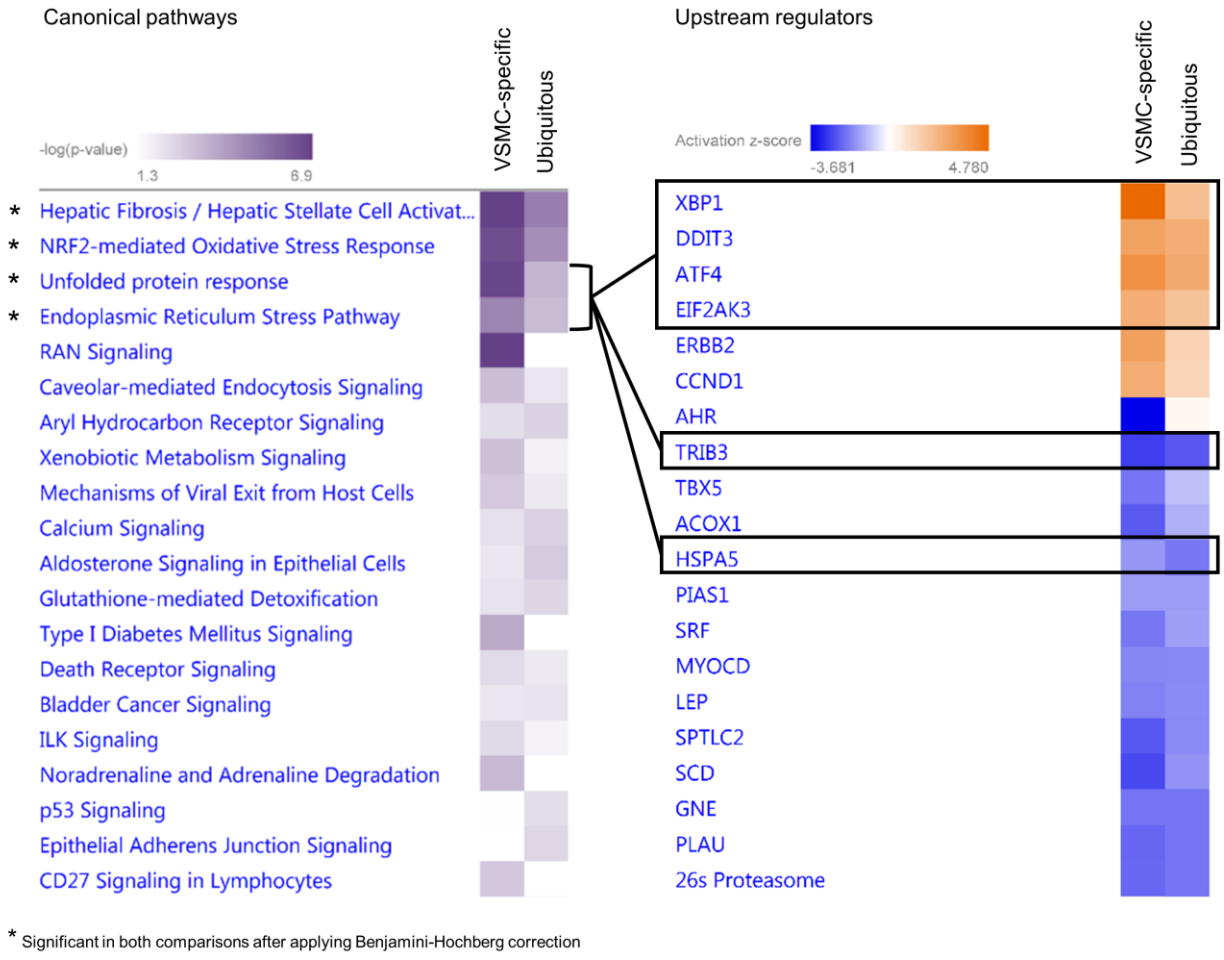

Figure 32. Progerin expression in vascular smooth muscle cell (VSMC)-rich aortic media activates endoplasmic reticulum (ER) stress and unfolded protein response (UPR). RNAseq results were analyzed using Ingenuity Pathway Analysis: (*left*) canonical pathway heatmap, showing processes affected by progerin expression in VSMC-rich medial aortas. Asterisk (*) indicates pathways which are significantly changed in both comparisons after applying the Benjamini-Hochberg correction for multiple testing; (*right*) upstream regulator heatmap, showing predicted activation states of transcriptional regulators (black boxes indicate key molecules involved in ER stress and UPR regulation).

To validate the RNAseq results, we performed quantitative real-time PCR on selected ER stress response and UPR genes that were significantly upregulated in aortic media from 8-week-old mice of both progeria models (**Fig. 33A**). This analysis confirmed progerin-induced upregulation of *Calr*, *Ddit3*, *Dnajb9*, *Hspa5*, *Hsp90b1*, and *Pdia4* in VSMC-rich aortic media in both models (**Fig. 33B, C**).

A

Gene symbol	Fold change (Ubiquitous progerin)	Fold change (VSMC-specific progerin)	Description	ID
Calr	1.29	1.80	calreticulin	ENSMUSG00000003814
Hspa5	1.95	3.07	heat shock protein 5	ENSMUSG00000026864
Hsp90b1	1.38	1.80	heat shock protein 90, beta (Grp94), member 1	ENSMUSG00000020048
Pdia4	1.27	1.84	protein disulfide isomerase associated 4	ENSMUSG00000025823
Dnajb9	1.43	1.64	DnaJ (Hsp40) homolog, subfamily B, member 9	ENSMUSG00000014905
Ddit3	1.37	1.64	DNA-damage inducible transcript 3	ENSMUSG00000025408

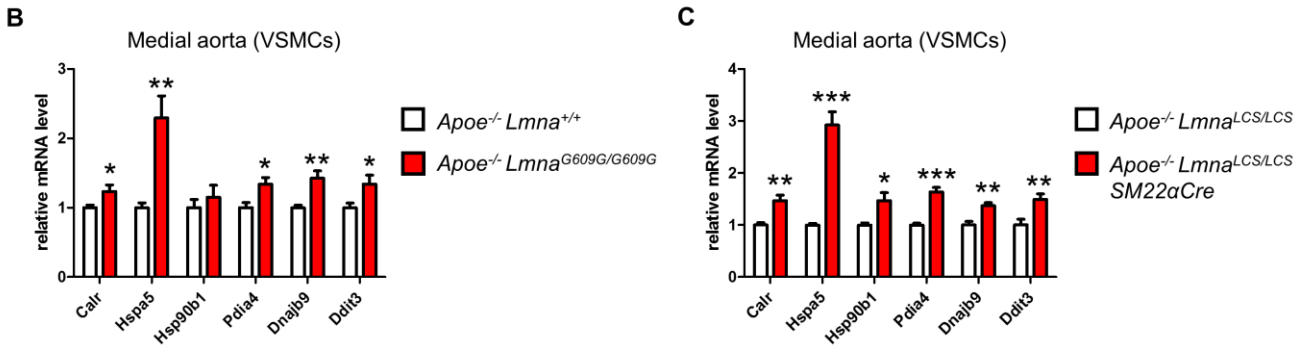

Figure 33. Endoplasmic reticulum (ER) stress and unfolded protein response (UPR) activation in progerin-expressing aortas from *Apoe*$^{-/-}$*Lmna*$^{G609G/G609G}$ mice (ubiquitous progerin) and *Apoe*$^{-/-}$*Lmna*$^{LCS/LCS}$*SM22αCre* mice (vascular smooth muscle cell (VSMC)-specific progerin). (A) Six ER stress/UPR pathway genes selected for qPCR validation from among of those detected as differentially expressed in RNAseq in both models. **(B, C)** qPCR results in pooled medial aortas (n=4) obtained from 8-week-old *Apoe*$^{-/-}$ *Lmna*$^{G609G/G609G}$ mice **(B)** and *Apoe*$^{-/-}$*Lmna*$^{LCS/LCS}$*SM22αCre* mice **(C)** and their corresponding controls. *Hprt* and *Gusb* were used for normalization. Data are mean ± SEM. Statistical differences were analyzed by one-tailed *t*-test. **P*<0.05, ***P*<0.01, ****P*<0.001.

We next assessed whether progerin activates the ER stress response and the UPR in other organs. Consistent with the ubiquity of progerin expression in *Apoe*$^{-/-}$*Lmna*$^{G609G/G609G}$ mice, induction of ER stress response and the UPR was noted in some organs of these animals, with kidney being the organ most affected and liver the least (**Fig. 34A**). As anticipated, no activation of this stress pathway was detected in kidney, liver, spleen, or heart from *Apoe*$^{-/-}$*Lmna*$^{LCS/LCS}$*SM22αCre* mice, confirming the specificity of the model (**Fig. 34B**). The variability in the ER stress and UPR activation across the organs of *Apoe*$^{-/-}$*Lmna*$^{G609G/G609G}$ mice may be in part attributed to different lamin A (and thus progerin) expression levels associated with tissue stiffness (*63, 64*). Moreover, distinct organs and tissues may

have different thresholds for tolerating misfolded protein load and therefore be more prone or resistant to ER stress.

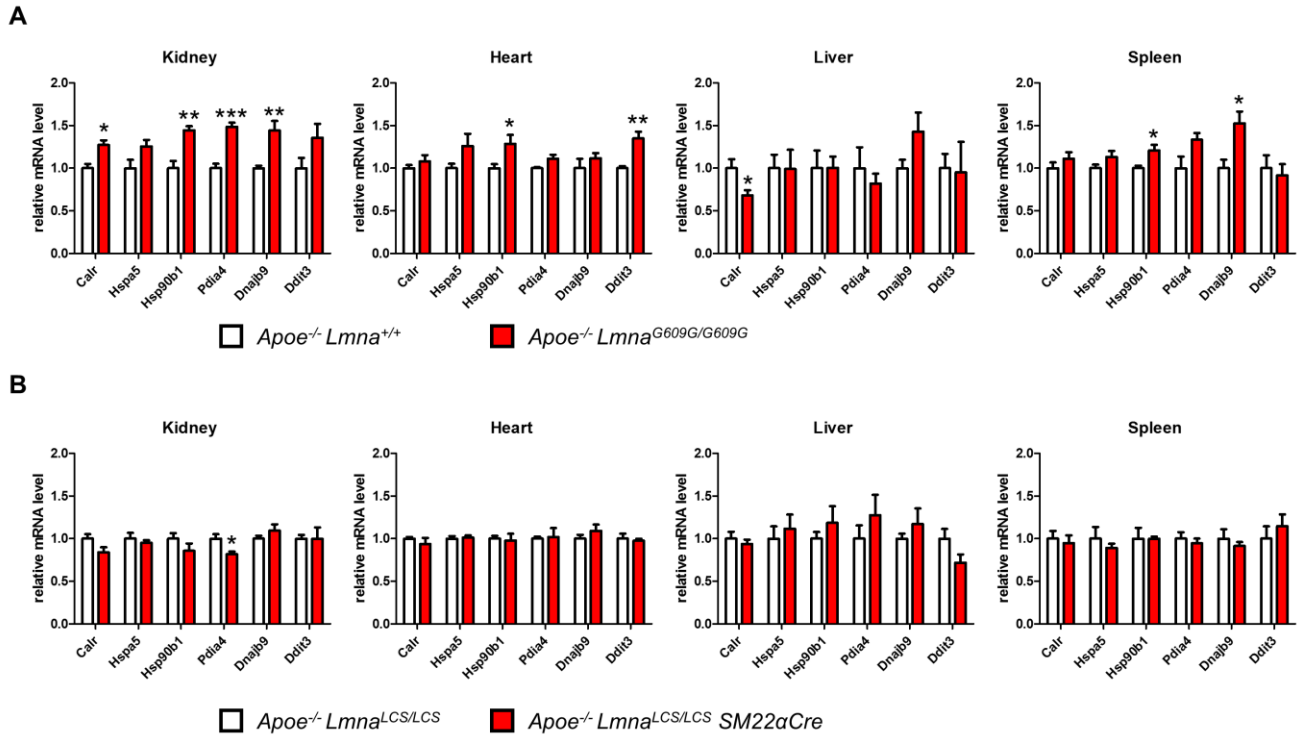

Figure 34. Endoplasmic reticulum (ER) stress and unfolded protein response (UPR) activation in different organs from *Apoe*$^{-/-}$*Lmna*$^{G609G/G609G}$ mice with ubiquitous progerin expression. qPCR results in organs from 8-week-old *Apoe*$^{-/-}$*Lmna*$^{G609G/G609G}$ mice **(A)** and *Apoe*$^{-/-}$*Lmna*$^{LCS/LCS}$*SM22αCre* mice **(B)** and their corresponding controls (n=4 per condition). Activation of some ER stress and UPR genes was observed in kidney, heart, and spleen of *Apoe*$^{-/-}$*Lmna*$^{G609G/G609G}$ mice but not in the same organs of *Apoe*$^{-/-}$*Lmna*$^{LCS/LCS}$*SM22αCre* mice. *Hprt* and *Gusb* were used for normalization. Data are mean ± SEM. Statistical differences were analyzed by two-tailed *t*-test. **P*<0.05, ***P*<0.01, ****P*<0.001.

Previous *in vitro* and *in vivo* studies have identified numerous pathways potentially contributing to HGPS. Most of them, however, are mutually dependent, making it challenging to distinguish primary from secondary mechanisms. Our RNAseq analysis of pre-disease aortic media from the ubiquitous and VSMC-specific progeria models identified the ER stress response and the related UPR as potential driver mechanisms of atherosclerosis in progeria. We hypothesize that accumulation of misfolded progerin due to defective post-translational processing triggers ER stress in VSMCs, which might be exaggerated by medial deposits of lipids, also known to activate ER stress (*165, 166*). At early stages, VSMCs attempt to restore homeostasis by activating the UPR, but cell death occurs when stress cannot be resolved. Because of continuous crosstalk between stress pathways, ER stress can lead to activation of other stress responses. For instance, ER stress can sensitize cells to DNA damage-induced apoptosis (*167*), providing a possible link between our findings and those of previous studies showing increased

DNA damage in HGPS cells (*101*). In accordance with recent studies in HGPS fibroblasts, which identified the NRF2 pathway as a major progerin target (*168*), our RNAseq analysis detected NRF2-mediated oxidative stress response as one of the main pathways affected by progerin expression in VSMCs. Oxidative stress induced by NRF2 is connected to ER stress through the protein kinase PERK, which phosphorylates the transcription factor NRF2 in response to ER stress (*169*). Moreover, ER stress is associated with inflammation, autophagy and mitochondrial dysfunction (*170*), processes that are affected in progeria (*171-173*). Our results identify an important upstream mechanism in VSMCs, which may link various stress pathways previously described in progeria. *In vitro* studies are thus warranted to further explore in detail the mechanisms linking ER stress, UPR and VSMC death in the setting of progeria, and the role of oxidized LDLs in this process. These studies could be performed with primary VSMCs from wild-type and progerin-expressing mice, and VSMCs differentiated from control and HGPS iPSCs (available from The Progeria Research Foundation).

IV.9. Therapeutic effects of ER stress response targeting in progeroid mice

Our RNAseq results strongly suggested a key role of ER stress response and the UPR as drivers of progerin-induced VSMC death and enhanced atherosclerosis in the ubiquitous and VSMC-specific progeria models. We therefore examined the potential benefits of targeting this pathway by chemical chaperone treatment. We selected TUDCA, a bile acid previously proven to efficiently alleviate ER stress and ameliorate experimental diabetes (*174*), aortic valve calcification (*175*), and myocardial infarction (*176*).

Before using progeric mice, we conducted a pilot study with *Apoe*$^{-/-}$*Lmna*$^{+/+}$ control mice fed normal chow to monitor for any adverse effects of prolonged TUDCA treatment. Animals received TUDCA (400 mg/kg) or PBS intraperitoneal injections 3 times weekly starting at 6 weeks of age. TUDCA- and PBS-treated mice appeared healthy and did not show any overt pathology. However, weight gain in the TUDCA-treated group was slightly diminished (**Fig. 35A**), likely due to an increase in energy expenditure, as described previously by da-Silva *et al.* (*177*). Analysis at 26 weeks of age revealed similar blood pressure in both experimental groups (**Fig. 35B**), and the absence of blood pressure and heart rate instability and variability (**Fig. 35C**). Similarly, except for a borderline significant reduction in the PR segment in TUDCA-treated mice, all ECG parameters at 26 weeks of age were similar in both experimental groups (**Fig. 35D**).

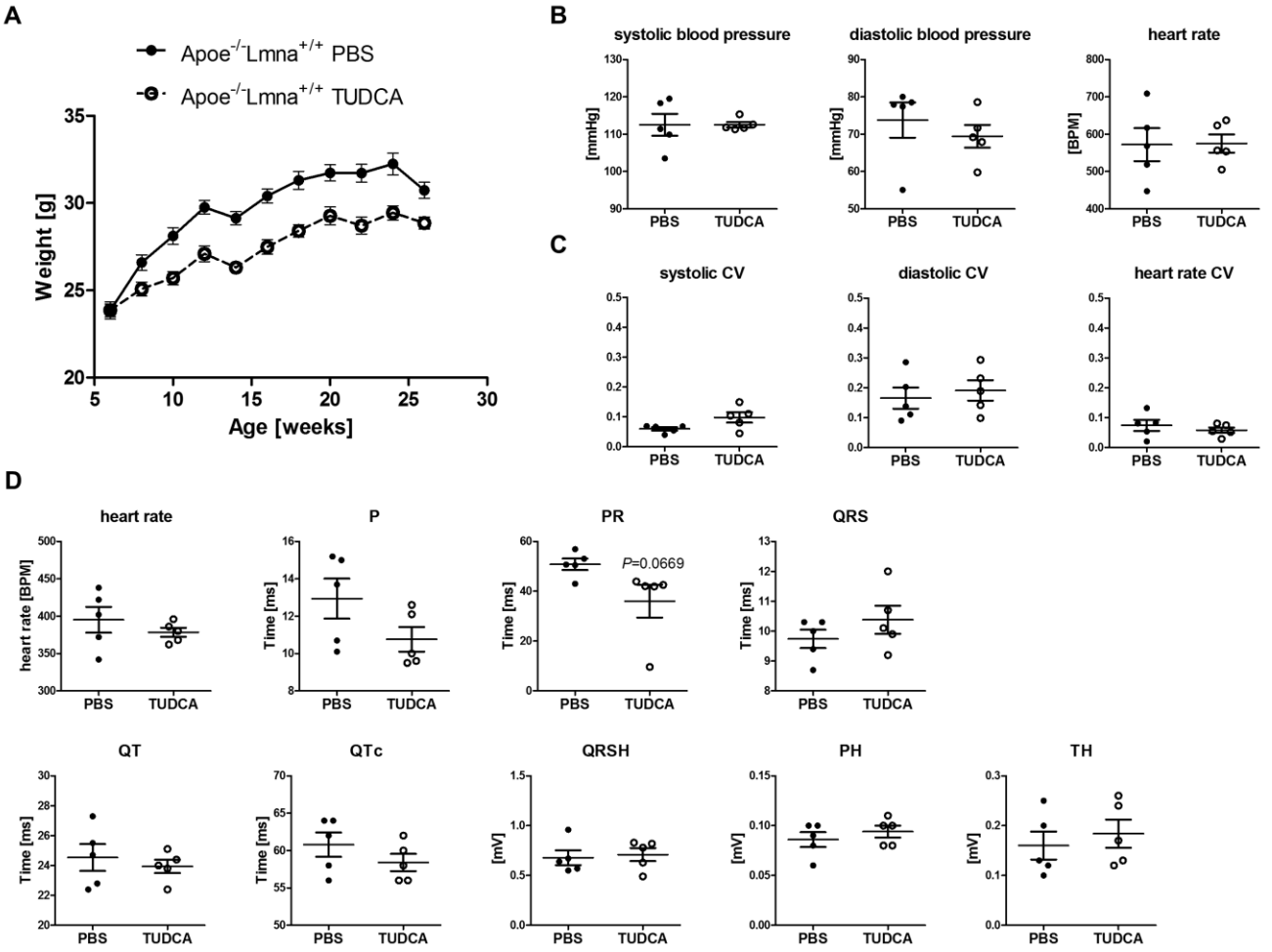

Figure 35. Prolonged tauroursodeoxycholic acid (TUDCA) treatment of *Apoe*$^{-/-}$*Lmna*$^{+/+}$ mice does not cause any severe alteration in blood pressure or electrocardiogram (ECG) parameters. *Apoe*$^{-/-}$*Lmna*$^{+/+}$ mice fed normal chow received either TUDCA (400 mg/kg) or PBS intraperitoneal injections 3 times a week starting at 6 weeks of age. **(A)** Body weight curves for TUDCA-treated and untreated mice. $P<0.0001$ **(B)** Heart rate, systolic and diastolic blood pressure analysis for TUDCA-treated and untreated mice at 26 weeks of age. **(C)** Variability in the heart rate, systolic and diastolic blood pressure for 26-week-old TUDCA-treated and untreated mice measured as coefficient of variation (CV). **(D)** ECG parameters for 26-week-old TUDCA-treated and untreated mice. n=5. Data are presented as mean ± SEM. Statistical analysis was performed by two-tailed *t*-test.

Necropsies of 27-week-old TUDCA- and PBS-treated mice did not reveal pathology in the intraperitoneal cavity (**Fig. 36A**), which might arise because of the multiple injections or the drug *per se*. We next analyzed the effect of TUDCA on atherosclerosis development as Erbay *et al.* found that the chemical chaperone 4-phenyl butyric acid (PBA) can delay atherosclerotic plaque formation via alleviating ER stress in macrophages (*178*). Importantly, this effect of PBA on atherosclerosis was independent of changes in lipids, lipoprotein profiles, glucose and insulin levels in the circulation (*178*). In agreement with these findings, we found a weak tendency toward reduced atherosclerosis in the aortic arch in mice treated with TUDCA, although differences did not reach statistical significance

(**Fig. 36B**). Our pilot study also revealed similar fasting serum levels of total and free cholesterol in both experimental groups, and significantly lower LDL in TUDCA-treated animals (**Fig. 36C**).

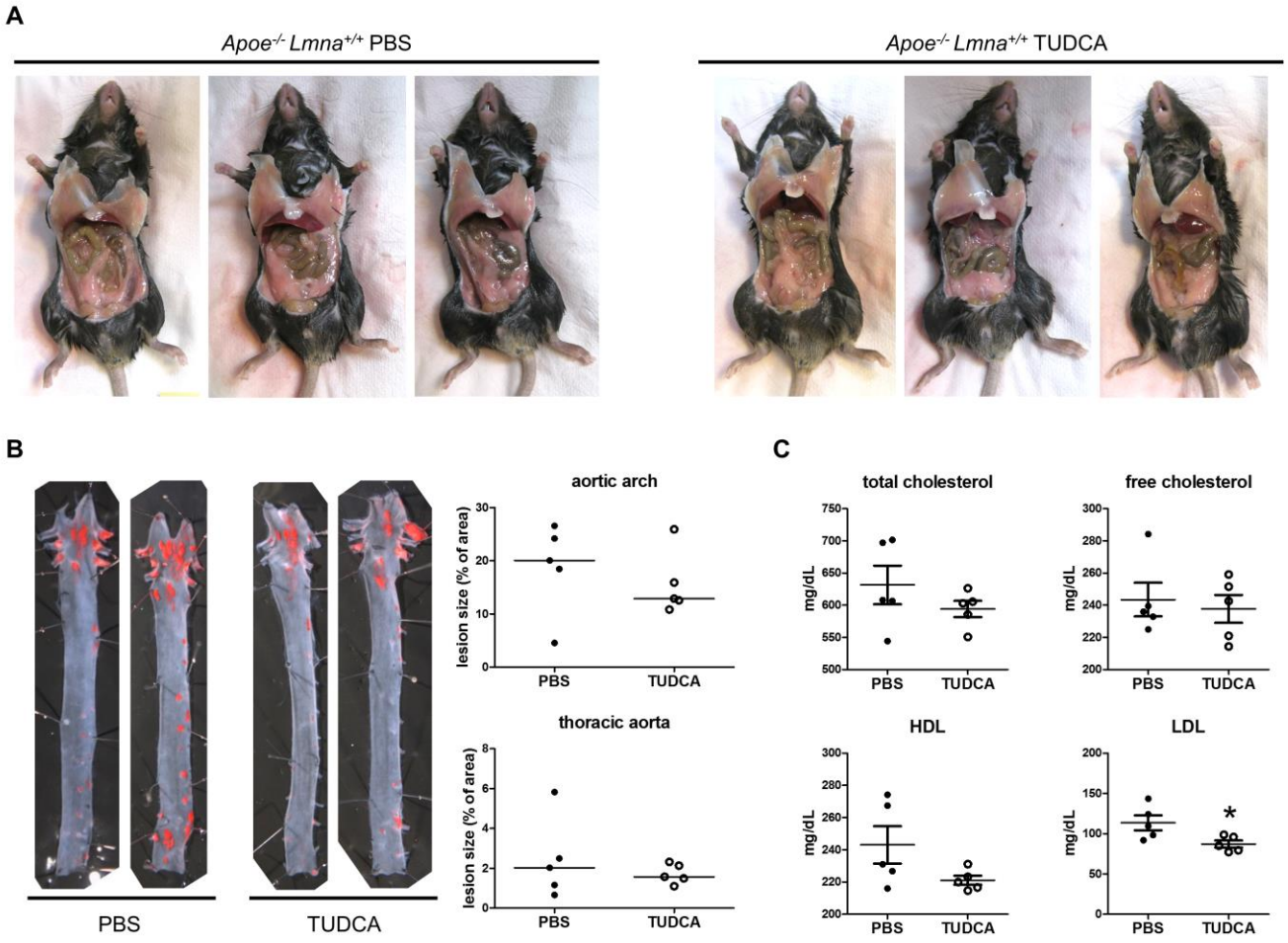

Figure 36. Prolonged tauroursodeoxycholic acid (TUDCA) treatment of *Apoe*$^{-/-}$*Lmna*$^{+/+}$ mice does not significantly affect atherosclerosis and has only minor effect on the lipid profile. *Apoe*$^{-/-}$*Lmna*$^{+/+}$ mice fed normal chow received either TUDCA (400 mg/kg) or PBS intraperitoneal injections 3 times a week starting at 6 weeks of age. Mice were sacrificed at 27 weeks of age. **(A)** Representative photographs of intraperitoneal cavity of TUDCA-treated and untreated mice. **(B)** Representative images of Oil Red O-stained aortas of TUDCA-treated and untreated mice; graphs show quantification of atherosclerosis burden in aortic arch and thoracic aorta. **(C)** Fasting serum levels of total cholesterol, free cholesterol, low-density lipoprotein (LDL), and high-density lipoprotein (HDL) in 27-week-old TUDCA-treated and mice. n=5. Data in **B** are shown as median; data in **C** are mean ± SEM. Statistical differences were analyzed by two-tailed Mann-Whitney test in **B** and two-tailed *t*-test in **C**. **P*<0.05.

We also observed that TUDCA induced some minor changes in the hematological parameters, including higher lymphocyte and lower monocyte percentage (**Fig. 37**). Whether these alterations are a cause or a consequence of diminished atherosclerosis burden should be addressed in a future study.

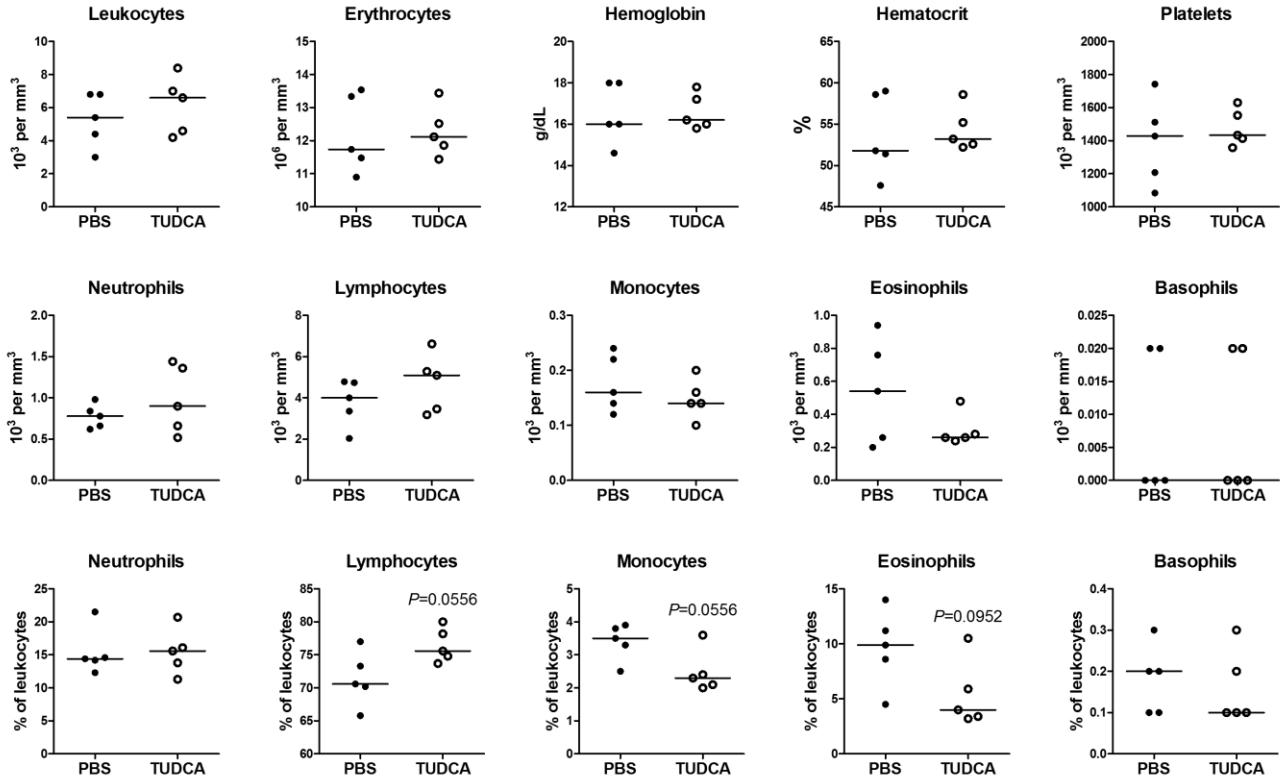

Figure 37. Prolonged tauroursodeoxycholic acid (TUDCA) treatment of *Apoe*$^{-/-}$*Lmna*$^{+/+}$ mice does not cause any significant alterations in hematological parameters. *Apoe*$^{-/-}$*Lmna*$^{+/+}$ mice fed normal chow received either TUDCA (400 mg/kg) or PBS intraperitoneal injections 3 times a week starting at 6 weeks of age. Hematology (fasting) results for 27-week-old TUDCA-treated and untreated (PBS) mice; n=5. Data are shown as median. Statistical differences were analyzed by two-tailed Mann-Whitney test.

After confirming that prolonged TUDCA treatment did not trigger any deleterious side effects, we performed experiments with ubiquitous and VSMC-specific progeroid mouse models. Animals were fed HFD for 8 weeks starting at 8 weeks of age. Additionally, mice received intraperitoneal injections of TUDCA (400 mg/kg) 3 times weekly starting at 6 weeks of age in the case of *Apoe*$^{-/-}$*Lmna*$^{G609G/G609G}$ and *Apoe*$^{-/-}$*Lmna*$^{+/+}$ or at 8 weeks of age in the case of *Apoe*$^{-/-}$*Lmna*$^{LCS/LCS}$*SM22αCre* and *Apoe*$^{-/-}$*Lmna*$^{LCS/LCS}$ mice. Control mice received PBS injections. TUDCA treatment in both HFD-fed *Apoe*$^{-/-}$*Lmna*$^{G609G/G609G}$ and *Apoe*$^{-/-}$*Lmna*$^{LCS/LCS}$*SM22αCre* mice inhibited atheroma lesion formation in the thoracic aorta (**Fig. 38A, B**) and alleviated aortic VSMC loss and adventitial thickening (**Fig. 38C-F**).

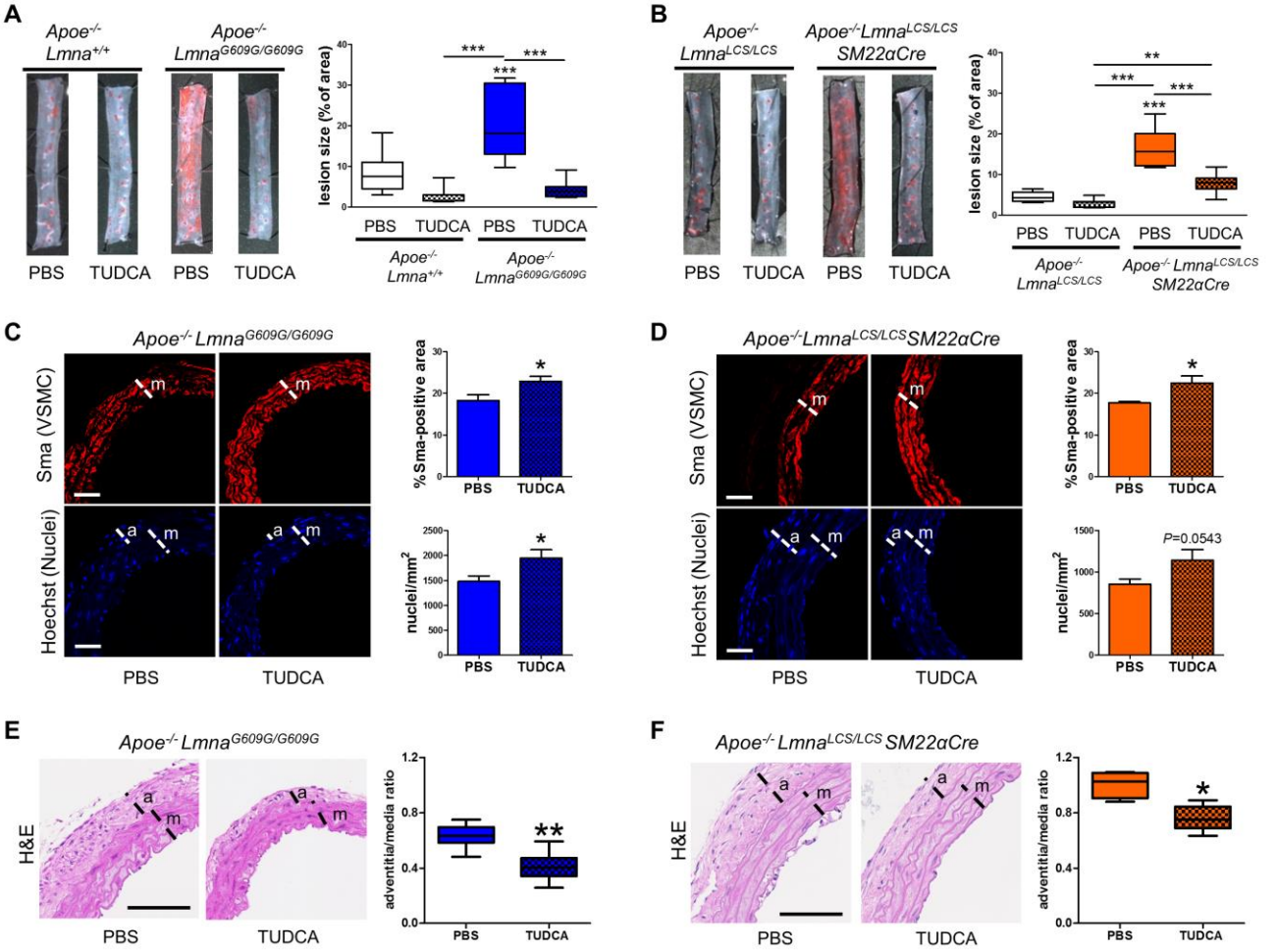

Figure 38. Tauroursodeoxycholic acid (TUDCA) treatment alleviates vascular pathology in progeroid mouse models. Mice were treated with TUDCA or vehicle (PBS), starting at 6 weeks of age for *Apoe*$^{-/-}$*Lmna*$^{+/+}$ and *Apoe*$^{-/-}$*Lmna*$^{G609G/G609G}$ mice, and at 8 weeks of age for *Apoe*$^{-/-}$*Lmna*$^{LCS/LCS}$ and *Apoe*$^{-/-}$*Lmna*$^{LCS/LCS}$*SM22αCre* mice. All mice were fed high-fat diet for 8 weeks starting at 8 weeks of age. **(A, B)** Representative images of thoracic aortas stained with Oil Red O and quantification of atherosclerosis burden in TUDCA-treated and untreated mice of the indicated genotypes (n=7-8 in **A**; n=6-8 in **B**). **(C, D)** Representative immunofluorescence images of aortas stained with anti-smooth muscle actin (Sma) antibody (red) and Hoechst3442 (blue). Graphs show quantification of vascular smooth muscle cell (VSMC) content in the media as either % of Sma-positive area (top) or number of nuclei/mm^2 (bottom); n=6 in **C** (*Apoe*$^{-/-}$*Lmna*$^{G609G/G609G}$), and n=4-5 in **D** (*Apoe*$^{-/-}$*Lmna*$^{LCS/LCS}$*SM22αCre*). Scale bar, 50 µm. **(E, F)** Representative histology sections of hematoxylin & eosin (H&E)-stained aortas. Graphs show quantification of adventitia-to-media thickness ratio; n=6 in **E** (*Apoe*$^{-/-}$*Lmna*$^{G609G/G609G}$), and n=4-5 in **F** (*Apoe*$^{-/-}$*Lmna*$^{LCS/LCS}$*SM22αCre*). Scale bar, 100 µm. Data in **A**, **B**, **E** and **F** are shown as median with interquartile range and minima and maxima; data in **C** and **D** are mean ± SEM. Statistical differences were analyzed by one-way ANOVA with Tukey´s post hoc test in **A** and **B**, one-tailed *t*-test in **C** and **D**, and one-tailed Mann-Whitney test in **E** and **F**. **P*<0.05, ***P*<0.01, ****P*<0.001. m: media, a: adventitia.

We next examined the effect of TUDCA on survival. Notably, TUDCA prolonged the median lifespan of *Apoe*$^{-/-}$*Lmna*$^{LCS/LCS}$*SM22αCre* mice by 35% (median survival: 61.4 weeks in TUDCA-

treated *versus* 45.35 weeks in untreated mice, *P*=0.0148), without affecting the survival of *Apoe*$^{-/-}$ *Lmna*$^{G609G/G609G}$ mice (**Fig. 39A**).

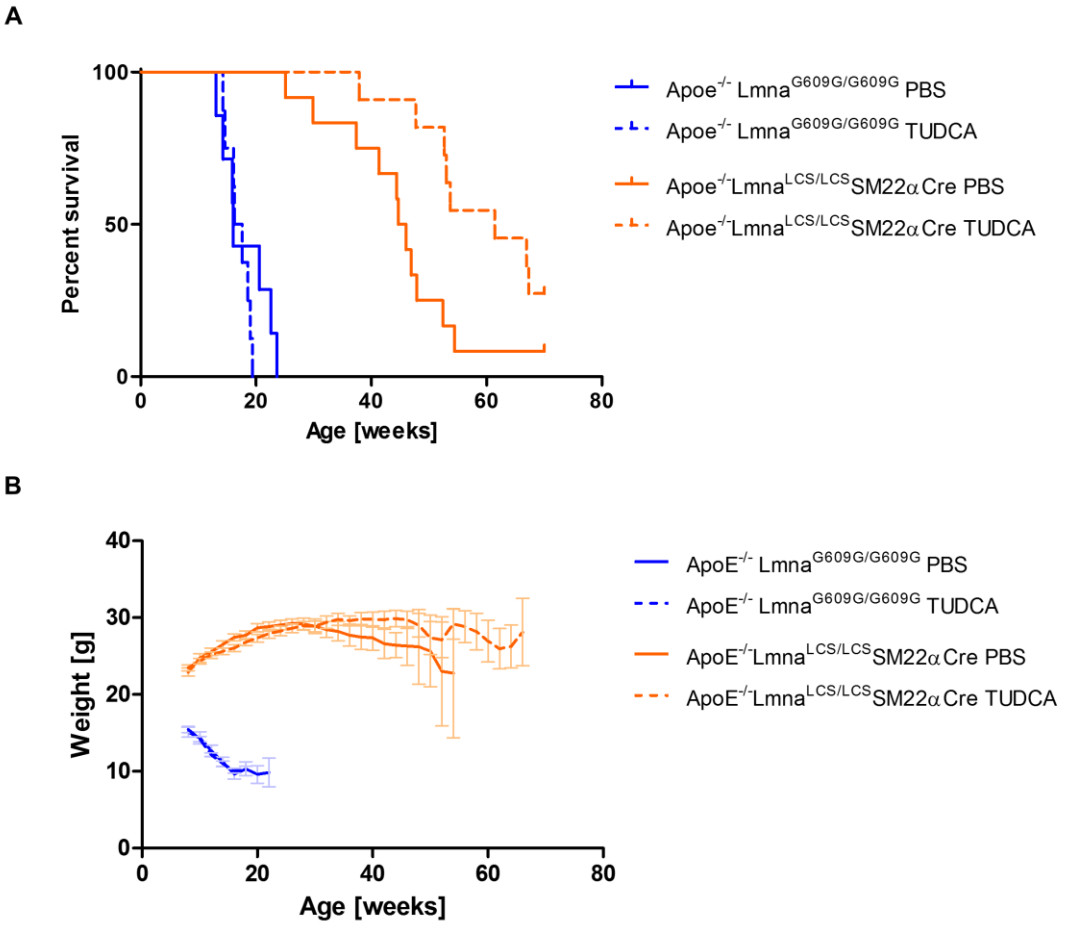

Figure 39. Tauroursodeoxycholic acid (TUDCA) treatment extends lifespan in *Apoe*$^{-/-}$*Lmna*$^{LCS/LCS}$*SM22αCre* mice. Mice were treated with TUDCA or vehicle (PBS), starting at 6 weeks of age for *Apoe*$^{-/-}$*Lmna*$^{+/+}$ and *Apoe*$^{-/-}$*Lmna*$^{G609G/G609G}$ mice, and at 8 weeks of age for *Apoe*$^{-/-}$*Lmna*$^{LCS/LCS}$ and *Apoe*$^{-/-}$*Lmna*$^{LCS/LCS}$*SM22αCre* mice. Graphs show Kaplan-Meier survival **(A)** and body weight **(B)** curves of TUDCA-treated and untreated (PBS) mice of the indicated genotypes (n=7-8 *Apoe*$^{-/-}$*Lmna*$^{G609G/G609G}$ mice; n=11-*12 Apoe*$^{-/-}$*Lmna*$^{LCS/LCS}$*SM22αCre* mice); *P*=0.0148 for TUDCA-treated *vs* untreated *Apoe*$^{-/-}$*Lmna*$^{LCS/LCS}$*SM22αCre* mice (median survival: 61.4 *vs* 45.35 weeks, respectively). Data in **B** are mean ± SEM. Statistical differences were analyzed by log-rank test in **A**.

These results show that whereas TUDCA treatment ameliorated vasculopathy in both progeria models, it failed to prolong lifespan in mice ubiquitously expressing progerin. In accord with this finding, ePPi treatment was shown to prevent vascular calcification in *Lmna*$^{G609G/G609G}$ mice, but had no effect on survival (*60*). This result may be explained by our previous studies on the cause of death of progeric mice, showing that *Apoe*$^{-/-}$*Lmna*$^{LCS/LCS}$*SM22αCre* mice, unlike *Apoe*$^{-/-}$*Lmna*$^{G609G/G609G}$ mice,

die of atherosclerosis-related causes. Thus, prevention of atherosclerosis by TUDCA in *Apoe*$^{-/-}$ *Lmna*$^{LCS/LCS}$*SM22αCre* mice was also associated with a significant prolongation of lifespan.

Although we did not detect any evident adverse effects of TUDCA treatment, we did observe that weight gain was lower in TUDCA-treated groups than in PBS-injected groups (**Fig. 35A** and **Fig. 39B**). Even though this diminished weight gain was usually not significant, it was present across different experiments in all analyzed genotypes and was independent of diet. This observation is in agreement with the work of da-Silva *et al.*, who showed that some chemical chaperones, including TUDCA, accelerate thyroid hormone activation and energy expenditure (*177*). Remarkably, progerin can also increase energy expenditure and mitochondrial activity, contributing to lipodystrophy; thus, caution should be exercised when calculating the TUDCA dose for progeric mice, to avoid possible harmful effects on adipose tissue. Nevertheless, four weeks of oral TUDCA treatment in obese patients was shown not to alter body weight and total body fat, indicating that the doses used in humans (1750 mg/day/person in this particular study) are unlikely to affect body weight and adipose tissue homeostasis (*179*).

The chemical chaperone TUDCA is a water-soluble bile acid that has been used successfully in Europe to treat cholestatic liver disease (*180, 181*). TUDCA represents around 0.13% of the bile acid pool in human serum (*182*), and is a high-abundance bile acid in American and Asiatic black bears (*183*). Various studies reported no adverse effects of TUDCA treatment (daily doses from 500 to 1750 mg per person) in obese, liver-transplanted, and primary biliary cirrhosis patients (*179, 184-186*). In general, chemical chaperones show exceptional *in vivo* safety, and some of them have been approved for clinical use by the U.S. Food and Drug Administration, for example, PBA for urea cycle disorders (*187, 188*) and ursodeoxycholic acid or primary biliary cirrhosis (*189-191*). Importantly, chemical chaperones have been used successfully in children (*187, 188*). Thus, the potential of chemical chaperone treatment to ameliorate atherosclerosis and associated ischemic events should be explored in children with HGPS. The use of a combination of drugs targeting different pathways may be an effective, therapeutic strategy until approaches directly targeting progerin production become available in humans.

V. CONCLUSIONS

In this PhD thesis, I have generated new mouse models to study the role of progerin in accelerating atherosclerosis and premature death, and to identify the underlying mechanisms and develop new therapies for the treatment of progeria in mice. The main conclusions derived from this thesis are the following:

1. *Apoe*$^{-/-}$ *Lmna*$^{G609G/G609G}$ mice with ubiquitous progerin expression display features of premature aging (shortened life span, reduced body weight, etc.), and exhibit early onset of vascular disease (including enhanced atherosclerosis, VSMC loss, increased lipid and collagen content in the media, and adventitial thickening). As these alterations mimic the main symptoms of HGPS, these mice constitute the first available preclinical model to study atherosclerosis in the context of HGPS.
2. *Apoe*$^{-/-}$ *Lmna*$^{LCS/LCS}$ *SM22αCre* mice with VSMC-specific progerin expression do not exhibit premature aging, but present the same vasculopathies as those observed in the ubiquitous progeria model (including accelerated atherosclerosis, VSMC loss, lipid retention in the media, adventitial thickening, etc.), and shortened life span. These findings demonstrate that progerin effects on VSMCs play a crucial role in CVD progression and premature death in HGPS.
3. *Apoe*$^{-/-}$ *Lmna*$^{LCS/LCS}$ *LysMCre* mice with macrophage (myeloid)-specific progerin expression do not show any premature aging or vascular phenotype.
4. Atherosclerotic lesions in *Apoe*$^{-/-}$ *Lmna*$^{G609G/G609G}$ and *Apoe*$^{-/-}$ *Lmna*$^{LCS/LCS}$ *SM22αCre* mice display characteristic features of vulnerable plaques, which may lead to myocardial infarction.
5. *Apoe*$^{-/-}$ *Lmna*$^{LCS/LCS}$ *SM22αCre* mice develop hypotension as they age.
6. *Apoe*$^{-/-}$ *Lmna*$^{G609G/G609G}$ mice, unlike *Apoe*$^{-/-}$ *Lmna*$^{LCS/LCS}$ *SM22αCre* mice, develop early cardiac electrical defects (prolonged QRS complex, QT and QTc intervals) and arrhythmias, which can lead to premature death.
7. *Apoe*$^{-/-}$ *Lmna*$^{LCS/LCS}$ *SM22αCre* mice, unlike *Apoe*$^{-/-}$ *Lmna*$^{G609G/G609G}$ mice, die of atherosclerosis-related causes.
8. High-throughput RNAseq analysis identified ER stress response and the subsequent UPR as major alterations in the tunica media of both *Apoe*$^{-/-}$ *Lmna*$^{G609G/G609G}$ and *Apoe*$^{-/-}$ *Lmna*$^{LCS/LCS}$ *SM22αCre* mice.
9. Targeting ER stress response and the UPR with the chemical chaperone TUDCA inhibits atherosclerosis, VSMC loss and adventitial thickening in *Apoe*$^{-/-}$ *Lmna*$^{G609G/G609G}$ and *Apoe*$^{-/-}$ *Lmna*$^{LCS/LCS}$ *SM22αCre* mice, and extends lifespan in the VSMC-specific model by 35%. These

findings establish the ER stress response and the UPR as driver mechanisms of progerin-induced VSMC death and accelerated atherosclerosis.

In summary, our results with progeroid mouse models suggest the possibility of chemical chaperone treatment for ameliorating atherosclerosis in children with HGPS. Since premature and physiological aging share many pathologies (including CVD), and progerin has been detected at low levels in cells and tissues of normally aging individuals, research on HGPS might shed light on the mechanisms of normal aging.

V. CONCLUSIONES

En esta tesis doctoral hemos generado nuevos modelos de ratón para estudiar el papel de la progerina en la aceleración de la aterosclerosis y la muerte prematura asociada a HGPS. Además, hemos identificado los mecanismos subyacentes y hemos desarrollado nuevas terapias para tratar la enfermedad en ratones progéricos. Las principales conclusiones derivadas de esta tesis son:

1. Los ratones *Apoe*$^{-/-}$ *Lmna*$^{G609G/G609G}$ con expresión ubicua de progerina muestran características de envejecimiento prematuro (pérdida de peso corporal, menor longevidad, etc.) y desarrollan con mucha rapidez enfermedad vascular (incluyendo aterosclerosis acelerada, pérdida de CMLVs, aumento del contenido de colágeno y retención de lípidos en la capa media, y fibrosis de la capa adventicia). Dado que estas alteraciones recapitulan los principales síntomas del HGPS, estos ratones son el primer modelo preclínico disponible para estudiar la aterosclerosis en el contexto de HGPS.
2. Los ratones *Apoe*$^{-/-}$*Lmna*$^{LCS/LCS}$ *SM22αCre* con expresión de progerina específica en CMLVs no muestran fenotipo progérico, pero presentan las mismas alteraciones vasculares observadas en el modelo de expresión ubicua de progeria, incluyendo aterosclerosis acelerada, pérdida de CMLVs, retención de lípidos en la capa media y fibrosis de la capa adventicia, así como menor longevidad. Estos hallazgos demuestran que los efectos de la progerina en las CMLVs juegan un papel crítico en la progresión de la ECV y la muerte prematura asociadas a HGPS.
3. Los ratones *Apoe*$^{-/-}$*Lmna*$^{LCS/LCS}$ *LysMCre* con expresión de progerina específica en macrófagos (línea mieloide) no muestran envejecimiento prematuro ni patología vascular.
4. Las lesiones ateroscleróticas en ratones *Apoe*$^{-/-}$ *Lmna*$^{G609G/G609G}$ y *Apoe*$^{-/-}$*Lmna*$^{LCS/LCS}$ *SM22αCre* presentan características de placas vulnerables, que pueden provocar infarto de miocardio.
5. Los ratones *Apoe*$^{-/-}$*Lmna*$^{LCS/LCS}$ *SM22αCre* desarrollan hipotensión a medida que envejecen.
6. Los ratones *Apoe*$^{-/-}$ *Lmna*$^{G609G/G609G}$, a diferencia de *Apoe*$^{-/-}$*Lmna*$^{LCS/LCS}$ *SM22αCre*, desarrollan tempranamente alteraciones electrocardiográficas (prolongación del complejo QRS, y de los intervalos QT y QTc) y arritmias. Estas anomalías pueden provocar muerte prematura.
7. Los ratones *Apoe*$^{-/-}$*Lmna*$^{LCS/LCS}$ *SM22αCre*, a diferencia de *Apoe*$^{-/-}$ *Lmna*$^{G609G/G609G}$, mueren por problemas relacionadas con la aterosclerosis.
8. Mediante RNAseq hemos identificado un aumento significativo de genes implicados en el estrés de RE y la respuesta a proteínas desplegadas (UPR) en la túnica de media de ratones con expresión de progerina ubicua *(Apoe*$^{-/-}$ *Lmna*$^{G609G/G609G}$*)* y específica de CMLVs *(Apoe*$^{-/-}$ *Lmna*$^{LCS/LCS}$ *SM22αCre).*

9. El tratamiento con TUDCA, una chaperona química que mejora la supervivencia celular en situaciones de estrés de RE y UPR, inhibe la aterosclerosis, la pérdida de CMLVs y el engrosamiento de la adventicia en ratones *Apoe*$^{-/-}$ *Lmna*$^{G609G/G609G}$ y *Apoe*$^{-/-}$*Lmna*$^{LCS/LCS}$ *SM22αCre*. Además, TUDCA prolonga en un 35% la supervivencia de los ratones *Apoe*$^{-/-}$ *Lmna*$^{LCS/LCS}$ *SM22αCre* con expresión de progerina específica en CMLVs. Estos resultados identifican la respuesta al estrés de RE y la UPR como un mecanismo clave en la inducción de muerte de las CMLVs y la aceleración de la aterosclerosis provocadas por progerina.

En resumen, nuestros resultados con modelos de ratón progérico sugieren la posibilidad de tratamiento con chaperonas químicas para mejorar la aterosclerosis en niños con HGPS. Teniendo en cuenta que el envejecimiento prematuro y fisiológico comparten muchos mecanismos y patologías (incluyendo ECV), y que se han detectado niveles bajos de expresión de progerina en células y tejidos de individuos sin HGPS, nuestra investigación en HGPS podría arrojar luz sobre el envejecimiento normal.

VI. REFERENCES

1. E. G. Lakatta, D. Levy, Arterial and cardiac aging: major shareholders in cardiovascular disease enterprises: Part I: aging arteries: a "set up" for vascular disease. *Circulation* **107**, 139-146 (2003).
2. S. S. Lim, T. Vos, A. D. Flaxman, G. Danaei, K. Shibuya, H. Adair-Rohani, M. Amann, H. R. Anderson, K. G. Andrews, M. Aryee, C. Atkinson, L. J. Bacchus, A. N. Bahalim, K. Balakrishnan, J. Balmes, S. Barker-Collo, A. Baxter, M. L. Bell, J. D. Blore, F. Blyth, C. Bonner, G. Borges, R. Bourne, M. Boussinesq, M. Brauer, P. Brooks, N. G. Bruce, B. Brunekreef, C. Bryan-Hancock, C. Bucello, R. Buchbinder, F. Bull, R. T. Burnett, T. E. Byers, B. Calabria, J. Carapetis, E. Carnahan, Z. Chafe, F. Charlson, H. Chen, J. S. Chen, A. T. Cheng, J. C. Child, A. Cohen, K. E. Colson, B. C. Cowie, S. Darby, S. Darling, A. Davis, L. Degenhardt, F. Dentener, D. C. Des Jarlais, K. Devries, M. Dherani, E. L. Ding, E. R. Dorsey, T. Driscoll, K. Edmond, S. E. Ali, R. E. Engell, P. J. Erwin, S. Fahimi, G. Falder, F. Farzadfar, A. Ferrari, M. M. Finucane, S. Flaxman, F. G. Fowkes, G. Freedman, M. K. Freeman, E. Gakidou, S. Ghosh, E. Giovannucci, G. Gmel, K. Graham, R. Grainger, B. Grant, D. Gunnell, H. R. Gutierrez, W. Hall, H. W. Hoek, A. Hogan, H. D. Hosgood, 3rd, D. Hoy, H. Hu, B. J. Hubbell, S. J. Hutchings, S. E. Ibeanusi, G. L. Jacklyn, R. Jasrasaria, J. B. Jonas, H. Kan, J. A. Kanis, N. Kassebaum, N. Kawakami, Y. H. Khang, S. Khatibzadeh, J. P. Khoo, C. Kok, F. Laden, R. Lalloo, Q. Lan, T. Lathlean, J. L. Leasher, J. Leigh, Y. Li, J. K. Lin, S. E. Lipshultz, S. London, R. Lozano, Y. Lu, J. Mak, R. Malekzadeh, L. Mallinger, W. Marcenes, L. March, R. Marks, R. Martin, P. McGale, J. McGrath, S. Mehta, G. A. Mensah, T. R. Merriman, R. Micha, C. Michaud, V. Mishra, K. Mohd Hanafiah, A. A. Mokdad, L. Morawska, D. Mozaffarian, T. Murphy, M. Naghavi, B. Neal, P. K. Nelson, J. M. Nolla, R. Norman, C. Olives, S. B. Omer, J. Orchard, R. Osborne, B. Ostro, A. Page, K. D. Pandey, C. D. Parry, E. Passmore, J. Patra, N. Pearce, P. M. Pelizzari, M. Petzold, M. R. Phillips, D. Pope, C. A. Pope, 3rd, J. Powles, M. Rao, H. Razavi, E. A. Rehfuess, J. T. Rehm, B. Ritz, F. P. Rivara, T. Roberts, C. Robinson, J. A. Rodriguez-Portales, I. Romieu, R. Room, L. C. Rosenfeld, A. Roy, L. Rushton, J. A. Salomon, U. Sampson, L. Sanchez-Riera, E. Sanman, A. Sapkota, S. Seedat, P. Shi, K. Shield, R. Shivakoti, G. M. Singh, D. A. Sleet, E. Smith, K. R. Smith, N. J. Stapelberg, K. Steenland, H. Stockl, L. J. Stovner, K. Straif, L. Straney, G. D. Thurston, J. H. Tran, R. Van Dingenen, A. van Donkelaar, J. L. Veerman, L. Vijayakumar, R. Weintraub, M. M. Weissman, R. A. White, H. Whiteford, S. T. Wiersma, J. D. Wilkinson, H. C. Williams, W. Williams, N. Wilson, A. D. Woolf, P. Yip, J. M. Zielinski, A. D. Lopez, C. J. Murray, M. Ezzati, M. A. AlMazroa, Z. A. Memish, A comparative risk assessment of burden

of disease and injury attributable to 67 risk factors and risk factor clusters in 21 regions, 1990-2010: a systematic analysis for the Global Burden of Disease Study 2010. *Lancet* **380**, 2224-2260 (2012).

3. E. J. Benjamin, M. J. Blaha, S. E. Chiuve, M. Cushman, S. R. Das, R. Deo, S. D. de Ferranti, J. Floyd, M. Fornage, C. Gillespie, C. R. Isasi, M. C. Jimenez, L. C. Jordan, S. E. Judd, D. Lackland, J. H. Lichtman, L. Lisabeth, S. Liu, C. T. Longenecker, R. H. Mackey, K. Matsushita, D. Mozaffarian, M. E. Mussolino, K. Nasir, R. W. Neumar, L. Palaniappan, D. K. Pandey, R. R. Thiagarajan, M. J. Reeves, M. Ritchey, C. J. Rodriguez, G. A. Roth, W. D. Rosamond, C. Sasson, A. Towfighi, C. W. Tsao, M. B. Turner, S. S. Virani, J. H. Voeks, J. Z. Willey, J. T. Wilkins, J. H. Wu, H. M. Alger, S. S. Wong, P. Muntner, C. American Heart Association Statistics, S. Stroke Statistics, Heart Disease and Stroke Statistics-2017 Update: A Report From the American Heart Association. *Circulation* **135**, e146-e603 (2017).
4. R. Virmani, A. P. Avolio, W. J. Mergner, M. Robinowitz, E. E. Herderick, J. F. Cornhill, S. Y. Guo, T. H. Liu, D. Y. Ou, M. O'Rourke, Effect of aging on aortic morphology in populations with high and low prevalence of hypertension and atherosclerosis. Comparison between occidental and Chinese communities. *The American journal of pathology* **139**, 1119-1129 (1991).
5. M. A. Lim, R. R. Townsend, Arterial compliance in the elderly: its effect on blood pressure measurement and cardiovascular outcomes. *Clinics in geriatric medicine* **25**, 191-205 (2009).
6. C. Vlachopoulos, K. Aznaouridis, C. Stefanadis, Prediction of cardiovascular events and all-cause mortality with arterial stiffness: a systematic review and meta-analysis. *Journal of the American College of Cardiology* **55**, 1318-1327 (2010).
7. S. J. Zieman, V. Melenovsky, D. A. Kass, Mechanisms, pathophysiology, and therapy of arterial stiffness. *Arteriosclerosis, thrombosis, and vascular biology* **25**, 932-943 (2005).
8. Z. Li, J. Froehlich, Z. S. Galis, E. G. Lakatta, Increased expression of matrix metalloproteinase-2 in the thickened intima of aged rats. *Hypertension* **33**, 116-123 (1999).
9. G. K. Hansson, P. Libby, I. Tabas, Inflammation and plaque vulnerability. *Journal of internal medicine* **278**, 483-493 (2015).
10. G. P. Kwon, J. L. Schroeder, M. J. Amar, A. T. Remaley, R. S. Balaban, Contribution of macromolecular structure to the retention of low-density lipoprotein at arterial branch points. *Circulation* **117**, 2919-2927 (2008).

11. D. R. Greaves, S. Gordon, Thematic review series: the immune system and atherogenesis. Recent insights into the biology of macrophage scavenger receptors. *Journal of lipid research* **46**, 11-20 (2005).
12. L. Hegyi, J. N. Skepper, N. R. Cary, M. J. Mitchinson, Foam cell apoptosis and the development of the lipid core of human atherosclerosis. *The Journal of pathology* **180**, 423-429 (1996).
13. C. Stefanadis, C. K. Antoniou, D. Tsiachris, P. Pietri, Coronary Atherosclerotic Vulnerable Plaque: Current Perspectives. *Journal of the American Heart Association* **6**, (2017).
14. J. Hutchinson, Congenital Absence of Hair and Mammary Glands with Atrophic Condition of the Skin and its Appendages, in a Boy whose Mother had been almost wholly Bald from Alopecia Areata from the age of Six. *Medico-chirurgical transactions* **69**, 473-477 (1886).
15. H. Gilford, On a Condition of Mixed Premature and Immature Development. *Medico-chirurgical transactions* **80**, 17-46 25 (1897).
16. R. C. Hennekam, Hutchinson-Gilford progeria syndrome: review of the phenotype. *American journal of medical genetics. Part A* **140**, 2603-2624 (2006).
17. M. A. Merideth, L. B. Gordon, S. Clauss, V. Sachdev, A. C. Smith, M. B. Perry, C. C. Brewer, C. Zalewski, H. J. Kim, B. Solomon, B. P. Brooks, L. H. Gerber, M. L. Turner, D. L. Domingo, T. C. Hart, J. Graf, J. C. Reynolds, A. Gropman, J. A. Yanovski, M. Gerhard-Herman, F. S. Collins, E. G. Nabel, R. O. Cannon, 3rd, W. A. Gahl, W. J. Introne, Phenotype and course of Hutchinson-Gilford progeria syndrome. *The New England journal of medicine* **358**, 592-604 (2008).
18. N. J. Ullrich, L. B. Gordon, Hutchinson-Gilford progeria syndrome. *Handb Clin Neurol* **132**, 249-264 (2015).
19. L. B. Gordon, I. A. Harten, M. E. Patti, A. H. Lichtenstein, Reduced adiponectin and HDL cholesterol without elevated C-reactive protein: clues to the biology of premature atherosclerosis in Hutchinson-Gilford Progeria Syndrome. *The Journal of pediatrics* **146**, 336-341 (2005).
20. M. Olive, I. Harten, R. Mitchell, J. K. Beers, K. Djabali, K. Cao, M. R. Erdos, C. Blair, B. Funke, L. Smoot, M. Gerhard-Herman, J. T. Machan, R. Kutys, R. Virmani, F. S. Collins, T. N. Wight, E. G. Nabel, L. B. Gordon, Cardiovascular pathology in Hutchinson-Gilford progeria: correlation with the vascular pathology of aging. *Arteriosclerosis, thrombosis, and vascular biology* **30**, 2301-2309 (2010).

21. W. E. Stehbens, S. J. Wakefield, E. Gilbert-Barness, R. E. Olson, J. Ackerman, Histological and ultrastructural features of atherosclerosis in progeria. *Cardiovascular pathology : the official journal of the Society for Cardiovascular Pathology* **8**, 29-39 (1999).
22. W. E. Stehbens, B. Delahunt, T. Shozawa, E. Gilbert-Barness, Smooth muscle cell depletion and collagen types in progeric arteries. *Cardiovascular pathology : the official journal of the Society for Cardiovascular Pathology* **10**, 133-136 (2001).
23. M. Gerhard-Herman, L. B. Smoot, N. Wake, M. W. Kieran, M. E. Kleinman, D. T. Miller, A. Schwartzman, A. Giobbie-Hurder, D. Neuberg, L. B. Gordon, Mechanisms of premature vascular aging in children with Hutchinson-Gilford progeria syndrome. *Hypertension* **59**, 92-97 (2012).
24. J. Blacher, J. A. Staessen, X. Girerd, J. Gasowski, L. Thijs, L. Liu, J. G. Wang, R. H. Fagard, M. E. Safar, Pulse pressure not mean pressure determines cardiovascular risk in older hypertensive patients. *Archives of internal medicine* **160**, 1085-1089 (2000).
25. A. Benetos, F. Thomas, L. Joly, J. Blacher, B. Pannier, C. Labat, P. Salvi, H. Smulyan, M. E. Safar, Pulse pressure amplification a mechanical biomarker of cardiovascular risk. *Journal of the American College of Cardiology* **55**, 1032-1037 (2010).
26. P. M. Rothwell, Limitations of the usual blood-pressure hypothesis and importance of variability, instability, and episodic hypertension. *Lancet* **375**, 938-948 (2010).
27. P. M. Rothwell, S. C. Howard, E. Dolan, E. O'Brien, J. E. Dobson, B. Dahlof, P. S. Sever, N. R. Poulter, Prognostic significance of visit-to-visit variability, maximum systolic blood pressure, and episodic hypertension. *Lancet* **375**, 895-905 (2010).
28. V. M. Silvera, L. B. Gordon, D. B. Orbach, S. E. Campbell, J. T. Machan, N. J. Ullrich, Imaging characteristics of cerebrovascular arteriopathy and stroke in Hutchinson-Gilford progeria syndrome. *AJNR. American journal of neuroradiology* **34**, 1091-1097 (2013).
29. M. W. Kieran, L. Gordon, M. Kleinman, New approaches to progeria. *Pediatrics* **120**, 834-841 (2007).
30. J. Rivera-Torres, C. J. Calvo, A. Llach, G. Guzman-Martinez, R. Caballero, C. Gonzalez-Gomez, L. J. Jimenez-Borreguero, J. A. Guadix, F. G. Osorio, C. Lopez-Otin, A. Herraiz-Martinez, N. Cabello, A. Vallmitjana, R. Benitez, L. B. Gordon, J. Jalife, J. M. Perez-Pomares, J. Tamargo, E. Delpon, L. Hove-Madsen, D. Filgueiras-Rama, V. Andres, Cardiac electrical defects in progeroid mice and Hutchinson-Gilford progeria syndrome patients with nuclear lamina alterations. *Proc Natl Acad Sci U S A* **113**, E7250-E7259 (2016).

31. K. Nair, P. Ramachandran, K. M. Krishnamoorthy, S. Dora, T. J. Achuthan, Hutchinson-Gilford progeria syndrome with severe calcific aortic valve stenosis and calcific mitral valve. *J Heart Valve Dis* **13**, 866-869 (2004).
32. N. B. Hanumanthappa, G. Madhusudan, J. Mahimarangaiah, C. N. Manjunath, Hutchinson-Gilford progeria syndrome with severe calcific aortic valve stenosis. *Ann Pediatr Cardiol* **4**, 204-206 (2011).
33. M. Eriksson, W. T. Brown, L. B. Gordon, M. W. Glynn, J. Singer, L. Scott, M. R. Erdos, C. M. Robbins, T. Y. Moses, P. Berglund, A. Dutra, E. Pak, S. Durkin, A. B. Csoka, M. Boehnke, T. W. Glover, F. S. Collins, Recurrent de novo point mutations in lamin A cause Hutchinson-Gilford progeria syndrome. *Nature* **423**, 293-298 (2003).
34. A. De Sandre-Giovannoli, R. Bernard, P. Cau, C. Navarro, J. Amiel, I. Boccaccio, S. Lyonnet, C. L. Stewart, A. Munnich, M. Le Merrer, N. Levy, Lamin a truncation in Hutchinson-Gilford progeria. *Science* **300**, 2055 (2003).
35. F. Lin, H. J. Worman, Structural organization of the human gene encoding nuclear lamin A and nuclear lamin C. *The Journal of biological chemistry* **268**, 16321-16326 (1993).
36. K. Furukawa, H. Inagaki, Y. Hotta, Identification and cloning of an mRNA coding for a germ cell-specific A-type lamin in mice. *Exp Cell Res* **212**, 426-430 (1994).
37. B. M. Machiels, A. H. Zorenc, J. M. Endert, H. J. Kuijpers, G. J. van Eys, F. C. Ramaekers, J. L. Broers, An alternative splicing product of the lamin A/C gene lacks exon 10. *The Journal of biological chemistry* **271**, 9249-9253 (1996).
38. V. Andres, J. M. Gonzalez, Role of A-type lamins in signaling, transcription, and chromatin organization. *The Journal of cell biology* **187**, 945-957 (2009).
39. L. A. Beck, T. J. Hosick, M. Sinensky, Isoprenylation is required for the processing of the lamin A precursor. *The Journal of cell biology* **110**, 1489-1499 (1990).
40. M. Sinensky, K. Fantle, M. Trujillo, T. McLain, A. Kupfer, M. Dalton, The processing pathway of prelamin A. *Journal of cell science* **107 (Pt 1)**, 61-67 (1994).
41. D. Holtz, R. A. Tanaka, J. Hartwig, F. McKeon, The CaaX motif of lamin A functions in conjunction with the nuclear localization signal to target assembly to the nuclear envelope. *Cell* **59**, 969-977 (1989).
42. D. P. Corrigan, D. Kuszczak, A. E. Rusinol, D. P. Thewke, C. A. Hrycyna, S. Michaelis, M. S. Sinensky, Prelamin A endoproteolytic processing in vitro by recombinant Zmpste24. *The Biochemical journal* **387**, 129-138 (2005).

43. A. M. Pendas, Z. Zhou, J. Cadinanos, J. M. Freije, J. Wang, K. Hultenby, A. Astudillo, A. Wernerson, F. Rodriguez, K. Tryggvason, C. Lopez-Otin, Defective prelamin A processing and muscular and adipocyte alterations in Zmpste24 metalloproteinase-deficient mice. *Nat Genet* **31**, 94-99 (2002).
44. K. Weber, U. Plessmann, P. Traub, Maturation of nuclear lamin A involves a specific carboxy-terminal trimming, which removes the polyisoprenylation site from the precursor; implications for the structure of the nuclear lamina. *FEBS letters* **257**, 411-414 (1989).
45. S. Vidak, R. Foisner, Molecular insights into the premature aging disease progeria. *Histochemistry and cell biology* **145**, 401-417 (2016).
46. S. Gonzalo, R. Kreienkamp, P. Askjaer, Hutchinson-Gilford Progeria Syndrome: A premature aging disease caused by LMNA gene mutations. *Ageing research reviews* **33**, 18-29 (2017).
47. C. L. Navarro, A. De Sandre-Giovannoli, R. Bernard, I. Boccaccio, A. Boyer, D. Genevieve, S. Hadj-Rabia, C. Gaudy-Marqueste, H. S. Smitt, P. Vabres, L. Faivre, A. Verloes, T. Van Essen, E. Flori, R. Hennekam, F. A. Beemer, N. Laurent, M. Le Merrer, P. Cau, N. Levy, Lamin A and ZMPSTE24 (FACE-1) defects cause nuclear disorganization and identify restrictive dermopathy as a lethal neonatal laminopathy. *Hum Mol Genet* **13**, 2493-2503 (2004).
48. C. L. Navarro, J. Cadinanos, A. De Sandre-Giovannoli, R. Bernard, S. Courrier, I. Boccaccio, A. Boyer, W. J. Kleijer, A. Wagner, F. Giuliano, F. A. Beemer, J. M. Freije, P. Cau, R. C. Hennekam, C. Lopez-Otin, C. Badens, N. Levy, Loss of ZMPSTE24 (FACE-1) causes autosomal recessive restrictive dermopathy and accumulation of Lamin A precursors. *Hum Mol Genet* **14**, 1503-1513 (2005).
49. C. L. Moulson, G. Go, J. M. Gardner, A. C. van der Wal, J. H. Smitt, J. M. van Hagen, J. H. Miner, Homozygous and compound heterozygous mutations in ZMPSTE24 cause the laminopathy restrictive dermopathy. *J Invest Dermatol* **125**, 913-919 (2005).
50. A. K. Agarwal, J. P. Fryns, R. J. Auchus, A. Garg, Zinc metalloproteinase, ZMPSTE24, is mutated in mandibuloacral dysplasia. *Hum Mol Genet* **12**, 1995-2001 (2003).
51. S. Reddy, L. Comai, Lamin A, farnesylation and aging. *Exp Cell Res* **318**, 1-7 (2012).
52. C. Lefevre, M. Auclair, F. Boccara, J. P. Bastard, J. Capeau, C. Vigouroux, M. Caron-Debarle, Premature senescence of vascular cells is induced by HIV protease inhibitors: implication of prelamin A and reversion by statin. *Arteriosclerosis, thrombosis, and vascular biology* **30**, 2611-2620 (2010).

53. P. Afonso, M. Auclair, F. Boccara, M. C. Vantyghem, C. Katlama, J. Capeau, C. Vigouroux, M. Caron-Debarle, LMNA mutations resulting in lipodystrophy and HIV protease inhibitors trigger vascular smooth muscle cell senescence and calcification: Role of ZMPSTE24 downregulation. *Atherosclerosis* **245**, 200-211 (2016).

54. P. Scaffidi, T. Misteli, Lamin A-dependent nuclear defects in human aging. *Science* **312**, 1059-1063 (2006).

55. D. McClintock, D. Ratner, M. Lokuge, D. M. Owens, L. B. Gordon, F. S. Collins, K. Djabali, The mutant form of lamin A that causes Hutchinson-Gilford progeria is a biomarker of cellular aging in human skin. *PloS one* **2**, e1269 (2007).

56. S. H. Yang, M. O. Bergo, J. I. Toth, X. Qiao, Y. Hu, S. Sandoval, M. Meta, P. Bendale, M. H. Gelb, S. G. Young, L. G. Fong, Blocking protein farnesyltransferase improves nuclear blebbing in mouse fibroblasts with a targeted Hutchinson-Gilford progeria syndrome mutation. *Proc Natl Acad Sci U S A* **102**, 10291-10296 (2005).

57. S. H. Yang, M. Meta, X. Qiao, D. Frost, J. Bauch, C. Coffinier, S. Majumdar, M. O. Bergo, S. G. Young, L. G. Fong, A farnesyltransferase inhibitor improves disease phenotypes in mice with a Hutchinson-Gilford progeria syndrome mutation. *J Clin Invest* **116**, 2115-2121 (2006).

58. R. Varga, M. Eriksson, M. R. Erdos, M. Olive, I. Harten, F. Kolodgie, B. C. Capell, J. Cheng, D. Faddah, S. Perkins, H. Avallone, H. San, X. Qu, S. Ganesh, L. B. Gordon, R. Virmani, T. N. Wight, E. G. Nabel, F. S. Collins, Progressive vascular smooth muscle cell defects in a mouse model of Hutchinson-Gilford progeria syndrome. *Proc Natl Acad Sci U S A* **103**, 3250-3255 (2006).

59. F. G. Osorio, C. L. Navarro, J. Cadinanos, I. C. Lopez-Mejia, P. M. Quiros, C. Bartoli, J. Rivera, J. Tazi, G. Guzman, I. Varela, D. Depetris, F. de Carlos, J. Cobo, V. Andres, A. De Sandre-Giovannoli, J. M. Freije, N. Levy, C. Lopez-Otin, Splicing-directed therapy in a new mouse model of human accelerated aging. *Science translational medicine* **3**, 106ra107 (2011).

60. R. Villa-Bellosta, J. Rivera-Torres, F. G. Osorio, R. Acin-Perez, J. A. Enriquez, C. Lopez-Otin, V. Andres, Defective extracellular pyrophosphate metabolism promotes vascular calcification in a mouse model of Hutchinson-Gilford progeria syndrome that is ameliorated on pyrophosphate treatment. *Circulation* **127**, 2442-2451 (2013).

61. J. M. Lee, C. Nobumori, Y. Tu, C. Choi, S. H. Yang, H. J. Jung, T. A. Vickers, F. Rigo, C. F. Bennett, S. G. Young, L. G. Fong, Modulation of LMNA splicing as a strategy to treat prelamin A diseases. *J Clin Invest* **126**, 1592-1602 (2016).

62. M. O. Bergo, B. Gavino, J. Ross, W. K. Schmidt, C. Hong, L. V. Kendall, A. Mohr, M. Meta, H. Genant, Y. Jiang, E. R. Wisner, N. Van Bruggen, R. A. Carano, S. Michaelis, S. M. Griffey, S. G. Young, Zmpste24 deficiency in mice causes spontaneous bone fractures, muscle weakness, and a prelamin A processing defect. *Proc Natl Acad Sci U S A* **99**, 13049-13054 (2002).

63. J. Swift, I. L. Ivanovska, A. Buxboim, T. Harada, P. C. Dingal, J. Pinter, J. D. Pajerowski, K. R. Spinler, J. W. Shin, M. Tewari, F. Rehfeldt, D. W. Speicher, D. E. Discher, Nuclear lamin-A scales with tissue stiffness and enhances matrix-directed differentiation. *Science* **341**, 1240104 (2013).

64. J. Swift, D. E. Discher, The nuclear lamina is mechano-responsive to ECM elasticity in mature tissue. *Journal of cell science* **127**, 3005-3015 (2014).

65. C. L. Moulson, L. G. Fong, J. M. Gardner, E. A. Farber, G. Go, A. Passariello, D. K. Grange, S. G. Young, J. H. Miner, Increased progerin expression associated with unusual LMNA mutations causes severe progeroid syndromes. *Hum Mutat* **28**, 882-889 (2007).

66. J. Reunert, R. Wentzell, M. Walter, S. Jakubiczka, M. Zenker, T. Brune, S. Rust, T. Marquardt, Neonatal progeria: increased ratio of progerin to lamin A leads to progeria of the newborn. *Eur J Hum Genet* **20**, 933-937 (2012).

67. J. Denecke, T. Brune, T. Feldhaus, H. Robenek, C. Kranz, R. J. Auchus, A. K. Agarwal, T. Marquardt, A homozygous ZMPSTE24 null mutation in combination with a heterozygous mutation in the LMNA gene causes Hutchinson-Gilford progeria syndrome (HGPS): insights into the pathophysiology of HGPS. *Hum Mutat* **27**, 524-531 (2006).

68. L. G. Fong, J. K. Ng, M. Meta, N. Cote, S. H. Yang, C. L. Stewart, T. Sullivan, A. Burghardt, S. Majumdar, K. Reue, M. O. Bergo, S. G. Young, Heterozygosity for Lmna deficiency eliminates the progeria-like phenotypes in Zmpste24-deficient mice. *Proc Natl Acad Sci U S A* **101**, 18111-18116 (2004).

69. S. H. Yang, S. Y. Chang, S. Ren, Y. Wang, D. A. Andres, H. P. Spielmann, L. G. Fong, S. G. Young, Absence of progeria-like disease phenotypes in knock-in mice expressing a non-farnesylated version of progerin. *Hum Mol Genet* **20**, 436-444 (2011).

70. B. S. Davies, R. H. Barnes, 2nd, Y. Tu, S. Ren, D. A. Andres, H. P. Spielmann, J. Lammerding, Y. Wang, S. G. Young, L. G. Fong, An accumulation of non-farnesylated prelamin A causes cardiomyopathy but not progeria. *Hum Mol Genet* **19**, 2682-2694 (2010).

71. J. I. Toth, S. H. Yang, X. Qiao, A. P. Beigneux, M. H. Gelb, C. L. Moulson, J. H. Miner, S. G. Young, L. G. Fong, Blocking protein farnesyltransferase improves nuclear shape in

fibroblasts from humans with progeroid syndromes. *Proc Natl Acad Sci U S A* **102**, 12873-12878 (2005).

72. L. G. Fong, D. Frost, M. Meta, X. Qiao, S. H. Yang, C. Coffinier, S. G. Young, A protein farnesyltransferase inhibitor ameliorates disease in a mouse model of progeria. *Science* **311**, 1621-1623 (2006).
73. B. C. Capell, M. Olive, M. R. Erdos, K. Cao, D. A. Faddah, U. L. Tavarez, K. N. Conneely, X. Qu, H. San, S. K. Ganesh, X. Chen, H. Avallone, F. D. Kolodgie, R. Virmani, E. G. Nabel, F. S. Collins, A farnesyltransferase inhibitor prevents both the onset and late progression of cardiovascular disease in a progeria mouse model. *Proc Natl Acad Sci U S A* **105**, 15902-15907 (2008).
74. I. Varela, S. Pereira, A. P. Ugalde, C. L. Navarro, M. F. Suarez, P. Cau, J. Cadinanos, F. G. Osorio, N. Foray, J. Cobo, F. de Carlos, N. Levy, J. M. Freije, C. Lopez-Otin, Combined treatment with statins and aminobisphosphonates extends longevity in a mouse model of human premature aging. *Nature medicine* **14**, 767-772 (2008).
75. L. B. Gordon, M. E. Kleinman, D. T. Miller, D. S. Neuberg, A. Giobbie-Hurder, M. Gerhard-Herman, L. B. Smoot, C. M. Gordon, R. Cleveland, B. D. Snyder, B. Fligor, W. R. Bishop, P. Statkevich, A. Regen, A. Sonis, S. Riley, C. Ploski, A. Correia, N. Quinn, N. J. Ullrich, A. Nazarian, M. G. Liang, S. Y. Huh, A. Schwartzman, M. W. Kieran, Clinical trial of a farnesyltransferase inhibitor in children with Hutchinson-Gilford progeria syndrome. *Proc Natl Acad Sci U S A* **109**, 16666-16671 (2012).
76. L. B. Gordon, J. Massaro, R. B. D'Agostino, Sr., S. E. Campbell, J. Brazier, W. T. Brown, M. E. Kleinman, M. W. Kieran, C. Progeria Clinical Trials, Impact of farnesylation inhibitors on survival in Hutchinson-Gilford progeria syndrome. *Circulation* **130**, 27-34 (2014).
77. L. B. Gordon, M. E. Kleinman, J. Massaro, R. B. D'Agostino, Sr., H. Shappell, M. Gerhard-Herman, L. B. Smoot, C. M. Gordon, R. H. Cleveland, A. Nazarian, B. D. Snyder, N. J. Ullrich, V. M. Silvera, M. G. Liang, N. Quinn, D. T. Miller, S. Y. Huh, A. A. Dowton, K. Littlefield, M. M. Greer, M. W. Kieran, Clinical Trial of the Protein Farnesylation Inhibitors Lonafarnib, Pravastatin, and Zoledronic Acid in Children With Hutchinson-Gilford Progeria Syndrome. *Circulation* **134**, 114-125 (2016).
78. A. Kalinowski, P. N. Yaron, Z. Qin, S. Shenoy, M. J. Buehler, M. Losche, K. N. Dahl, Interfacial binding and aggregation of lamin A tail domains associated with Hutchinson-Gilford progeria syndrome. *Biophys Chem* **195**, 43-48 (2014).

79. Z. Qin, A. Kalinowski, K. N. Dahl, M. J. Buehler, Structure and stability of the lamin A tail domain and HGPS mutant. *J Struct Biol* **175**, 425-433 (2011).
80. R. D. Goldman, D. K. Shumaker, M. R. Erdos, M. Eriksson, A. E. Goldman, L. B. Gordon, Y. Gruenbaum, S. Khuon, M. Mendez, R. Varga, F. S. Collins, Accumulation of mutant lamin A causes progressive changes in nuclear architecture in Hutchinson-Gilford progeria syndrome. *Proc Natl Acad Sci U S A* **101**, 8963-8968 (2004).
81. K. N. Dahl, P. Scaffidi, M. F. Islam, A. G. Yodh, K. L. Wilson, T. Misteli, Distinct structural and mechanical properties of the nuclear lamina in Hutchinson-Gilford progeria syndrome. *Proc Natl Acad Sci U S A* **103**, 10271-10276 (2006).
82. S. J. Lee, Y. S. Jung, M. H. Yoon, S. M. Kang, A. Y. Oh, J. H. Lee, S. Y. Jun, T. G. Woo, H. Y. Chun, S. K. Kim, K. J. Chung, H. Y. Lee, K. Lee, G. Jin, M. K. Na, N. C. Ha, C. Barcena, J. M. Freije, C. Lopez-Otin, G. Y. Song, B. J. Park, Interruption of progerin-lamin A/C binding ameliorates Hutchinson-Gilford progeria syndrome phenotype. *J Clin Invest* **126**, 3879-3893 (2016).
83. M. X. Ibrahim, V. I. Sayin, M. K. Akula, M. Liu, L. G. Fong, S. G. Young, M. O. Bergo, Targeting isoprenylcysteine methylation ameliorates disease in a mouse model of progeria. *Science* **340**, 1330-1333 (2013).
84. K. Cao, J. J. Graziotto, C. D. Blair, J. R. Mazzulli, M. R. Erdos, D. Krainc, F. S. Collins, Rapamycin reverses cellular phenotypes and enhances mutant protein clearance in Hutchinson-Gilford progeria syndrome cells. *Sci Transl Med* **3**, 89ra58 (2011).
85. J. J. Graziotto, K. Cao, F. S. Collins, D. Krainc, Rapamycin activates autophagy in Hutchinson-Gilford progeria syndrome: implications for normal aging and age-dependent neurodegenerative disorders. *Autophagy* **8**, 147-151 (2012).
86. S. J. Lee, S. H. Park, Arterial ageing. *Korean Circ J* **43**, 73-79 (2013).
87. A. Buxboim, J. Swift, J. Irianto, K. R. Spinler, P. C. Dingal, A. Athirasala, Y. R. Kao, S. Cho, T. Harada, J. W. Shin, D. E. Discher, Matrix elasticity regulates lamin-A,C phosphorylation and turnover with feedback to actomyosin. *Current biology : CB* **24**, 1909-1917 (2014).
88. J. T. Philip, K. N. Dahl, Nuclear mechanotransduction: response of the lamina to extracellular stress with implications in aging. *J Biomech* **41**, 3164-3170 (2008).
89. E. A. Booth, S. T. Spagnol, T. A. Alcoser, K. N. Dahl, Nuclear stiffening and chromatin softening with progerin expression leads to an attenuated nuclear response to force. *Soft Matter* **11**, 6412-6418 (2015).

90. V. L. Verstraeten, J. Y. Ji, K. S. Cummings, R. T. Lee, J. Lammerding, Increased mechanosensitivity and nuclear stiffness in Hutchinson-Gilford progeria cells: effects of farnesyltransferase inhibitors. *Aging Cell* **7**, 383-393 (2008).
91. M. Song, H. San, S. A. Anderson, R. O. Cannon, 3rd, D. Orlic, Shear stress-induced mechanotransduction protein deregulation and vasculopathy in a mouse model of progeria. *Stem Cell Res Ther* **5**, 41 (2014).
92. J. A. Brassard, N. Fekete, A. Garnier, C. A. Hoesli, Hutchinson-Gilford progeria syndrome as a model for vascular aging. *Biogerontology* **17**, 129-145 (2016).
93. T. Katsumoto, A. Mitsushima, T. Kurimura, The role of the vimentin intermediate filaments in rat 3Y1 cells elucidated by immunoelectron microscopy and computer-graphic reconstruction. *Biol Cell* **68**, 139-146 (1990).
94. G. H. Liu, B. Z. Barkho, S. Ruiz, D. Diep, J. Qu, S. L. Yang, A. D. Panopoulos, K. Suzuki, L. Kurian, C. Walsh, J. Thompson, S. Boue, H. L. Fung, I. Sancho-Martinez, K. Zhang, J. Yates, 3rd, J. C. Izpisua Belmonte, Recapitulation of premature ageing with iPSCs from Hutchinson-Gilford progeria syndrome. *Nature* **472**, 221-225 (2011).
95. D. Kinoshita, A. Nagasawa, I. Shimizu, T. K. Ito, Y. Yoshida, M. Tsuchida, A. Iwama, T. Hayano, T. Minamino, Progerin impairs vascular smooth muscle cell growth via the DNA damage response pathway. *Oncotarget*, (2017).
96. H. Zhang, Z. M. Xiong, K. Cao, Mechanisms controlling the smooth muscle cell death in progeria via down-regulation of poly(ADP-ribose) polymerase 1. *Proc Natl Acad Sci U S A* **111**, E2261-2270 (2014).
97. C. D. Ragnauth, D. T. Warren, Y. Liu, R. McNair, T. Tajsic, N. Figg, R. Shroff, J. Skepper, C. M. Shanahan, Prelamin A acts to accelerate smooth muscle cell senescence and is a novel biomarker of human vascular aging. *Circulation* **121**, 2200-2210 (2010).
98. Y. Liu, I. Drozdov, R. Shroff, L. E. Beltran, C. M. Shanahan, Prelamin A accelerates vascular calcification via activation of the DNA damage response and senescence-associated secretory phenotype in vascular smooth muscle cells. *Circ Res* **112**, e99-109 (2013).
99. A. M. Cobb, D. Larrieu, D. T. Warren, Y. Liu, S. Srivastava, A. J. Smith, R. P. Bowater, S. P. Jackson, C. M. Shanahan, Prelamin A impairs 53BP1 nuclear entry by mislocalizing NUP153 and disrupting the Ran gradient. *Aging Cell*, (2016).
100. B. Liu, J. Wang, K. M. Chan, W. M. Tjia, W. Deng, X. Guan, J. D. Huang, K. M. Li, P. Y. Chau, D. J. Chen, D. Pei, A. M. Pendas, J. Cadinanos, C. Lopez-Otin, H. F. Tse, C.

Hutchison, J. Chen, Y. Cao, K. S. Cheah, K. Tryggvason, Z. Zhou, Genomic instability in laminopathy-based premature aging. *Nature medicine* **11**, 780-785 (2005).

101. B. Liu, Z. Wang, S. Ghosh, Z. Zhou, Defective ATM-Kap-1-mediated chromatin remodeling impairs DNA repair and accelerates senescence in progeria mouse model. *Aging Cell* **12**, 316-318 (2013).
102. B. Liu, Z. Wang, L. Zhang, S. Ghosh, H. Zheng, Z. Zhou, Depleting the methyltransferase Suv39h1 improves DNA repair and extends lifespan in a progeria mouse model. *Nat Commun* **4**, 1868 (2013).
103. G. A. Garinis, G. T. van der Horst, J. Vijg, J. H. Hoeijmakers, DNA damage and ageing: new-age ideas for an age-old problem. *Nature cell biology* **10**, 1241-1247 (2008).
104. M. Salamat, P. K. Dhar, D. L. Neagu, J. B. Lyon, Aortic calcification in a patient with hutchinson-gilford progeria syndrome. *Pediatr Cardiol* **31**, 925-926 (2010).
105. J. C. Kovacic, P. Moreno, E. G. Nabel, V. Hachinski, V. Fuster, Cellular senescence, vascular disease, and aging: part 2 of a 2-part review: clinical vascular disease in the elderly. *Circulation* **123**, 1900-1910 (2011).
106. I. Quiros-Gonzalez, P. Roman-Garcia, C. Alonso-Montes, S. Barrio-Vazquez, N. Carrillo-Lopez, M. Naves-Diaz, M. I. Mora, F. J. Corrales, F. J. Lopez-Hernandez, M. P. Ruiz-Torres, J. B. Cannata-Andia, J. L. Fernandez-Martin, Lamin A is involved in the development of vascular calcification induced by chronic kidney failure and phosphorus load. *Bone* **84**, 160-168 (2016).
107. P. Scaffidi, T. Misteli, Lamin A-dependent misregulation of adult stem cells associated with accelerated ageing. *Nature cell biology* **10**, 452-459 (2008).
108. S. G. Frangos, V. Gahtan, B. Sumpio, Localization of atherosclerosis: role of hemodynamics. *Arch Surg* **134**, 1142-1149 (1999).
109. L. Rouleau, J. Rossi, R. L. Leask, The response of human aortic endothelial cells in a stenotic hemodynamic environment: effect of duration, magnitude, and spatial gradients in wall shear stress. *J Biomech Eng* **132**, 071015 (2010).
110. N. Bonello-Palot, S. Simoncini, S. Robert, P. Bourgeois, F. Sabatier, N. Levy, F. Dignat-George, C. Badens, Prelamin A accumulation in endothelial cells induces premature senescence and functional impairment. *Atherosclerosis* **237**, 45-52 (2014).
111. T. B. Kirkwood, S. N. Austad, Why do we age? *Nature* **408**, 233-238 (2000).
112. N. Kourtis, N. Tavernarakis, Cellular stress response pathways and ageing: intricate molecular relationships. *The EMBO journal* **30**, 2520-2531 (2011).

113. D. Lindholm, H. Wootz, L. Korhonen, ER stress and neurodegenerative diseases. *Cell death and differentiation* **13**, 385-392 (2006).
114. H. Yoshida, ER stress and diseases. *The FEBS journal* **274**, 630-658 (2007).
115. J. H. Lin, P. Walter, T. S. Yen, Endoplasmic reticulum stress in disease pathogenesis. *Annual review of pathology* **3**, 399-425 (2008).
116. M. Schroder, R. J. Kaufman, The mammalian unfolded protein response. *Annual review of biochemistry* **74**, 739-789 (2005).
117. D. Ron, P. Walter, Signal integration in the endoplasmic reticulum unfolded protein response. *Nature reviews. Molecular cell biology* **8**, 519-529 (2007).
118. P. Walter, D. Ron, The unfolded protein response: from stress pathway to homeostatic regulation. *Science* **334**, 1081-1086 (2011).
119. C. R. Prostko, M. A. Brostrom, C. O. Brostrom, Reversible phosphorylation of eukaryotic initiation factor 2 alpha in response to endoplasmic reticular signaling. *Molecular and cellular biochemistry* **127-128**, 255-265 (1993).
120. R. J. Kaufman, Stress signaling from the lumen of the endoplasmic reticulum: coordination of gene transcriptional and translational controls. *Genes & development* **13**, 1211-1233 (1999).
121. R. Y. Hampton, ER stress response: getting the UPR hand on misfolded proteins. *Current biology : CB* **10**, R518-521 (2000).
122. C. Hetz, The unfolded protein response: controlling cell fate decisions under ER stress and beyond. *Nature reviews. Molecular cell biology* **13**, 89-102 (2012).
123. E. Szegezdi, S. E. Logue, A. M. Gorman, A. Samali, Mediators of endoplasmic reticulum stress-induced apoptosis. *EMBO reports* **7**, 880-885 (2006).
124. A. Bertolotti, Y. Zhang, L. M. Hendershot, H. P. Harding, D. Ron, Dynamic interaction of BiP and ER stress transducers in the unfolded-protein response. *Nature cell biology* **2**, 326-332 (2000).
125. H. P. Harding, I. Novoa, Y. Zhang, H. Zeng, R. Wek, M. Schapira, D. Ron, Regulated translation initiation controls stress-induced gene expression in mammalian cells. *Molecular cell* **6**, 1099-1108 (2000).
126. D. Han, A. G. Lerner, L. Vande Walle, J. P. Upton, W. Xu, A. Hagen, B. J. Backes, S. A. Oakes, F. R. Papa, IRE1alpha kinase activation modes control alternate endoribonuclease outputs to determine divergent cell fates. *Cell* **138**, 562-575 (2009).
127. J. Hollien, J. S. Weissman, Decay of endoplasmic reticulum-localized mRNAs during the unfolded protein response. *Science* **313**, 104-107 (2006).

128. J. Hollien, J. H. Lin, H. Li, N. Stevens, P. Walter, J. S. Weissman, Regulated Ire1-dependent decay of messenger RNAs in mammalian cells. *The Journal of cell biology* **186**, 323-331 (2009).

129. G. Kroemer, G. Marino, B. Levine, Autophagy and the integrated stress response. *Molecular cell* **40**, 280-293 (2010).

130. K. Haze, H. Yoshida, H. Yanagi, T. Yura, K. Mori, Mammalian transcription factor ATF6 is synthesized as a transmembrane protein and activated by proteolysis in response to endoplasmic reticulum stress. *Molecular biology of the cell* **10**, 3787-3799 (1999).

131. J. Ye, R. B. Rawson, R. Komuro, X. Chen, U. P. Dave, R. Prywes, M. S. Brown, J. L. Goldstein, ER stress induces cleavage of membrane-bound ATF6 by the same proteases that process SREBPs. *Molecular cell* **6**, 1355-1364 (2000).

132. K. Haze, T. Okada, H. Yoshida, H. Yanagi, T. Yura, M. Negishi, K. Mori, Identification of the G13 (cAMP-response-element-binding protein-related protein) gene product related to activating transcription factor 6 as a transcriptional activator of the mammalian unfolded protein response. *The Biochemical journal* **355**, 19-28 (2001).

133. K. Lee, W. Tirasophon, X. Shen, M. Michalak, R. Prywes, T. Okada, H. Yoshida, K. Mori, R. J. Kaufman, IRE1-mediated unconventional mRNA splicing and S2P-mediated ATF6 cleavage merge to regulate XBP1 in signaling the unfolded protein response. *Genes & development* **16**, 452-466 (2002).

134. C. E. Shamu, P. Walter, Oligomerization and phosphorylation of the Ire1p kinase during intracellular signaling from the endoplasmic reticulum to the nucleus. *The EMBO journal* **15**, 3028-3039 (1996).

135. M. Calfon, H. Zeng, F. Urano, J. H. Till, S. R. Hubbard, H. P. Harding, S. G. Clark, D. Ron, IRE1 couples endoplasmic reticulum load to secretory capacity by processing the XBP-1 mRNA. *Nature* **415**, 92-96 (2002).

136. H. Yoshida, T. Matsui, A. Yamamoto, T. Okada, K. Mori, XBP1 mRNA is induced by ATF6 and spliced by IRE1 in response to ER stress to produce a highly active transcription factor. *Cell* **107**, 881-891 (2001).

137. A. H. Lee, N. N. Iwakoshi, L. H. Glimcher, XBP-1 regulates a subset of endoplasmic reticulum resident chaperone genes in the unfolded protein response. *Molecular and cellular biology* **23**, 7448-7459 (2003).

138. D. Acosta-Alvear, Y. Zhou, A. Blais, M. Tsikitis, N. H. Lents, C. Arias, C. J. Lennon, Y. Kluger, B. D. Dynlacht, XBP1 controls diverse cell type- and condition-specific transcriptional regulatory networks. *Molecular cell* **27**, 53-66 (2007).
139. R. Sriburi, S. Jackowski, K. Mori, J. W. Brewer, XBP1: a link between the unfolded protein response, lipid biosynthesis, and biogenesis of the endoplasmic reticulum. *The Journal of cell biology* **167**, 35-41 (2004).
140. Z. Liu, Y. Lv, N. Zhao, G. Guan, J. Wang, Protein kinase R-like ER kinase and its role in endoplasmic reticulum stress-decided cell fate. *Cell death & disease* **6**, e1822 (2015).
141. N. Naidoo, ER and aging-Protein folding and the ER stress response. *Ageing research reviews* **8**, 150-159 (2009).
142. K. Ameri, A. L. Harris, Activating transcription factor 4. *The international journal of biochemistry & cell biology* **40**, 14-21 (2008).
143. I. Novoa, H. Zeng, H. P. Harding, D. Ron, Feedback inhibition of the unfolded protein response by GADD34-mediated dephosphorylation of eIF2alpha. *The Journal of cell biology* **153**, 1011-1022 (2001).
144. N. Naidoo, The endoplasmic reticulum stress response and aging. *Reviews in the neurosciences* **20**, 23-37 (2009).
145. L. Wang, J. Meng, W. Cao, Q. Li, Y. Qiu, B. Sun, L. M. Li, Induction of apoptosis through ER stress and TP53 in MCF-7 cells by the nanoparticle [Gd@C82(OH)22]n: A systems biology study. *Methods* **67**, 394-406 (2014).
146. J. Zhang, Q. Lian, G. Zhu, F. Zhou, L. Sui, C. Tan, R. A. Mutalif, R. Navasankari, Y. Zhang, H. F. Tse, C. L. Stewart, A. Colman, A human iPSC model of Hutchinson Gilford Progeria reveals vascular smooth muscle and mesenchymal stem cell defects. *Cell Stem Cell* **8**, 31-45 (2011).
147. B. E. Clausen, C. Burkhardt, W. Reith, R. Renkawitz, I. Forster, Conditional gene targeting in macrophages and granulocytes using LysMcre mice. *Transgenic Res* **8**, 265-277 (1999).
148. R. Agarwal, Regulation of circadian blood pressure: from mice to astronauts. *Current opinion in nephrology and hypertension* **19**, 51-58 (2010).
149. F. Halberg, H. Mult, G. Cornelissen, D. Hillman, L. A. Beaty, S. Hong, O. Schwartzkopff, Y. Watanabe, K. Otsuka, J. Siegelova, Chronobiologically Interpreted Ambulatory Blood Pressure Monitoring in Health and Disease. *Global advances in health and medicine* **1**, 66-123 (2012).
150. S. Andrews, FastQC: a quality control tool for high throughput sequence data. 2010.

151. M. Martin, Cutadapt removes adapter sequences from high-throughput sequencing reads. *2011* **17**, (2011).
152. B. Li, C. N. Dewey, RSEM: accurate transcript quantification from RNA-Seq data with or without a reference genome. *BMC Bioinformatics* **12**, 323 (2011).
153. M. D. Robinson, D. J. McCarthy, G. K. Smyth, edgeR: a Bioconductor package for differential expression analysis of digital gene expression data. *Bioinformatics* **26**, 139-140 (2010).
154. T. Hulsen, J. de Vlieg, W. Alkema, BioVenn - a web application for the comparison and visualization of biological lists using area-proportional Venn diagrams. *BMC Genomics* **9**, 488 (2008).
155. S. H. Yang, X. Qiao, E. Farber, S. Y. Chang, L. G. Fong, S. G. Young, Eliminating the synthesis of mature lamin A reduces disease phenotypes in mice carrying a Hutchinson-Gilford progeria syndrome allele. *The Journal of biological chemistry* **283**, 7094-7099 (2008).
156. J. J. Fuster, A. I. Castillo, C. Zaragoza, B. Ibanez, V. Andres, Animal models of atherosclerosis. *Prog Mol Biol Transl Sci* **105**, 1-23 (2012).
157. P. Libby, G. K. Hansson, Inflammation and immunity in diseases of the arterial tree: players and layers. *Circ Res* **116**, 307-311 (2015).
158. I. C. Lopez-Mejia, M. de Toledo, C. Chavey, L. Lapasset, P. Cavelier, C. Lopez-Herrera, K. Chebli, P. Fort, G. Beranger, L. Fajas, E. Z. Amri, F. Casas, J. Tazi, Antagonistic functions of LMNA isoforms in energy expenditure and lifespan. *EMBO reports* **15**, 529-539 (2014).
159. M. C. Clarke, N. Figg, J. J. Maguire, A. P. Davenport, M. Goddard, T. D. Littlewood, M. R. Bennett, Apoptosis of vascular smooth muscle cells induces features of plaque vulnerability in atherosclerosis. *Nature medicine* **12**, 1075-1080 (2006).
160. S. A. Kamath, P. Meo Neto Jde, R. M. Canham, F. Uddin, K. H. Toto, L. L. Nelson, P. A. Kaiser, J. A. de Lemos, M. H. Drazner, Low voltage on the electrocardiogram is a marker of disease severity and a risk factor for adverse outcomes in patients with heart failure due to systolic dysfunction. *American heart journal* **152**, 355-361 (2006).
161. J. Gehrmann, S. Frantz, C. T. Maguire, M. Vargas, A. Ducharme, H. Wakimoto, R. T. Lee, C. I. Berul, Electrophysiological characterization of murine myocardial ischemia and infarction. *Basic research in cardiology* **96**, 237-250 (2001).
162. N. Clausell, J. Butany, P. Gladstone, E. Lonn, P. Liu, C. Cardella, C. Feindel, P. A. Daly, Myocardial vacuolization, a marker of ischemic injury, in surveillance cardiac biopsies posttransplant: Correlations with morphologic vascular disease and endothelial dysfunction.

Cardiovascular pathology : the official journal of the Society for Cardiovascular Pathology **5**, 29-37 (1996).

163. R. B. Driesen, F. K. Verheyen, P. Dijkstra, F. Thone, J. P. Cleutjens, M. H. Lenders, F. C. Ramaekers, M. Borgers, Structural remodelling of cardiomyocytes in the border zone of infarcted rabbit heart. *Molecular and cellular biochemistry* **302**, 225-232 (2007).
164. J. S. Pirolo, G. M. Hutchins, G. W. Moore, Myocyte vacuolization in infarct border zones is reversible. *The American journal of pathology* **121**, 444-450 (1985).
165. B. Feng, P. M. Yao, Y. Li, C. M. Devlin, D. Zhang, H. P. Harding, M. Sweeney, J. X. Rong, G. Kuriakose, E. A. Fisher, A. R. Marks, D. Ron, I. Tabas, The endoplasmic reticulum is the site of cholesterol-induced cytotoxicity in macrophages. *Nature cell biology* **5**, 781-792 (2003).
166. D. A. Cunha, P. Hekerman, L. Ladriere, A. Bazarra-Castro, F. Ortis, M. C. Wakeham, F. Moore, J. Rasschaert, A. K. Cardozo, E. Bellomo, L. Overbergh, C. Mathieu, R. Lupi, T. Hai, A. Herchuelz, P. Marchetti, G. A. Rutter, D. L. Eizirik, M. Cnop, Initiation and execution of lipotoxic ER stress in pancreatic beta-cells. *Journal of cell science* **121**, 2308-2318 (2008).
167. C. Mlynarczyk, R. Fahraeus, Endoplasmic reticulum stress sensitizes cells to DNA damage-induced apoptosis through p53-dependent suppression of p21(CDKN1A). *Nat Commun* **5**, 5067 (2014).
168. N. Kubben, W. Zhang, L. Wang, T. C. Voss, J. Yang, J. Qu, G. H. Liu, T. Misteli, Repression of the Antioxidant NRF2 Pathway in Premature Aging. *Cell* **165**, 1361-1374 (2016).
169. S. B. Cullinan, D. Zhang, M. Hannink, E. Arvisais, R. J. Kaufman, J. A. Diehl, Nrf2 is a direct PERK substrate and effector of PERK-dependent cell survival. *Molecular and cellular biology* **23**, 7198-7209 (2003).
170. D. Senft, Z. A. Ronai, UPR, autophagy, and mitochondria crosstalk underlies the ER stress response. *Trends Biochem Sci* **40**, 141-148 (2015).
171. F. G. Osorio, C. Barcena, C. Soria-Valles, A. J. Ramsay, F. de Carlos, J. Cobo, A. Fueyo, J. M. Freije, C. Lopez-Otin, Nuclear lamina defects cause ATM-dependent NF-kappaB activation and link accelerated aging to a systemic inflammatory response. *Genes & development* **26**, 2311-2324 (2012).
172. J. Rivera-Torres, R. Acin-Perez, P. Cabezas-Sanchez, F. G. Osorio, C. Gonzalez-Gomez, D. Megias, C. Camara, C. Lopez-Otin, J. A. Enriquez, J. L. Luque-Garcia, V. Andres, Identification of mitochondrial dysfunction in Hutchinson-Gilford progeria syndrome through

use of stable isotope labeling with amino acids in cell culture. *J Proteomics* **91**, 466-477 (2013).

173. G. Marino, A. P. Ugalde, N. Salvador-Montoliu, I. Varela, P. M. Quiros, J. Cadinanos, I. van der Pluijm, J. M. Freije, C. Lopez-Otin, Premature aging in mice activates a systemic metabolic response involving autophagy induction. *Hum Mol Genet* **17**, 2196-2211 (2008).
174. U. Ozcan, E. Yilmaz, L. Ozcan, M. Furuhashi, E. Vaillancourt, R. O. Smith, C. Z. Gorgun, G. S. Hotamisligil, Chemical chaperones reduce ER stress and restore glucose homeostasis in a mouse model of type 2 diabetes. *Science* **313**, 1137-1140 (2006).
175. Z. Cai, F. Li, W. Gong, W. Liu, Q. Duan, C. Chen, L. Ni, Y. Xia, K. Cianflone, N. Dong, D. W. Wang, Endoplasmic reticulum stress participates in aortic valve calcification in hypercholesterolemic animals. *Arteriosclerosis, thrombosis, and vascular biology* **33**, 2345-2354 (2013).
176. A. L. Rivard, C. J. Steer, B. T. Kren, C. M. Rodrigues, R. E. Castro, R. W. Bianco, W. C. Low, Administration of tauroursodeoxycholic acid (TUDCA) reduces apoptosis following myocardial infarction in rat. *Am J Chin Med* **35**, 279-295 (2007).
177. W. S. da-Silva, S. Ribich, R. Arrojo e Drigo, M. Castillo, M. E. Patti, A. C. Bianco, The chemical chaperones tauroursodeoxycholic and 4-phenylbutyric acid accelerate thyroid hormone activation and energy expenditure. *FEBS letters* **585**, 539-544 (2011).
178. E. Erbay, V. R. Babaev, J. R. Mayers, L. Makowski, K. N. Charles, M. E. Snitow, S. Fazio, M. M. Wiest, S. M. Watkins, M. F. Linton, G. S. Hotamisligil, Reducing endoplasmic reticulum stress through a macrophage lipid chaperone alleviates atherosclerosis. *Nature medicine* **15**, 1383-1391 (2009).
179. M. Kars, L. Yang, M. F. Gregor, B. S. Mohammed, T. A. Pietka, B. N. Finck, B. W. Patterson, J. D. Horton, B. Mittendorfer, G. S. Hotamisligil, S. Klein, Tauroursodeoxycholic Acid may improve liver and muscle but not adipose tissue insulin sensitivity in obese men and women. *Diabetes* **59**, 1899-1905 (2010).
180. A. Crosignani, P. M. Battezzati, K. D. Setchell, P. Invernizzi, G. Covini, M. Zuin, M. Podda, Tauroursodeoxycholic acid for treatment of primary biliary cirrhosis. A dose-response study. *Dig Dis Sci* **41**, 809-815 (1996).
181. A. Larghi, A. Crosignani, P. M. Battezzati, G. De Valle, M. Allocca, P. Invernizzi, M. Zuin, M. Podda, Ursodeoxycholic and tauro-ursodeoxycholic acids for the treatment of primary biliary cirrhosis: a pilot crossover study. *Aliment Pharmacol Ther* **11**, 409-414 (1997).

182. K. Bentayeb, R. Batlle, C. Sanchez, C. Nerin, C. Domeno, Determination of bile acids in human serum by on-line restricted access material-ultra high-performance liquid chromatography-mass spectrometry. *J Chromatogr B Analyt Technol Biomed Life Sci* **869**, 1-8 (2008).

183. L. R. Hagey, D. L. Crombie, E. Espinosa, M. C. Carey, H. Igimi, A. F. Hofmann, Ursodeoxycholic acid in the Ursidae: biliary bile acids of bears, pandas, and related carnivores. *Journal of lipid research* **34**, 1911-1917 (1993).

184. M. Angelico, G. Tisone, L. Baiocchi, G. Palmieri, F. Pisani, S. Negrini, A. Anselmo, G. Vennarecci, C. U. Casciani, One-year pilot study on tauroursodeoxycholic acid as an adjuvant treatment after liver transplantation. *Italian journal of gastroenterology and hepatology* **31**, 462-468 (1999).

185. K. D. Setchell, C. M. Rodrigues, M. Podda, A. Crosignani, Metabolism of orally administered tauroursodeoxycholic acid in patients with primary biliary cirrhosis. *Gut* **38**, 439-446 (1996).

186. P. Invernizzi, K. D. Setchell, A. Crosignani, P. M. Battezzati, A. Larghi, N. C. O'Connell, M. Podda, Differences in the metabolism and disposition of ursodeoxycholic acid and of its taurine-conjugated species in patients with primary biliary cirrhosis. *Hepatology* **29**, 320-327 (1999).

187. N. E. Maestri, S. W. Brusilow, D. B. Clissold, S. S. Bassett, Long-term treatment of girls with ornithine transcarbamylase deficiency. *The New England journal of medicine* **335**, 855-859 (1996).

188. A. B. Burlina, H. Ogier, H. Korall, F. K. Trefz, Long-term treatment with sodium phenylbutyrate in ornithine transcarbamylase-deficient patients. *Molecular genetics and metabolism* **72**, 351-355 (2001).

189. K. D. Lindor, E. R. Dickson, W. P. Baldus, R. A. Jorgensen, J. Ludwig, P. A. Murtaugh, J. M. Harrison, R. H. Wiesner, M. L. Anderson, S. M. Lange, et al., Ursodeoxycholic acid in the treatment of primary biliary cirrhosis. *Gastroenterology* **106**, 1284-1290 (1994).

190. E. J. Heathcote, K. Cauch-Dudek, V. Walker, R. J. Bailey, L. M. Blendis, C. N. Ghent, P. Michieletti, G. Y. Minuk, S. C. Pappas, L. J. Scully, et al., The Canadian Multicenter Double-blind Randomized Controlled Trial of ursodeoxycholic acid in primary biliary cirrhosis. *Hepatology* **19**, 1149-1156 (1994).

191. R. E. Poupon, A. M. Bonnand, Y. Chretien, R. Poupon, Ten-year survival in ursodeoxycholic acid-treated patients with primary biliary cirrhosis. The UDCA-PBC Study Group. *Hepatology* **29**, 1668-1671 (1999).

VII. ANNEX

Publications related to the thesis:

1. **Hamczyk MR**, Villa-Bellosta R, Gonzalo P, Andrés-Manzano MJ, López-Otín C, Andrés V. Ubiquitous and smooth muscle-specific progerin expression in apolipoprotein E-deficient mice accelerates atherosclerosis and induces premature death (under preparation).

2. **Hamczyk MR**, Villa-Bellosta R, Quesada V, Gonzalo P, Andrés-Manzano MJ, López-Otín C, Andrés V. Targeting the ER stress response delays atherosclerosis and associated death in progeroid mice (under preparation).

Other publications prepared during the thesis:

1. **Hamczyk MR*,** del Campo L*, Andrés V. Aging in the Cardiovascular System: Lessons from Hutchinson-Gilford progeria syndrome (under revision in Ann Rev Physiol). * *equal contribution*

2. Villa-Bellosta R, **Hamczyk MR**, Andrés V. Novel phosphate-activated macrophages prevent ectopic calcification by increasing extracellular ATP and pyrophosphate. PLoS One. 2017 Mar 31;12(3):e0174998.

3. Villa-Bellosta R, **Hamczyk MR**, Andrés V. Alternatively activated macrophages exhibit an anticalcifying activity dependent on extracellular ATP/pyrophosphate metabolism. Am J Physiol Cell Physiol. 2016 May 15;310(10):C788-99.

4. **Hamczyk MR**, Villa-Bellosta R, Andrés V. In Vitro Macrophage Phagocytosis Assay. Methods Mol Biol. 2015;1339:235-46.

5. Villa-Bellosta R, **Hamczyk MR**. Isolation and Culture of Aortic Smooth Muscle Cells and In Vitro Calcification Assay. Methods Mol Biol. 2015;1339:119-29.